3-2018

Control of PV Connected Power Grid using LQR and Fuzzy Logic Control

Samar Emara
sae8228@rit.edu

Control of PV Connected Power Grid using LQR and Fuzzy Logic Control

by

Samar Emara

A Thesis Submitted in Partial Fulfillment of the

Requirements for the Degree of Master of Science in Electrical Engineering

Department of Electrical Engineering and Computing Sciences

Rochester Institute of Technology, Dubai UAE

March 2018

Control of PV Connected Power Grid using LQR and Fuzzy Logic Control

by

Samar Emara

A Thesis Submitted in Partial Fulfilment of the Requirements
for the Degree of Master of Science in Electrical Engineering
Department of Electrical Engineering and Computing Sciences

Approved By:

Date:

Dr. Abdulla Ismail

Thesis Advisor – Department of Electrical Engineering

Date:

Dr. Yousef Al Assaf

Committee Member – Department of Electrical Engineering

Date:

Dr. Ghalib Kahwaji

Committee Member – Department of Mechanical Engineering

Acknowledgements

I would like to express my sincere gratitude to Dr. Abdulla Ismail, the advisor of this thesis, for his continuous support and guidance. Without him the completion of this research would not have been possible. His door was always open to help me in my thesis and I am honored to have him as my thesis advisor.

I would also like to thank Dr. Ali Sayyad for his helpful guidance and valuable comments on my thesis work and for all the time he dedicated to help me. Many thanks also to my colleagues at RIT Dubai and my professors for their support and encouragement.

My sincere thanks and appreciation to Dr. Yousef Al Assaf, president of RIT Dubai and Dr. Ghalib Kahwaji, head of the Mechanical Engineering at RIT Dubai, for giving me from their time to read and evaluate this thesis.

Last but not least, I would like to deeply thank my parents for their continuous support and encouragement throughout this journey. Their support always leads me to success and prosperity.

Dedicated to my parents

Abstract

As the contribution of renewable energy to the current power grid is becoming an essential part of the global energy system, it is of critical importance to study the effects of this increased penetration of the renewable sources on the power system. Focusing on solar energy, its intermittent nature makes it difficult to predict the output when connecting to the power grid. Therefore, well-structured control methods should be used to assure a continuous and steady system performance with regard to the system frequency variation.

In this thesis, a PV system is modelled and connected to a grid served by a conventional thermal power system with 45% penetration level. Then, the system frequency errors due to load changes are studied in this PV connected power grid. Appropriate and effective controllers are designed to regulate these errors to keep the system response within the required specifications.

In addition, single-area as well as two-area interconnected power systems are considered in this research. The power exchange among the two areas will add another significant parameter that is essential in the efficient operation of the system and that affects the behavior of the system in terms of the frequency error response.

Two advanced control methods, namely Linear Quadratic Regulator (LQR) and Fuzzy Logic Control (FLC) are applied to control the single-area and the two-area systems. The appropriate controllers are designed, assessed and the responses are analyzed and compared. These designed controllers demonstrated a superior performance in the controlled system by achieving the required specifications of undershoot, settling time and steady state error for the system frequency. For the single-area PV connected power system, the LQR controller gave the best response in comparison to the two other types of controllers, while in the two-area system the fuzzy logic controller was the most suitable as it met the specifications to the best possible extent.

Table of Contents

List of Figures

List of Tables

List of Main Symbols

Δf	Deviation of system frequency from 50Hz
ΔP_{load}	Change of load power
ΔP	Reference power
ΔP_{pv}	Change of the photovoltaic system output power (input to thermal power system)
ΔP_{tie}	Excess of scheduled power exchange between area 1 and area 2 in the power system
A	System state matrix
Q	State Weighted Matrix in LQR controller
R	Control Weighted Matrix in LQR controller
P	Costate matrix in the Riccati equation
K	Optimal state feedback gains in LQR
μ	Membership function
k_i	Integral controller gain
k_p	Proportional controller gain
ΔP_m	Turbine mechanical power
e	Error
$\dot{e}$	Derivative of error
u	Controller output
V_1	Output voltage from the PV array (V)
V_2	Voltage after the DC-DC boost converter (compatible with the grid voltage) (V)
m	The gain between the DC voltage and the AC voltage in the system
M_1	Boost converter gain
I_1	Output current from the PV array (amp)
I_2	Current after the DC-DC boost converter in the PV system (amp)
i_{AC}	The inverted current in the PV system (amp)
p	Instantaneous power of the PV system (W)
P_{avg}	Average power of the PV system (W)
V_m	Phase grid voltage (V)
w	System frequency (rad/s)

List of Main Abbreviations

PV	Photovoltaic
FLC	Fuzzy Logic Controller
PI	Proportional and Integral Controller
LQR	Linear Quadratic Regulator
LFC	Load Frequency Control
MPPT	Maximum Power Point Tracking
MPP	Maximum Power Point
SSE	Steady State Error
p.u.	Per unit system
NB	Negative Big
NM	Negative Medium
NS	Negative Small
ZZ	Zero change
PS	Positive Small
PM	Positive Medium
PB	Positive Big

List of Publications

1- S. Emara and A. Ismail, “Design of fuzzy logic controller for a PV grid connected two-area load frequency control system,” *International Research Journal of Engineering and Technology (IRJET),* Vol. 05, issue: 02, February 2018.

2- S. Emara, A. Ismail and A. Sayyad, “Mathematical model of a photovoltaic grid connected two-area power system,” *International Research Journal of Engineering and Technology (IRJET),* Vol. 05, issue: 02, February 2018.

3- S. Emara, A. Ismail and A. Sayyad, “Optimal controller of a PV grid connected two-area power system,” *International Research Journal of Engineering and Technology (IRJET),* Vol. 05, issue: 02, February 2018.

4- S. Emara, A. Ismail and A. Sayyad, “Fuzzy logic control of a single-area PV grid connected power system”, 4th International Conference on Automatic Control, Dubai UAE, June 2018.

Chapter 1: Introduction

This chapter explains the motivation behind choosing the current research topic as well as some general information concerning its importance. In addition, it explains the detailed objectives of this research that will be focused on throughout the thesis. Finally, the organization of the thesis report is explained for each of the subsequent chapters and associated sections.

1.1 Research Motivation

It is estimated that more than 14% of the supply of the energy nowadays is from renewable energy sources. However, there are always challenges to their implementation because they have to meet certain requirements of voltage and frequency regulations in order to be connected smoothly with the current power systems [1].

Many papers have studied PV connected grids and showed the direct connection of PV to the load [2]. Those studies do not show the connection with the actual model of the conventional power system as shown in Figure 1.1.

Control system design research has been conducted on performance enhancement of isolated photovoltaic systems. Similarly, other works have been reported with regard to the photovoltaic (PV) connected grid [3,4]. However, very few research has been conducted on the effect of this interconnection on the system frequency and voltage profiles. Moreover, some research has been conducted on the solar thermal power plant [5] connected to the conventional power system and its effect on the system frequency variation.

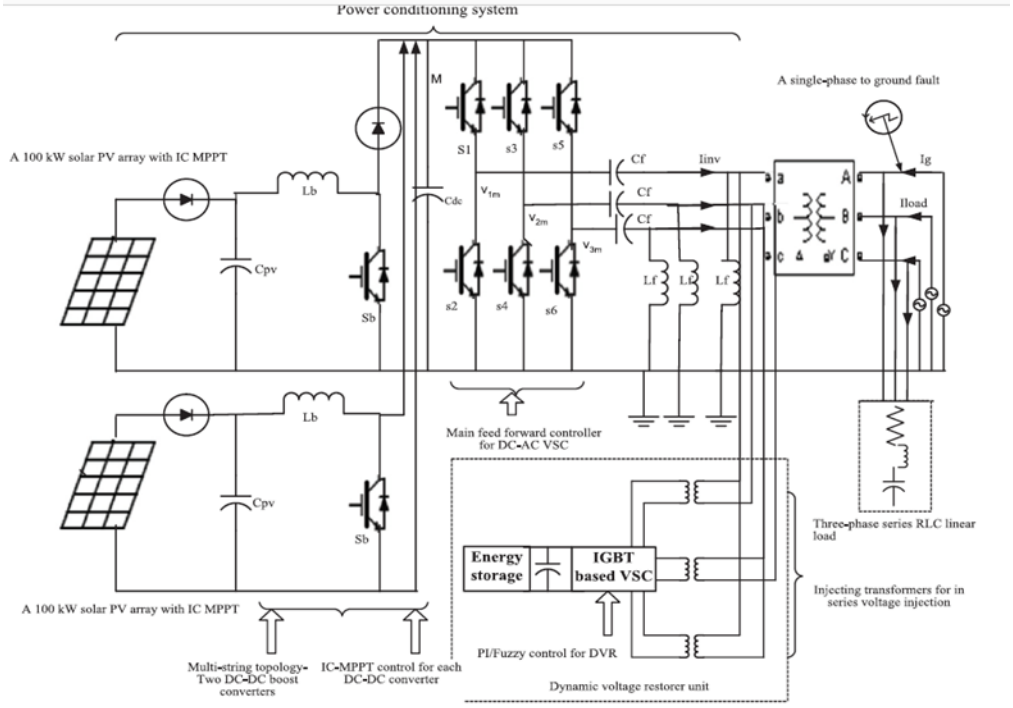

Figure 1.1 a PV system connected to the load in the grid directly [6].

It has been shown in some work that the penetration of renewable energy has an effect on the system frequency and voltage [1]. Keeping the system frequency at an acceptable constant level is a direct indicator of the power system real power and load balance [7]. Therefore, the frequency change will be the main parameter of study in this research. In order to achieve a high penetration level of PV, with its intermittent nature [8], the operation and control of power systems need to account for the associated high variability and uncertainty [9].

As PV is connected to the grid at the lower voltage side (for example, 11kV), thus, the voltage imbalance is not of a lesser concern than the system frequency. Since there are few papers that tackle the issue of frequency control in the PV connected grids with explaining the full model of both the PV and the thermal power system, this was the main motivation behind choosing the focus area of this thesis.

1.2 Research Objectives

The objectives of this research can be summarized as follows:

1- Model a PV system that could properly be connected to a thermal power grid and to model a single-area and two-area thermal power systems connected to it.
2- Design LQR, PI and FL controllers for a single-area and two-area power system connected to the PV system with 45% penetration level.
3- Study the effect of load changes on the system frequency of a single-area and two-area power system connected to PV.
4- Regulate the system frequency error Δf by maintaining the following standard performance specifications:
    a. Settling time < 3s
    b. Undershoot <0.02Hz
    c. Steady state error of Δf = 0
    d. Steady state error of $\Delta P_{tie} = 0$ (for the two-area system)

When the power demand at the load side increases, it causes a drop of system frequency. Since the reference frequency is 50Hz in the power grids in UAE, the tolerance of this undershoot in frequency is 50Hz$\pm$0.02Hz. As to the steady state error of Δf it should equal zero implying that there is no change in frequency from the reference value of 50Hz; i.e. f=50Hz. The exchange of power (ΔP_{tie}) between areas will be explained throughout the report.

1.3 Thesis Organization

Chapter 1 of this thesis explains the objectives of this research and the motivation behind it. Chapter 2 shows the literature review of the recent relevant topics to this research. Chapter 3 explains the mathematical model of the photovoltaic system, the single-area thermal power system, the two-area thermal power system, and the connection between the given PV system and the thermal power system.

Chapter 4 shows the designs of the three controllers (LQR, PI and FL controllers) for the single-area and two-area PV grid connected systems. It shows several cases for each design to study the effect of various load changes on the system frequency error response

and the power exchange between areas with these controllers integrated. In the last chapter, the analysis of the responses of the controlled systems has been studied along with the comparison between all controllers for different cases. The conclusion chapter summarizes the main findings and recommends future work.

Chapter 2: Literature Review

In this chapter, selected recent works on the subject are cited. The selected information presented in this chapter explains the basic knowledge for each system that will be studied and for each type of controller applied to these systems. This is essential in the controller design stage, after studying the details of the systems and the controllers design process.

2.1 Photovoltaic Systems

The smallest unit of a PV array is the solar cell, from which numerous arranged solar cells are used to create a PV array. Based on knowledge of semiconductors physics, a solar cell can be represented as a PN diode that produces DC current affected by the changes of temperature, solar irradiance and the load [8]. The PN junction diode from which a PV cell is created, has two different semiconductor elements; one that is doped with excess positively charged holes (p-type) and another that is doped with excess negatively charged electrons (n-type). The PN junction is the area that separates both sides from each other and it is the area through which the current flows from the high intensity of electrons (n-type) to the high intensity of holes (p-type). The sunlight excites more electrons to move from the n-type to the p-type region creating the DC current which is the output of the PV cell. Thus, this semiconductor structure takes the input and transforms it into electric current by creating the PN junction described. This makes the output current moves only in one direction (from the high intensity of electrons to the high intensity of holes) [10].

Due to the DC output nature of the PV cell, it adds no kinetic energy to the system [11]. Equations 2.1 and 2.2 describe the current produced from a single cell obtained from the ideal PV cell based on semiconductor physics [12].

$$I = I_{pv,cell} - \frac{I_{o,cell}\left[\exp\left(\frac{qV}{\propto KT}\right) - 1\right]}{I_d} \tag{2.1}$$

$$I_d = I_{o,cell}\left\{\exp\left[\frac{qV}{A} \times k \times T\right] - 1\right\} \quad (2.2)$$

I is the output current of the cell, $I_{pv,cell}$ is the current generated by the incident light of the sun on the cell, I_d is the diode current since the PV cell operates as a diode and $I_{o,cell}$ is the diode reverse saturation value. V is the output voltage, A is the area of the junction, T is the temperature at the current time and q and k are constants determined from the specifications of the PN junction diode.

In order to connect the PV array to a power grid, power electronics and devices are required in the connection [13]. After obtaining the power output from the array, the first stage of this connection with the thermal power grid is the boost converter. It increases the voltage to a suitable level to be used as an input to the second stage which is the inverter. The inverter produces an AC current which should be compatible with the AC nature of the power grid. This requires compatibility with the grid voltage and current [14]. Capacitors are used to absorb the harmonics that are not desired of the low frequency current [15]. Figure 2.1 shows the different stages of this connection. The output of the inverter in Figure 2.1 is the input to the thermal power grid from the PV system.

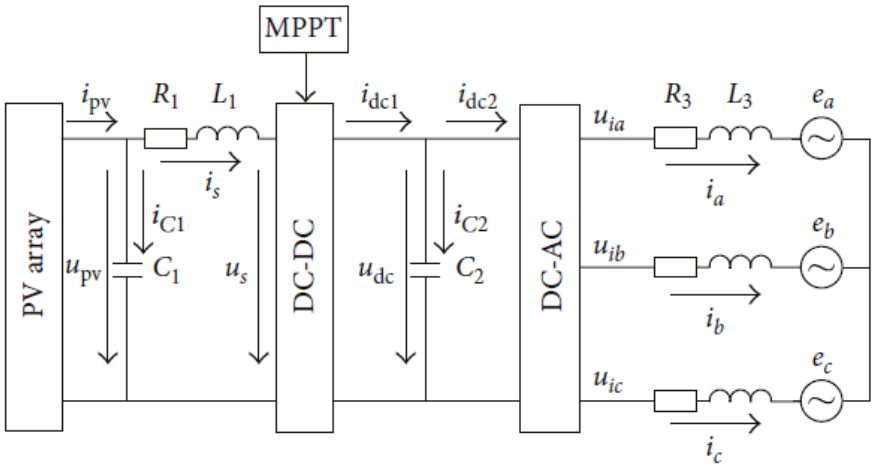

Figure 2.1 Stages of connection of PV array output to the three-phase power grid [15].

As to the effect of this connection of PV to the thermal power system, it has been shown in [16] and [17] that the more the penetration of the photovoltaic array output to the conventional power grid, the less the deviation of the frequency output. In [8], it is demonstrated that since PV only provides real power, then any clouds that pass will only

affect the frequency negatively at the transmission level, not at the utility grid side. Therefore, the effect of PV connection to the grid has a positive effect on the frequency which will be explained further in this work.

Nevertheless, the frequency still needs to be controlled to meet the required specifications. The source in the PV arrays (which is the sun) cannot be controlled unlike the conventional power systems where the amount of fluid can be controlled based on the demand [18]. However, control can be performed in the photovoltaic system connection to the grid in the DC-AC inverters [19]. It increases the efficiency of the system and ensures the operation at Maximum Power Point (MPP). This is the point at which the maximum output power is obtained. It occurs only at a certain voltage value; therefore, the output voltage tracks the MPP in PV cells [19]. The Maximum Power Point Tracker (MPPT) is the controller that tracks the maximum power point and ensures that the system operates at this point most of the time [10].

This MPP occurs, as shown in Figure 2.2, when the slope of the load resistance connected at the output of the PV array side happens to be the diagonal of the largest rectangle that could be drawn on the IV characteristics curve of the PV array.

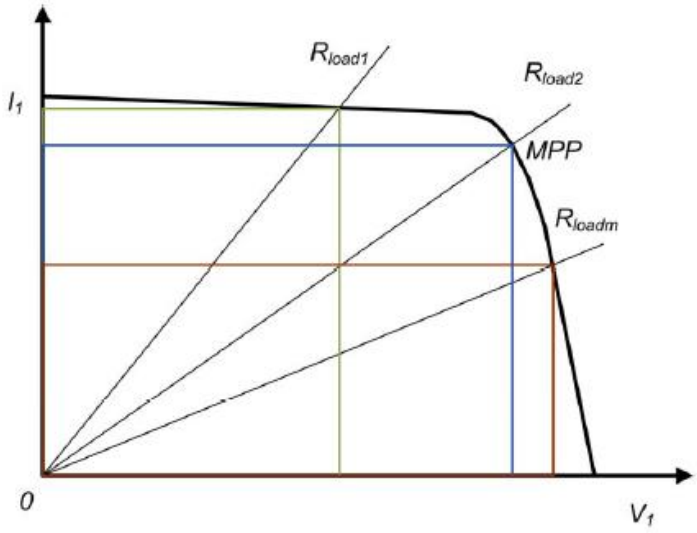

Figure 2.2 IV characteristics of PV array showing the point at which MPP occurs [14].

Another control possibility in the PV system is the following case. When the input to the grid due to PV is more than the load demand at a certain point, power is inverted and is injected back to the AC side. The photovoltaic system can be controlled if there is a battery connected to it to improve the frequency control of the grid system [11].

Figure 2.3 shows actual data of the changes of the PV input along with the changes in load throughout a day [20]. It can be seen that the peak of load demand happens in the solar noon when the PV input is also at its maximum. PV input is minimum after 6pm, then load starts decreasing after a while from that time as well. The part of the day studied in this thesis is in the time when PV is at its maximum.

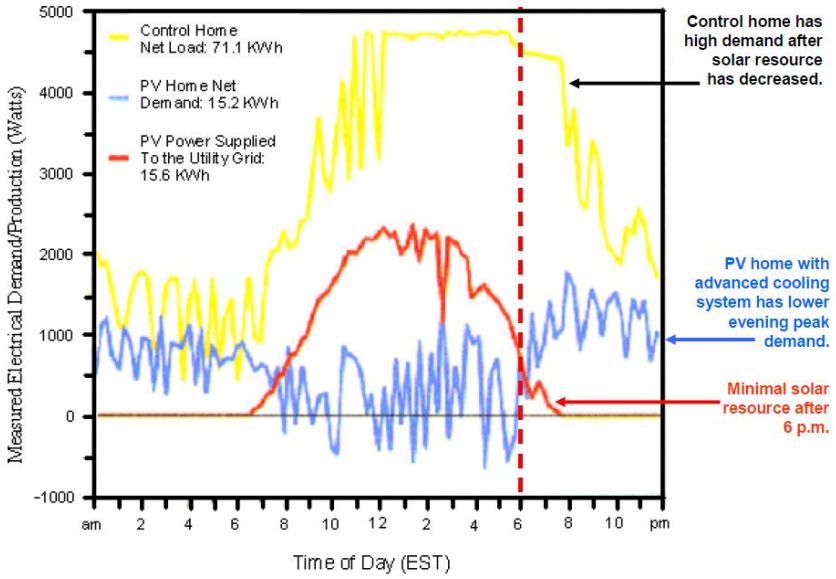

Figure 2.3 Changes of load demand and PV input throughout a day in a residential application.

2.2 Thermal Power System

The general block diagram of a single-area thermal power system is shown in Figure 2.4 in which ΔP represents the speed changer (input to the system), ΔP_{load} represents a disturbance in the form of load power changes, and Δf represents the deviation of the system frequency from the nominal frequency value (50Hz). The first component in this block diagram (the governor) is used to monitor and measure the system speed changes and to control the valve. The turbine is the component that transforms the input energy (in this case coming from the steam) into mechanical energy that could then be an input to the

generator which will transform this mechanical energy into electrical energy. The reheater makes the system more efficient as it reheats the steam to keep the same high temperature of the steam that entered the governor [21]. The generator transforms the mechanical energy into the electrical energy required.

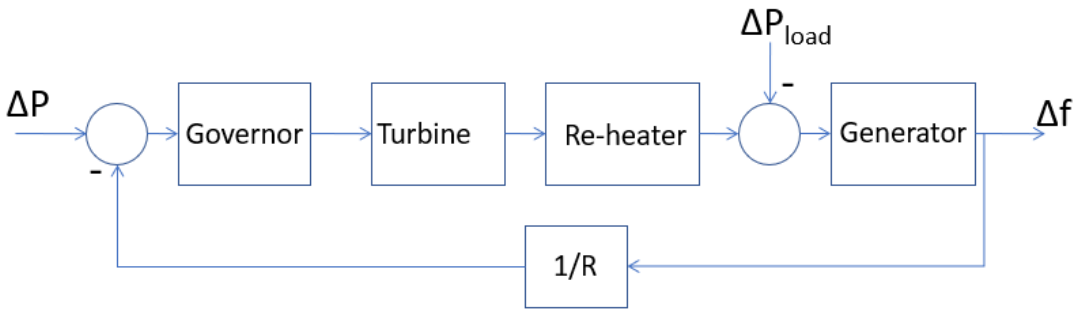

Figure 2.4 General diagram of the main components of a single-area thermal power system.

The control of this thermal power system is conducted through a standard generation called Automatic Generation Control (AGC) consists of two control loops: Automatic Voltage Regulator (AVR) and Load Frequency Control (LFC) [22]. The focus of this thesis is on the LFC to regulate the system frequency due to load demand changes. When the load increases, the generator becomes slower [23]. This is because more power is required to keep up with the same frequency level. Also, the generator in thermal power system cannot go beyond a certain rated speed which limits the standard system frequency to 50Hz. Therefore, when the load increases, the generator speed slows down and the resulting frequency decreases [24]. This drop in frequency is not desired, and an appropriate controller should be used to help the system retrieve its nominal frequency of 50Hz. This matching of the load should be performed as quickly as possible and with minimal undershoot. No matter how much the load changes, the system should maintain a frequency of 50Hz with minimal fluctuations. This is done by manipulating the fuel inlet valve that allows the steam to reach the turbine as shown in Figure 2.5.

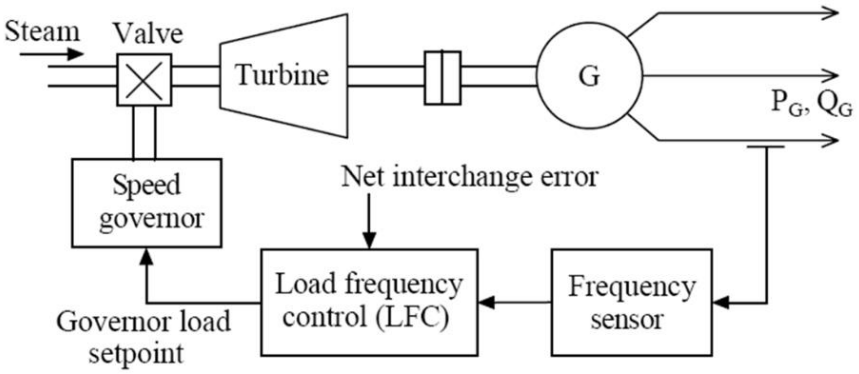

Figure 2.5 Load frequency control mechanism [23].

This valve operation is controlled primarily through Speed Regulation or Droop (R). A droop is defined as the ratio between the changes in the frequency (Δf) and the change in the output power of the generator (ΔP_G) [22]. For instance, a value of 5% for the speed regulation or droop implies that when the frequency deviates by 5%, it will cause a 100% change in the output power of the generator, i.e. a 100% change in the position of the valve. The higher the droop, the better the regulation [23].

This droop is the primary control action for the system [11]. However, the response due to the droop only is not sufficient as will be shown later. More reliable controllers are needed to regulate the system frequency within the required limits of the settling time and the undershoot.

As to the two-area system; where two separate power systems are interconnected, the same concept applies with the addition of having tie-line power exchange (ΔP_{tie}). The tie-line is the transmission line that carries power between the two areas [21]. The excess of power exchange of the tie-line between the two areas should also have a zero steady state error when a load disturbance occurs [23]. When this change in the tie-line power is zero, it implies that there is no excess power interchange between areas than the amount scheduled between the two areas.

The frequency bias (b_i) is also another parameter that is associated with the two-area system rather than single-area. When a disturbance occurs (change in load power), the frequency bias indicates the amount of interaction that will happen between both areas.

Area Control Error (ACE) represents the accumulative error of both the frequency error and the power exchange between both areas, while considering the effect of this frequency bias [17]. The value of ACE should be kept zero or at a value very close to zero all the time [25].

2.3 Linear Quadratic Regulators

The Linear Quadratic Regulator (LQR) is a standard optimal control technique. To design an optimal controller, a performance measure should be chosen, which is the objective that is required to be minimized or maximized by the optimal controller [26].

A certain state trajectory is defined after applying the controller signal obtained from the optimal controller over a certain period of time along with an initial state for the system at t_0. The optimal control problem is defined as finding an optimal control u^* for the system in (2.3).

$$\dot{x}(t) = f(x(t), u(t), t) \tag{2.3}$$

which makes it follow an optimal trajectory x^* that minimizes or maximizes the targeted performance measure J given in Equation 2.4 where h and g are scalar functions.

$$\begin{aligned} J &= h(x_{tf}, t_f) + \int_{t_0}^{t_f} g(x(t), u(t), t) \\ &= \frac{1}{2}[z(t_f) - y(t_f)]' F(t_f)[z(t_f) - y(t_f)] \\ &+ \frac{1}{2}\int_{t_o}^{t_f} \{[z(t) - y(t)]' Q(t)[z(t) - y(t)] + u'(t)R(t)u(t)\}dt \end{aligned} \tag{2.4}$$

z(t) represents the desired output vector and y(t) represents the output vector. Q and R are the matrices that should be chosen in order to give the minimum value of the performance index (J). Q is the error weighted matrix, and it should be positive semidefinite. The more focus is required on minimizing a certain parameter, the larger the weight that should be attributed to its corresponding state variable in the Q matrix. R is the control weighted matrix and it should be positive definite [26]. At the final time (t_f), the terminal cost term ($F(t_f)$) should be 0, therefore, the first term of Equation 2.4 is cancelled.

When the optimal values of Q and R matrices are substituted in the Riccati equation (Equation 2.5), it provides the optimal costate matrix (P) [27].

$$\dot{P(t)} + P(t)A(t) + A'(t)P(t) + Q(t) - P(t)B(t)R^{-1}(t)B'(t)P(t) = 0 \quad (2.5)$$

This costate matrix (P) is substituted into the optimal controller $u^*(t)$ (Equation 2.6) in the form of state feedback gains (*K*), as follows.

$$u^*(t) = R^{-1}(t)B'(t)P(t)x^*(t) = -K(t)x^*(t) \quad (2.6)$$

The optimal controller is implemented by feeding back these gains to their corresponding state variables to obtain the optimal response of the system.

An optimal controller does not always exist for every system. In order to check if an optimal controller exists for the system under study, the controllability and observability matrices have to be obtained. If both matrices have ranks that are equal to the rank of the system state matrix A from the state space model of the system, then an optimal controller can be designed for this system, and the system is controllable and observable [26]. This is important to ensure that the inputs are accessible, thus, can be controlled, and the outputs are accessible, thus, can be observed and feedback to the system for the controller to operate properly. Thus, for all systems in this thesis, the controllability and observability matrices have been checked.

If the system is controllable and observable, and an optimal controller exists for the system, the main challenge remaining in LQR is a suitable choice of the Q and R matrices that are chosen based on the user experience [27]. An algebraic approach has been proposed to calculate Q and R systematically [28]. The idea behind this approach is to compare between the actual and the desired characteristic equations of the system. The desired characteristic equation can be obtained for second and third order systems easily because it is pre-defined according to the specifications of undershoot and settling time required. Then, the comparison with the actual characteristic equation (in terms of P matrix elements) is possible, and the P matrix would be obtained. This would solve the Riccati equation. Based on that, and with assuming a certain value for the R matrix, the Q matrix can be obtained by calculation rather than assumption.

However, this method has been tried for the systems presented in this thesis but could not yield reasonable results. This is because the method presented in [28] is for second and third order systems. However, the desired characteristic equation for higher order systems has no pre-defined standard formulas related to the specifications (settling time and undershoot). They rather depend on the choice of the desired closed loop poles, which by their turn depend on user experience. Moreover, not all the elements in the P matrix can be obtained by the comparison of both equations leaving behind many variables that need to be tuned based on trial and error for higher order systems, which leads to a very high cost function most of the time. Therefore, the best way to design LQR based controller for a higher order system is by creating an optimization code and tuning the system manually according to optimization results, which has been implemented in this thesis.

2.4 Fuzzy Logic Controllers

Zadeh was the first to introduce the concept of fuzzy logic in 1965, then the controllers based on fuzzy logic were introduced by Mamdani in 1974 [29]. The concept of fuzzy logic is based on a concept similar to that of the binary logic (0,1). However, in the binary logic, any value can either be in a set (therefore, having a value of 1) or not in a set (having a value of 0). Things in the binary logic are either black or white. But in fuzzy logic, each value can be considered as a member of a set by a certain percentage (either a low or a high percentage). Thus, the values in fuzzy logic have partial memberships in the set [30]. For example, if a certain set denotes old people, then it would be difficult to give values of 0 and 1 for people who fit or do not fit strictly in this category. Fuzzy logic gives the flexibility of assigning percentages to how much each person belongs to the category "old"; for example, it could be considered that a person belongs to the set of "old" by 30% if the age is 65 years old in a range of 50-100 years for the membership function of "old".

In order to determine the percentage, the scale should be determined first. This is done by determining the age of the person under study and defining the extreme limits of the age for "youngest = 0 years old" and "oldest = 120 years old" as an example. "Old" and "young" in this case are known as the membership functions (μ). The element x and the associated membership function μ from which we determine how much this element

belongs to the set together are called the fuzzy set [31]. Equation 2.7 shows a general fuzzy set (A) that consists of the membership function μ_A and the element x which belongs to the range of all possible values (X).

$$A = \{(x, \mu_A(x)) | x \epsilon X) \tag{2.7}$$

Several variables can be defined that belong to the same subset (A) or to different subsets (A and B) with different degrees, and the members of these subsets are the values of each variable. The min operator in fuzzy logic rather than binary logic gives the intersection between both fuzzy sets as shown in Figure 2.6 [32]. The degree of overlap between the fuzzy sets depends on the concept being studied in the fuzzy logic example [33].

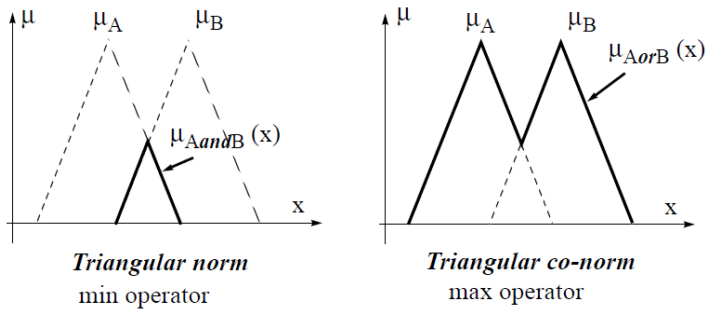

Figure 2.6 Difference between min and max operators for fuzzy inference stage.

As to defining the membership functions, it depends on the choice of the individual and in most cases the shape of these membership functions does not affect the results significantly. Figure 2.7 shows an example of these shapes: triangular.

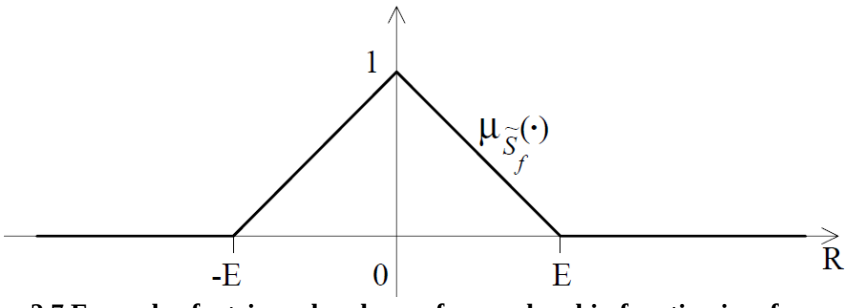

Figure 2.7 Example of a triangular shape of a membership function in a fuzzy set.

A value of 1 corresponding to the variable $x = 0$ means that we are 100% sure that the variable belongs to this membership function. For $x = \frac{E}{2}$ for example, we are 50% certain that this variable belongs to this membership function [34].

The range [-E, E] represent the universe of discourse, i.e. all the possible range of values in this set [29]. If there are several membership functions, this means that there are several subsets. [-E, E] would be the original set from which the smaller subsets and their membership functions are defined. Usually, these values are normalized (between -1 and 1) by mapping [-1, 1] to the original values in the range [-E, E] [29].

Figure 2.8 shows the general steps of designing a fuzzy logic controller (FLC) for a system. After defining the input(s) of the FLC, membership functions and the ranges corresponding to each should be determined through the stage called Fuzzification. The number of these membership functions and what each one represents are determined.

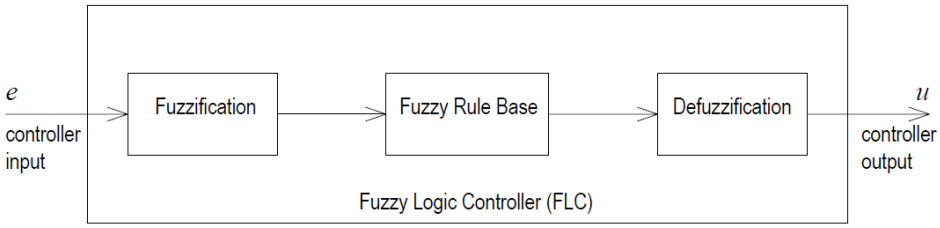

Figure 2.8 General fuzzy logic controller design stages.

Next stage is to design the rule base which consist of the square of the number of membership functions chosen. For example, if 5 membership functions are chosen, this would produce 25 rules that should be designed based on the experience of the engineer. The rules are designed as a rule set and they are the intermediate step that give a value of the output based on the input(s). It creates the required controller actions in fuzzy terms based on the inputs and the required response [30]. The relation between the variables could be “AND” or “OR” or any other logical relationship in the rules depending on the application.

Two or more variables can be related to each other to produce another variable (which is the output of FLC) by rules. These rules are fuzzy rules indicating for example:

If a $\in$ A is true with a truth value (degree of membership) $\mu_A(a)$ and b $\in$ B is true with a truth value $\mu_B(b)$ then

$$\mu_{rule}(\text{a} \Rightarrow \text{b}) = \min\{\mu_A(a), \mu_B(b)\} \quad (2.8)$$

It means that we are certain of the statement (a is A and b is B) by a probability that equals $\mu_{rule}(\text{a} \Rightarrow \text{b}) = \min\{\mu_A(a), \mu_B(b)\}$ [30]. Notice that (a is A and b is B then c is C) is a fuzzy logic rule. Therefore, this value of $\min\{\mu_A(a), \mu_B(b)\}$ implies how much we are certain that this rule is the most suitable rule to be applied by the controller at a certain point of time [34]. If the value of this $\mu_{rule}(\text{a} \Rightarrow \text{b})$ for rule 1 is greater than that of another rule at time t, it means that rule 1 is more relevant to the situation at time t. This fuzzy measure process is called the inference system according to which the control rule that will be used at a certain point in time in the FLC is chosen [34].

Thus, the inference system provides all the rules that are relevant at a certain time t, but it will never give more than 4 relevant rules for one time (if there are 2 inputs to the FLC). The output of the fuzzy logic controller is obtained based on these rule as a fuzzy value, then the last stage (defuzzification) occurs to transform it from a fuzzy value to a numerical value. The most commonly used defuzzification method is the Centre-of-Gravity (Centroid) by weighing all the membership functions for all variables (by weighing the control actions) [30].

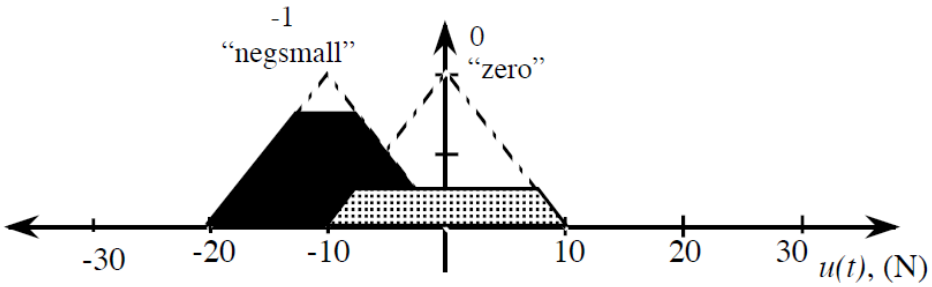

Figure 2.9 Example of two rules obtained from inference mechanism.

For example, consider that the rule determined from inference method is as shown in Figure 2.9 with rule 1 being 25% certain to be "zero" and rule 2 being 75% certain to be "negsmall". The area under the shaded parts of the triangle which represent these

probabilities can be calculated from Equation 2.9 where w is the width and h is the height of the shaded region [34].

$$A = w(h - \frac{h^2}{2}) \tag{2.9}$$

The center of these two triangles are $b_1 = 0$ and $b_2 = -10$ and the width and height for each are $w = 20, h_1 = 0.25, h_2 = 0.75$, thus the areas could be calculated as in Equations 2.10 and 2.11.

$$A_1 = w\left(h_1 - \frac{{h_1}^2}{2}\right) = 20\left(0.25 - \frac{0.25^2}{2}\right) = 4.375 \tag{2.10}$$

$$A_2 = w\left(h_2 - \frac{{h_2}^2}{2}\right) = 20\left(0.75 - \frac{0.75^2}{2}\right) = 9.375 \tag{2.11}$$

Equation 2.12 shows the method of calculating the output of FLC by Centre-of-Gravity (COG) for the previous example [34]. This method of defuzzification has been chosen as it is the most common type used in FLC and as it takes the average of values by weighting the membership functions involved and there are no abrupt changes. The output of the controller (u) is inserted to the system as a negative feedback.

$$u = \frac{\sum b_i \times membership\ value}{\sum membership\ values} = \frac{(0 \times 4.375) + (-10 \times 9.375)}{(4.375 + 9.375)} = -6.81 \tag{2.12}$$

The biggest advantage of using fuzzy logic controllers is that it is not necessary to have knowledge of the mathematical model of the system [22]. As will be demonstrated in this thesis, fuzzy logic becomes very useful when the model of the system becomes mathematically uncertain. Also, it is useful to enhance the system performance more than what PI controllers alone can achieve [29]. Moreover, PI controller alone cannot cope with the nonlinearities and the uncertainties in the system, while FLC deals with this matter efficiently [18].

Chapter 3: Uncontrolled System Modeling

This chapter presents the mathematical models of the photovoltaic system, the single-area power system, the connection between PV and single-area, and the two-area power system connected to PV. The responses of these uncontrolled systems are presented for various changes in system loads. All the system variables responses are obtained without added controllers to the system. The integral controller is the only controller that has been added to some of the system models in this chapter and it will be indicated where it has been included. This is to ensure a zero steady state error as we proceed to the advanced controller designs in the following chapter.

3.1 Model of the Photovoltaic System

The input to the PV system connected to the grid is the output of the PV array which is a DC current as previously explained. The system in this work consists of 150 30kW connected arrays with a constant voltage source of 6 kV at the PV array side [35]. The PV is at a low voltage and low power side, usually in inverter-based PV systems connected to grids, with the power in order of 1kW to a few MW [1]. The maximum power point (MPP) of this connection of solar arrays is at $I_1 = 750A$ which gives an MPP of 4.5MW. This is suitable for the current application because the maximum load of the thermal power system is 10MVA.

As explained earlier, the output of the solar cell is always DC and nonlinear over a long span of time (hours). However, in terms of seconds (which is the period dealt with here for the control parts) it can be considered as a constant DC. Even when a change occurs over a long period of time due to a change of temperature or solar irradiance, it varies from a certain DC value to another DC value (different amplitude but it remains a constant DC).

Moreover, because the PV array acts as a simple PN junction diode and the output is a DC current, the ideal PV array circuit has no order; i.e. does not add state variables to

the system model. That is why the output from that solar array is taken directly into the PV system, as it will not affect the calculations of the overall system state space model.

Before proceeding to the details of each system building block, all the parameters that will be used in the PV systems were summarized in the list of symbols at the beginning of this thesis. Figure 3.1 shows the process of the photovoltaic system designed for the grid in this thesis.

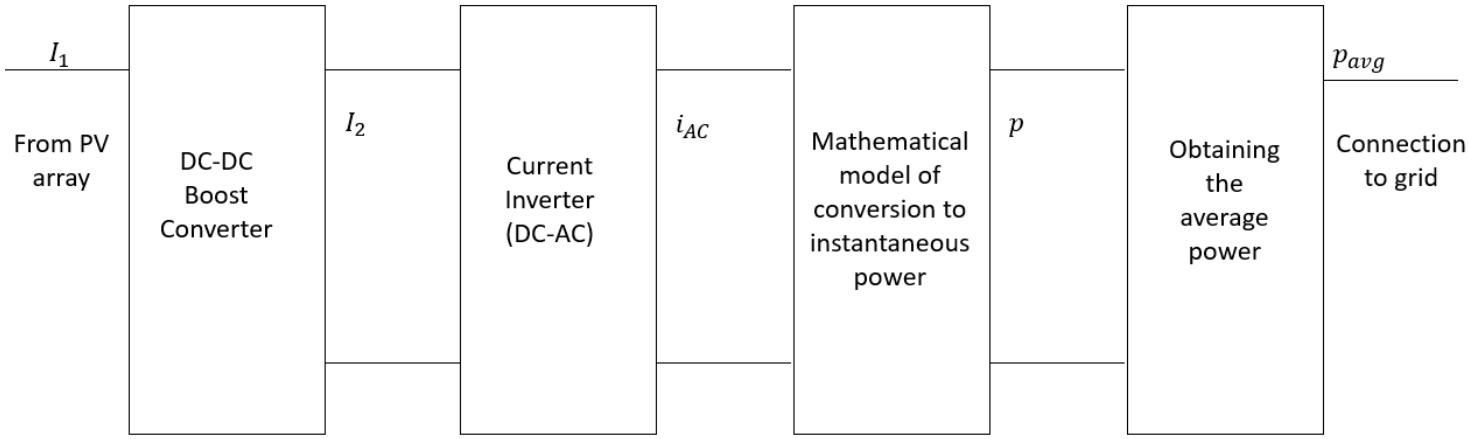

Figure 3.1 General mathematical model of the connection between the PV array and the grid.

The first block in connecting the PV system to the grid after getting the output from the PV array is the DC-DC boost converter. In the ideal case, this converter is just a gain. To obtain this gain, it is important to know the total gain required between the DC voltage and the amplitude of the final AC voltage (m) as shown in Equation 3.1.

$$m = \frac{V_{DC}}{V_{AC}} \tag{3.1}$$

The value of m is ideally less than 0.866, and it has been chosen in this model to be 0.7. The PV system operates at a constant DC voltage $V_{DC} = 6kV$, while the output current and power of the PV arrays change according to the irradiance of the sun and the temperature. Since this DC value is constant, by choosing m for this specific system, the amplitude of the AC voltage will also remain constant, leaving the AC current and power to vary along with the changes.

This m can now be used in the calculations to find the value of the voltage required after the boost converter (V_2) as shown in Equation 3.2. The PV system is applied at the low voltage side of the grid and the RMS value of the grid line voltage of the conventional system that is considered here is 11kV. This means that the grid phase voltage is $V_m = V_{AC,rms=}11/\sqrt{3}$kV. This is the value that will be used since in this photovoltaic system only a single phase is considered.

$$V_2 = \frac{V_m}{m} = \frac{11/\sqrt{3}}{0.7} = 9.07kV \tag{3.2}$$

Accordingly, the boost converter gain can be calculated as

$$M_1 = \frac{V_2}{V_1} = \frac{9.07kV}{6kV} = 1.51167 \tag{3.3}$$

Since $M_1 = \frac{V_2}{V_1} = \frac{I_1}{I_2}$ [14], therefore, assuming an ideal DC-DC boost converter (with the switching frequency much higher than the system dynamics), the gain for the boost converter is $\frac{1}{M_1} = \frac{1}{1.5}$ representing the first transfer gain as follows:

$$G_1 = \frac{1}{1.5} \tag{3.4}$$

The next stage is the DC-AC inverter which converts this DC current to an AC current that will be suitable for the connection with the conventional AC based power system. The transfer function can be obtained by dividing the Laplace transform of each term.

The AC current (i_{AC}) is simply given by the form $I_m\cos(wt)$, and this has a Laplace transform of $\frac{s}{s^2+w^2}$, where $w = 2\pi f = 2\pi(50) = 314.159\, rad/s$. Similarly, I_2 (the current after the boost converter) is a DC value so it has the Laplace transform of $\frac{1}{s}$. Therefore, the transfer function of the second block (current inverter) is given as follows:

$$G_2(s) = \frac{i_{AC}(s)}{I_2(s)} = \frac{s}{s^2 + w^2} \div \frac{1}{s} = \frac{s^2}{s^2 + w^2} = \frac{s^2}{s^2 + 98700} \tag{3.5}$$

Figure 3.2 shows the current that is inverted to AC through the DC-AC inversion block in this model. Two periods in the graph are between 45ms and 5ms which is 40ms, therefore, the frequency of the current is 2/40ms=50Hz, which is the system's frequency as expected.

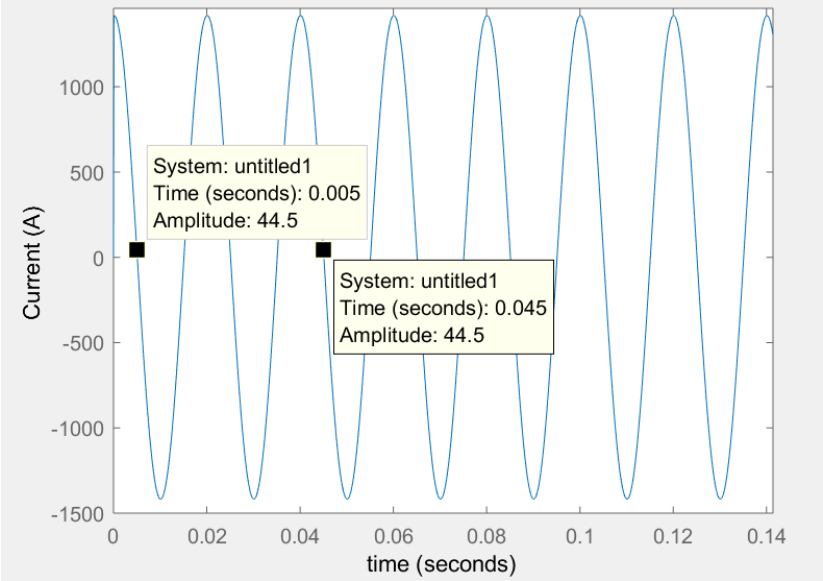

Figure 3.2 Current Inversion from DC (after boost converter) to AC with 50Hz (system frequency).

The third stage is to convert this current to instantaneous power because the output of the conventional power system is power, thus, the input from the PV system to the grid should also be in terms of power. The transfer function of this block can be obtained similar to the method of obtaining G_2. First, the instantaneous power *p(t)* is given by

$$p(t) = \frac{V_m}{I_m} {i_{AC}}^2 = \frac{V_m}{I_m}(I_m \cos(wt))^2 = \frac{V_m I_m}{2} + \frac{V_m I_m\,(\cos(2wt))}{2} \tag{3.6}$$

The gain $\frac{V_m}{I_m}$ is an impedance which is real without an imaginary part because the load is purely resistive. Taking the Laplace transform of (3.6) gives,

$$P(s) = \frac{V_m I_m}{2s} + \frac{V_m I_m}{2}\frac{s}{s^2 + (2w)^2} \tag{3.7}$$

where i_{AC} is the same expression obtained previously. Therefore, the transfer function for the conversion from AC current to instantaneous power is:

$$G_3(s) = \frac{P(s)}{i_{AC}(s)} = \left(\frac{V_m I_m}{2s} + \frac{V_m I_m}{2}\frac{s}{s^2 + (2w)^2}\right) \div (I_m \cos(wt)) \qquad (3.8)$$

$$= V_m\left(\frac{(s^2 + w^2)(s^2 + (2w)^2)}{s^2(s^2 + (4w)^2)}\right)$$

$$= \frac{6351s^4 + (1.88 \times 10^9)s^2 + (1.237 \times 10^{14})}{s^4 + (3.948 \times 10^5)s^2}$$

It is noticed that the instantaneous power has double the frequency of the inverted current because the equation of instantaneous power is given by the multiplication of two cosine waves (the current and the voltage) each of which has a frequency of 50Hz, and by the trigonometric identities which produces a cosine wave of double the frequency. Thus, a frequency of 100Hz can be observed from Figure 3.3 for the instantaneous power. One period occurs between 2.6ms and 12.6ms, i.e. 10ms giving a frequency of 1/10ms=100Hz. The voltage and the current are in phase, therefore there is no reactive power going from the PV array to the grid [14].

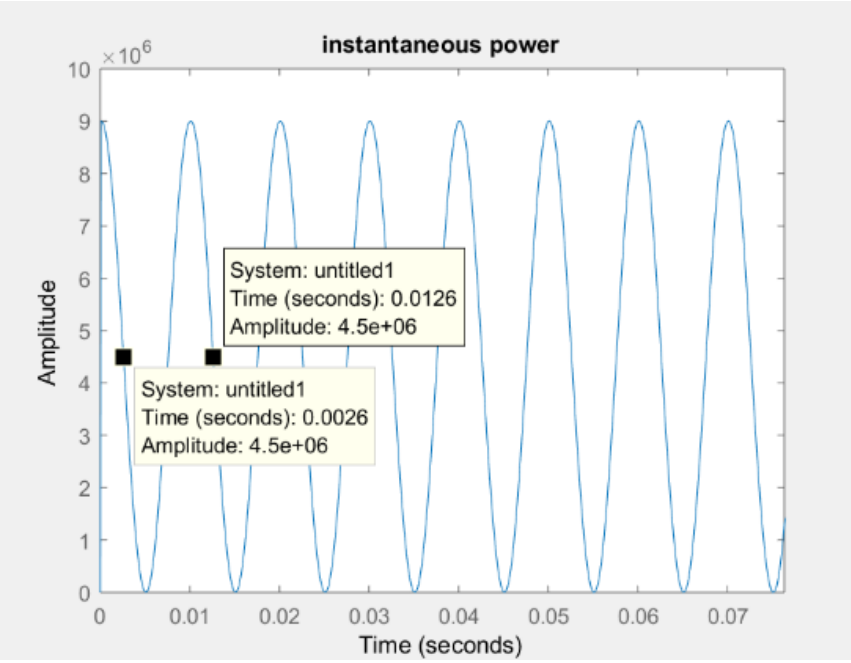

Figure 3.3 Instantaneous power from the photovoltaic system (100 Hz).

Since the load in the photovoltaic systems is purely resistive, the instantaneous power graph is expected to be completely offset in the positive y-axis (above the x-axis)

which is the case in Figure 3.3. This explains why the instantaneous power has double the amplitude (9MW instead of 4.5MW), because the real negative peak of the original sine wave is at -4.5MW, but with the offset that occurred, the negative amplitude shifted to the positive side making the -4.5 start from 0 and the 4.5 peak to shift to 9MW.

However, the required output power of the PV system that will be an input to the conventional power system is the average power not the instantaneous in order to make them compatible with each other [14]. Thus, the last stage here is to convert the instantaneous power to average power. The equation for the average power in the time domain is given by

$$P_{avg} = \frac{1}{T}\int_0^T v_{AC} \times i_{AC}\, dt = \frac{1}{T}\int_0^T V_m \cos(wt)\,.\, I_m \cos(wt)\; dt \qquad (3.9)$$
$$= \frac{1}{T}\int_0^T \frac{V_m I_m}{2} + \frac{V_m I_m\,(\cos(2wt))}{2}\; dt = \frac{V_m I_m}{2}$$

This is expected since the load is purely resistive, and the average power would be a constant. The Laplace transform of the average power (P_{avg}) is given by

$$\frac{V_m I_m}{2s} \qquad (3.10)$$

To obtain the transfer function of the conversion from instantaneous power to average power after simplification is given next as,

$$G_4(s) = \frac{P_{avg}(s)}{p(s)} = \frac{V_m I_m}{2s} \div \left(\frac{V_m I_m}{2s} + \frac{V_m I_m}{2}\frac{s}{s^2 + (2w)^2}\right) = \frac{s^2 + (4w)^2}{2(s^2 + (2w)^2)} \qquad (3.11)$$
$$= \frac{s^2 + (3.948 \times 10^5)}{2s^2 + (3.948 \times 10^5)}$$

Figure 3.4 shows the final output of the PV system which is the MPP average power (4.5 MW) as expected because this is half of the amplitude of the offset instantaneous power graph. If the power was not purely resistive, then the real power will be less than

4.5MW because part of the graph of the instantaneous power will be below the x axis depicting reactive power.

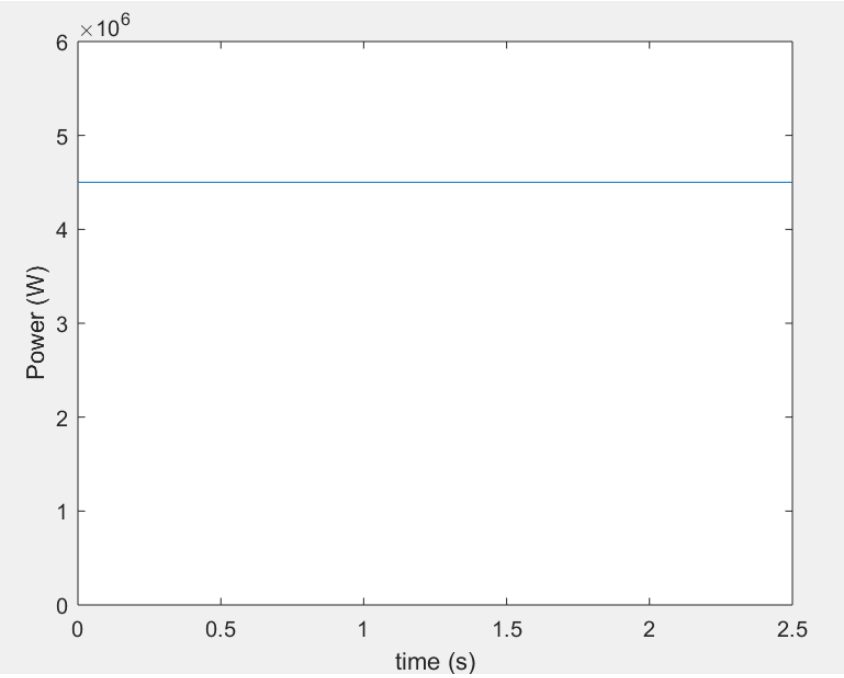

Figure 3.4 Average power output of the PV (second input to conventional power system).

Putting all the above blocks together leads to the full PV system which is shown in Figure 3.5.

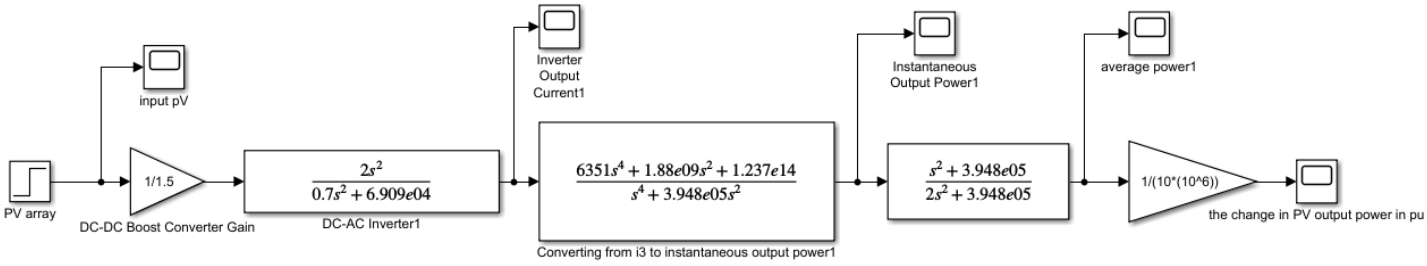

Figure 3.5 PV system designed model.

To get the state space model of this PV system, the form chosen here is the controllable canonical one. This would lead to the state space model of the system in the standard form of

$$\dot{x}(t) = Ax(t) + Bu(t) \tag{3.12}$$

$$y(t) = Cx(t) + Du(t)$$

Starting with the DC-AC inverter block:

$$G_2(s) = \frac{i_{AC}(s)}{I_2(s)} = \frac{s^2}{s^2 + 98700} \tag{3.13}$$

The controllable canonical form is obtained from the following state equations,

$$\dot{x_7} = x_8 \tag{3.14}$$

$$\dot{x_8} = -98700x_7 + \Delta P_i \tag{3.15}$$

$$y = -98700x_7 + \Delta P_i \tag{3.16}$$

ΔP_i in the following equations represent the input to each sub-system, giving the following state space model,

$$\begin{bmatrix} \dot{x_7} \\ \dot{x_8} \end{bmatrix} = \begin{bmatrix} 0 & 1 \\ -98700 & 0 \end{bmatrix} \begin{bmatrix} x_7 \\ x_8 \end{bmatrix} + \begin{bmatrix} 0 \\ 1 \end{bmatrix} \Delta P_i \tag{3.17}$$

$$y = \begin{bmatrix} -98700 & 0 \end{bmatrix} \begin{bmatrix} x_7 \\ x_8 \end{bmatrix} + [1]\Delta P_i \tag{3.18}$$

Realizing this state space model as a block diagram is shown in Figure 3.6 below.

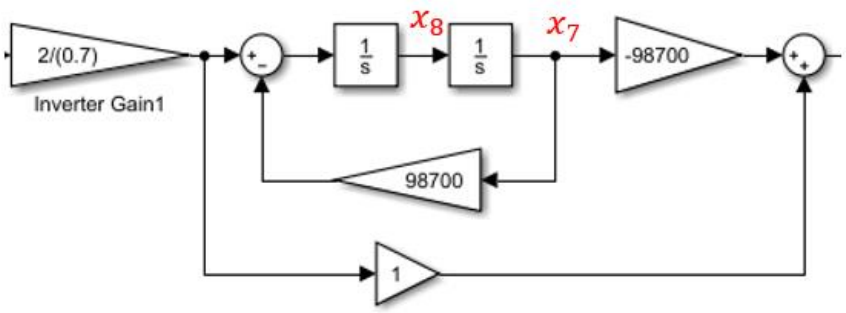

Figure 3.6 DC-AC inverter block to obtain controllable canonical form.

As to $G_3(s)$, the same steps are applied to obtain the state space equations as follows:

$$\dot{x_3} = x_4 \tag{3.19}$$

$$\dot{x_4} = x_5 \tag{3.20}$$

$$\dot{x_5} = x_6 \tag{3.21}$$

$$\dot{x_6} = -3.948 \times 10^5 x_5 + \Delta P_i \tag{3.22}$$

$$y = 1.237 \times 10^{14} x_3 - 6.27375 \times 10^8 x_5 + 6351 \Delta P_i \tag{3.23}$$

This leads to the state space model

$$\begin{bmatrix} \dot{x_3} \\ \dot{x_4} \\ \dot{x_5} \\ \dot{x_6} \end{bmatrix} = \begin{bmatrix} 0 & 1 & 0 & 0 \\ 0 & 0 & 1 & 0 \\ 0 & 0 & 0 & 1 \\ 0 & 0 & -3.948 \times 10^5 & 0 \end{bmatrix} \begin{bmatrix} x_3 \\ x_4 \\ x_5 \\ x_6 \end{bmatrix} + \begin{bmatrix} 0 \\ 0 \\ 0 \\ 1 \end{bmatrix} \Delta P_i \tag{3.24}$$

$$y = \begin{bmatrix} 1.237 \times 10^{14} & 0 & -6.27375 \times 10^8 & 0 \end{bmatrix} \begin{bmatrix} x_3 \\ x_4 \\ x_5 \\ x_6 \end{bmatrix} + [6351] \Delta P_i \tag{3.25}$$

Figure 3.7 shows the detailed block diagram in canonical form for $\boldsymbol{G_3}$.

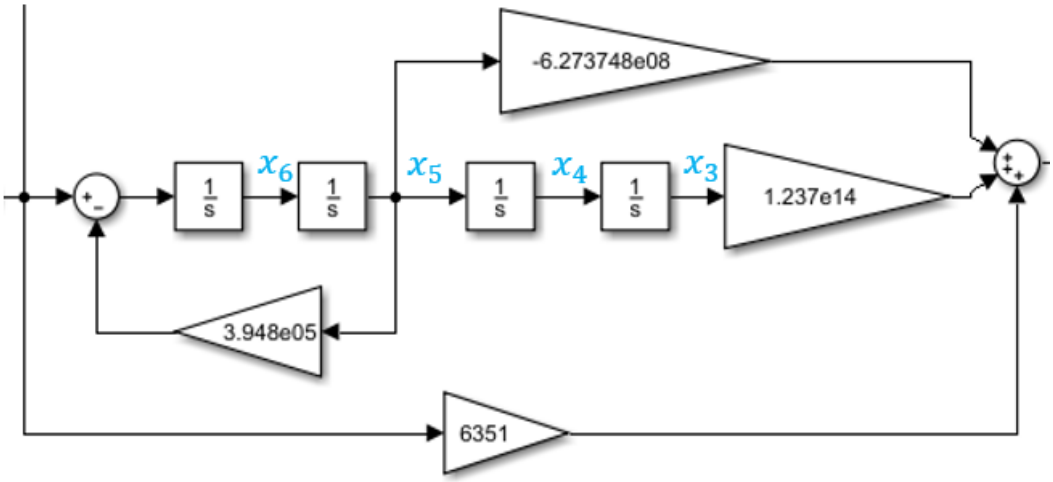

Figure 3.7 Instantaneous power blocks to obtain controllable canonical form.

Similarly, $G_4(s)$ state space model is given as follows:

$$\dot{x_1} = x_2 \tag{3.26}$$

$$\dot{x_2} = -197400 x_1 + \Delta P_i \tag{3.27}$$

$$y = 197400x_1 + \frac{1}{2}\Delta P_i \tag{3.28}$$

In matrix form, we have

$$\begin{bmatrix} \dot{x}_1 \\ \dot{x}_2 \end{bmatrix} = \begin{bmatrix} 0 & 1 \\ -197400 & 0 \end{bmatrix} \begin{bmatrix} x_1 \\ x_2 \end{bmatrix} + \begin{bmatrix} 0 \\ 1 \end{bmatrix} \Delta P_i \tag{3.29}$$

$$y = [197400 \quad 0] \begin{bmatrix} x_1 \\ x_2 \end{bmatrix} + [1/2]\Delta P_i \tag{3.30}$$

Figure 3.8 shows the corresponding block diagram in canonical form.

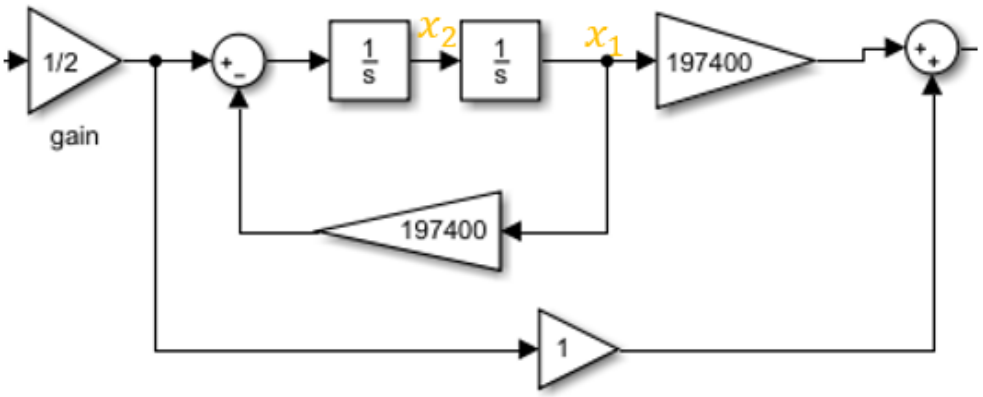

Figure 3.8 Average power block to obtain controllable canonical form.

Combining all these state space models for the sub-blocks into one state space model gives the overall state space matrix (3.31). G_2 is circled in red, G_3 is circled in blue, and G_4 is circled in yellow.

$$A = \begin{bmatrix} 0 & 1 & 0 & 0 & 0 & 0 & 0 & 0 \\ -197400 & 0 & 6.185 \times 10^{13} & 0 & 3.1368 \times 10^{8} & 0 & 3.13422 \times 10^{8} & 0 \\ 0 & 0 & 0 & 1 & 0 & 0 & 0 & 0 \\ 0 & 0 & 0 & 0 & 1 & 0 & 0 & 0 \\ 0 & 0 & 0 & 0 & 0 & 1 & 0 & 0 \\ 0 & 0 & 0 & 0 & -3.948 \times 10^{5} & 0 & -98700 & 0 \\ 0 & 0 & 0 & 0 & 0 & 0 & 0 & 1 \\ 0 & 0 & 0 & 0 & 0 & 0 & -98700 & 0 \end{bmatrix} \tag{3.31}$$

$$B=\begin{bmatrix} 0 \\ 6048 \\ 0 \\ 0 \\ 0 \\ \frac{1}{1.5}\times\frac{2}{0.7} \\ 0 \\ \frac{1}{1.5}\times\frac{2}{0.7} \end{bmatrix} \quad (3.32)$$

$$C=[0 \quad 1 \quad 0 \quad 0 \quad 0 \quad 0 \quad 0 \quad 0] \quad (3.33)$$

$$D=[6048.57] \quad (3.34)$$

Notice that these sub-blocks are interconnected, therefore, these extra connections need to be accounted for. The values written in green in the state matrix show the values that accounted for the connection between the blocks.

To get these values of the interconnection, some state equations needed to be modified. The modified state Equations 3.36 and 3.37 demonstrate how these values were obtained. The term ΔP_i here in the full state matrix represents the input of the photovoltaic system rather than the input of each sub-block separately.

$$\dot{x_2} = -197400x_1 + \frac{1}{2}\left[6351\left(-98700x_7 + \left(\frac{1}{1.5}\times\frac{2}{0.7}\right)\Delta P_i\right] - \left(\frac{1}{2}\times 6.2737\times 10^8 x_5\right) + \left(\frac{1}{2}\times 1.237\times 10^{14}x_3\right) \quad (3.35)$$

Simplifying Equation 3.35 gives:

$$\dot{x_2} = -197400x_1 + 6.185\times 10^{13}x_3 - 3.1368\times 10^8 x_5 + 3.13422\times 10^8 x_7 + 6048.57\Delta P_i \quad (3.36)$$

$$\dot{x_6} = -3.948\times 10^5 x_5 - 98700x_7 + \left(\frac{1}{1.5}\times\frac{2}{0.7}\right)\Delta P_i \quad (3.37)$$

In addition, to get the D matrix, the following calculation has been done by tracking how the output is directly related to the input. Or, it can also be obtained directly from the final $\dot{x_2}$ equation.

$$\frac{1}{2} \times 6351 \times \frac{2}{0.7} \times \frac{1}{1.5} = 6048.57 \tag{3.38}$$

The full system in the form that allows us to deduce the state space matrix and cast it in the controllable canonical form is given in Figure 3.9. An additional model that was also useful in some calculations is the full transfer function of the PV system shown in Equation 3.39, where $\Delta P_i = PV_{array}$; or the output of the PV array which is the input to the PV system.

$$\frac{P_{avg}}{PV_{array}} = \frac{8402\ s^8 + (5.805e09)\ s^6 + (1.146e15)\ s^4 + (6.462e19)\ s^2}{1.4\ s^8 + \ (9.672e05)\ s^6 + (1.909e11)\ s^4 + (1.077e16)\ s^2} \tag{3.39}$$

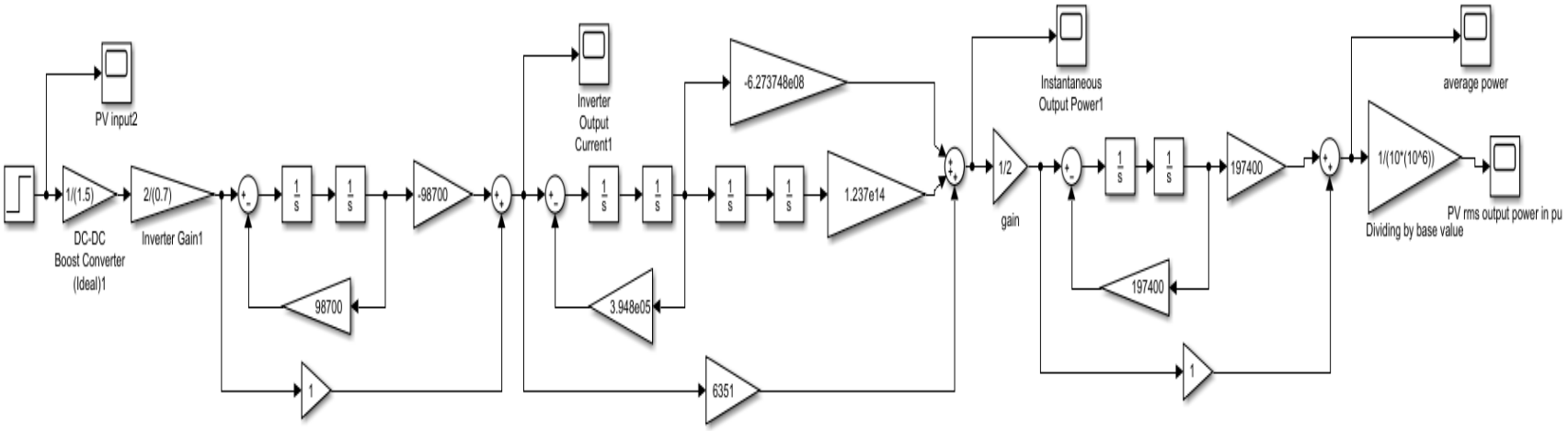

Figure 3.9 The full PV system model from which the controllable canonical form was obtained.

3.2 Thermal Power System – Single Area

The state space model of the single-area power system (thermal) with only the integral controller is presented in this section. Table 3.1 shows the parameters that were used in the modeling of the thermal power system under study and their definition.

Table 3.1 Parameters of the thermal power system.

Parameter	Definition	Value
T_g	Governor time constant	0.08
R	Droop	2.4
T_t	Turbine time constant	0.3
T_r	Reheater time constant	10
K_r	Reheater gain	0.5
T_p	Generator time constant	20
K_p	Gain constant	120

Figure 3.10 shows this part of the system without any controller. The first input to this system is the speed changer ΔP that determines the amount of fuel coming in to the system by operating the valve. The state space model (in Equations 3.40 and 3.41) with ΔP_{load} being the second input which represents the changes in the power system load (disturbance).

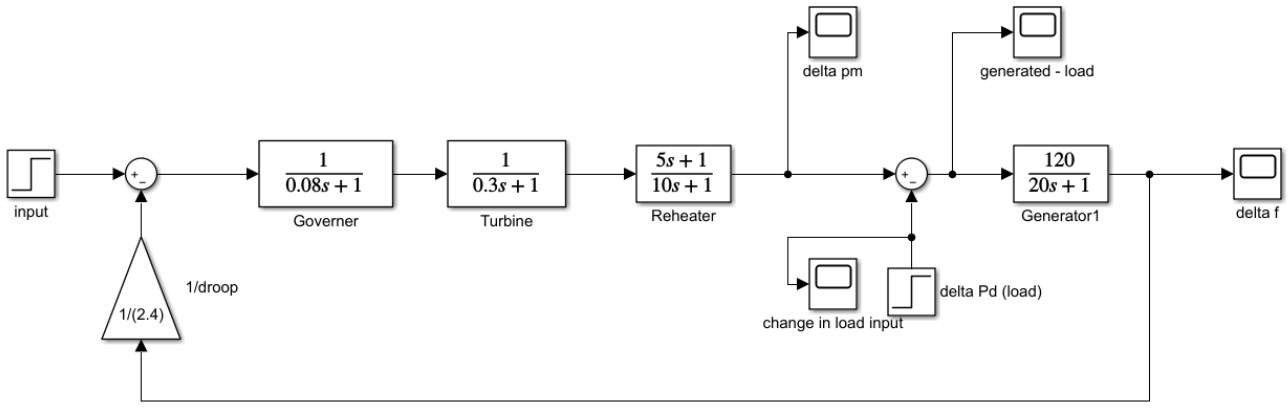

Figure 3.10 Block diagram of the single-area thermal power system without any controller.

$$\begin{bmatrix} \dot{x_1} \\ \dot{x_2} \\ \dot{x_3} \\ \dot{x_4} \end{bmatrix} = \begin{bmatrix} \frac{-1}{20} & 6 & 0 & 0 \\ 0 & -0.1 & -1.566 & \frac{5}{3} \\ 0 & 0 & \frac{-1}{0.3} & \frac{-1}{0.3} \\ -5.21 & 0 & 0 & -12.5 \end{bmatrix} \begin{bmatrix} x_1 \\ x_2 \\ x_3 \\ x_4 \end{bmatrix} + \begin{bmatrix} -6 \\ 0 \\ 0 \\ 0 \end{bmatrix} \Delta P_{load} \quad (3.40)$$

$$y = [1 \quad 0 \quad 0 \quad 0] \begin{bmatrix} x_1 \\ x_2 \\ x_3 \\ x_4 \end{bmatrix} \quad (3.41)$$

The frequency error response of this system due to a sudden 50% increase in the load is given in Figure 3.11 with the corresponding response specifications in Table 3.2. SSE represents the steady state error.

Table 3.2 Response summary due to a 50% increase in load.

Settling Time (s)	18.2
Undershoot (Hz)	-2.33299
SSE (Hz)	-1.175

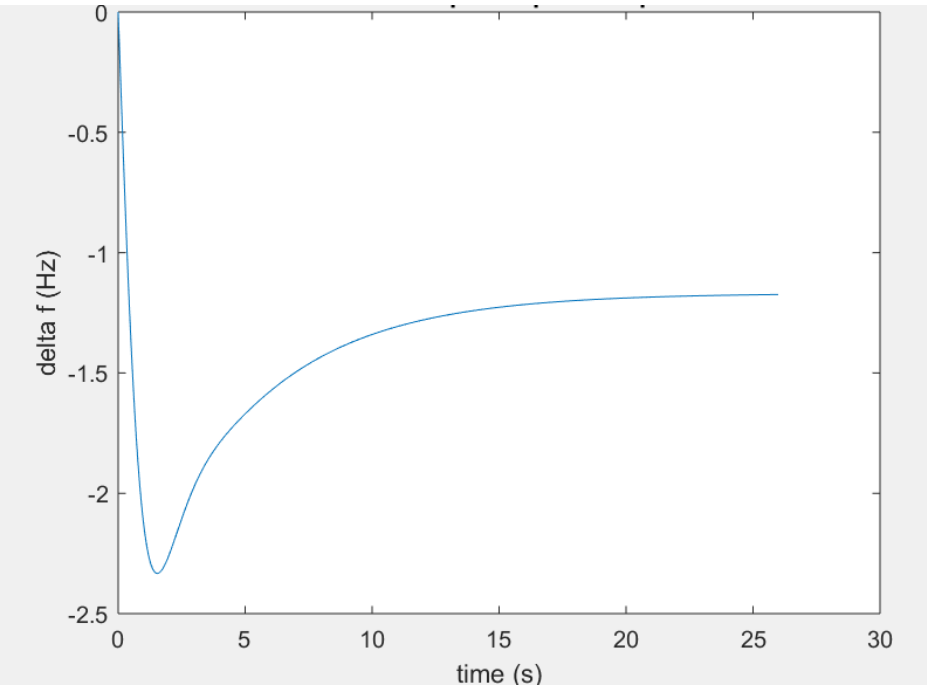

Figure 3.11 Response of the single-area thermal power system due to a 50% increase in load without any controller.

Since one of the main criteria to be met in the system is a zero steady state frequency error, the addition of an integral controller is needed for this purpose. In this section, the integral controller is integrated in the state space model since it will introduce an additional state variable in the original state space model. Thus, to apply the other controllers later, it is important to work with this updated state space model so that the final steady state error criteria is ensured to be met. Therefore, from this point onwards in this work, the model will always have an integral controller integrated. This way SSE will always be 0, and only the settling time and undershoot are to be considered. Adding an integral controller to the system increases the number of state variables by 1, thus, the system now has a total of 5 state variables. Figure 3.12 shows the thermal power system with the integral controller.

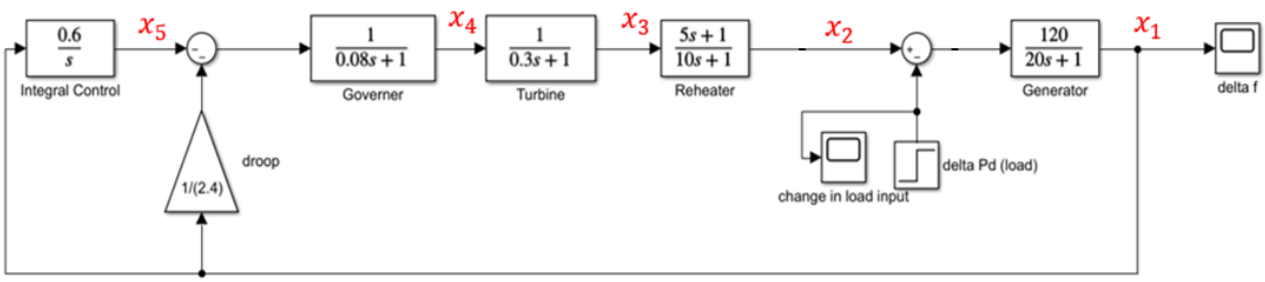

Figure 3.12 Block diagram of the single-area thermal power system with integral controller only.

After adding the integral controller and tuning its gain value to the one that produced the best response ($k_i = 0.6$), the new state equations become,

$$\dot{x_1} = \frac{1}{20}x_1 + 6x_2 - 6\Delta P_{load} \tag{3.42}$$

$$\dot{x_3} = \frac{1}{0.3}x_3 - \frac{1}{0.3}x_4 \tag{3.42}$$

Substituting this expression of $\dot{x_3}$ into the equation of $\dot{x_2}$ gives

$$\dot{x_2} = -0.1x_2 - 1.566x_3 + \frac{5}{3}x_4 \tag{3.43}$$

The remaining two state equations to complete the 5 are:

$$\dot{x_4} = -\frac{1}{2.4 \times 0.08} x_1 - \frac{1}{0.08} x_4 - \frac{1}{0.08} x_5 \tag{3.44}$$

$$\dot{x_5} = k_i \times x_1 \tag{3.45}$$

Accordingly, the state space model of the thermal power system with an integral controller is given in (3.46) and (3.47). The first input to the thermal power system is replaced by the effect of adding the integral controller, thus, only ΔP_{load} remains as the input here.

$$\begin{bmatrix} \dot{x_1} \\ \dot{x_2} \\ \dot{x_3} \\ \dot{x_4} \\ \dot{x_5} \end{bmatrix} = \begin{bmatrix} \frac{-1}{20} & 6 & 0 & 0 & 0 \\ 0 & -0.1 & -1.566 & \frac{5}{3} & 0 \\ 0 & 0 & \frac{-1}{0.3} & \frac{1}{0.3} & 0 \\ -5.21 & 0 & 0 & -12.5 & -12.5 \\ k_i & 0 & 0 & 0 & 0 \end{bmatrix} \begin{bmatrix} x_1 \\ x_2 \\ x_3 \\ x_4 \\ x_5 \end{bmatrix} + \begin{bmatrix} -6 \\ 0 \\ 0 \\ 0 \\ 0 \end{bmatrix} \Delta P_{load} \tag{3.46}$$

$$y = \begin{bmatrix} 1 & 0 & 0 & 0 & 0 \end{bmatrix} \begin{bmatrix} x_1 \\ x_2 \\ x_3 \\ x_4 \\ x_5 \end{bmatrix} \tag{3.47}$$

Figure 3.13 shows the frequency error response of this updated state space model. Table 3.3 summarizes the key response specification values from the response.

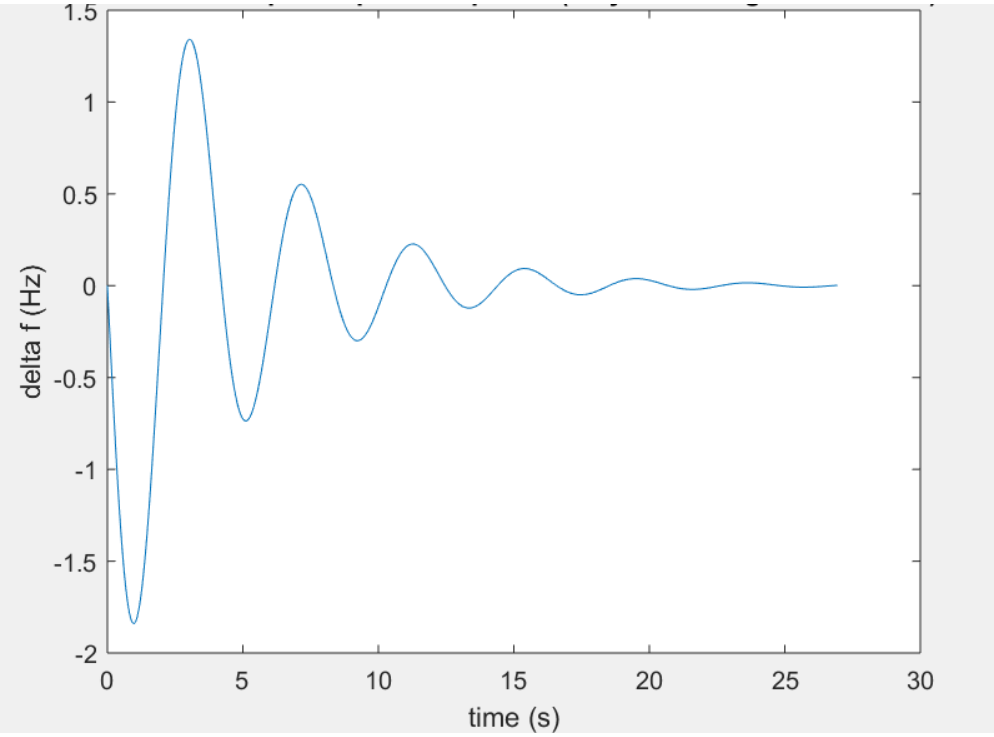

Figure 3.13 Single-area thermal power system frequency error response to a 50% increase in load (with integral controller only).

Table 3.3 Response summary of the single-area thermal power system for a 50% increase in load.

Settling Time (s)	19.716575
Undershoot (Hz)	-1.8399269
SSE (Hz)	0

The controllability and observability of the system are checked to ensure that the system can be controlled. Both the controllability matrix and observability matrix have a rank of 5 which is equal to the number of state variables. Therefore, the system is controllable and observable, and controllers can be designed and applied to the system.

In addition, to check the stability of the open loop system, the eigenvalues were verified, and they are: -12.875, -2.475, -0.1995, -0.2168 + 1.525i and -0.2168 -1.525i indicating that the system is stable.

In the state space model, x_1 represents the output (the change of frequency obtained from the generator) and x_2 represents ΔP_m which is the output after the turbine and reheater

(the power generated mechanically to match the load). Since the photovoltaic system has not been connected yet, the thermal power system has to provide the system with all what the load demand requires. Therefore, in Figure 3.14 ΔP_m settles at a value of 0.5p.u.MVA, which is equivalent to a 50% increase in load according to the base value of the system, and this is the value of the load power specified in this example.

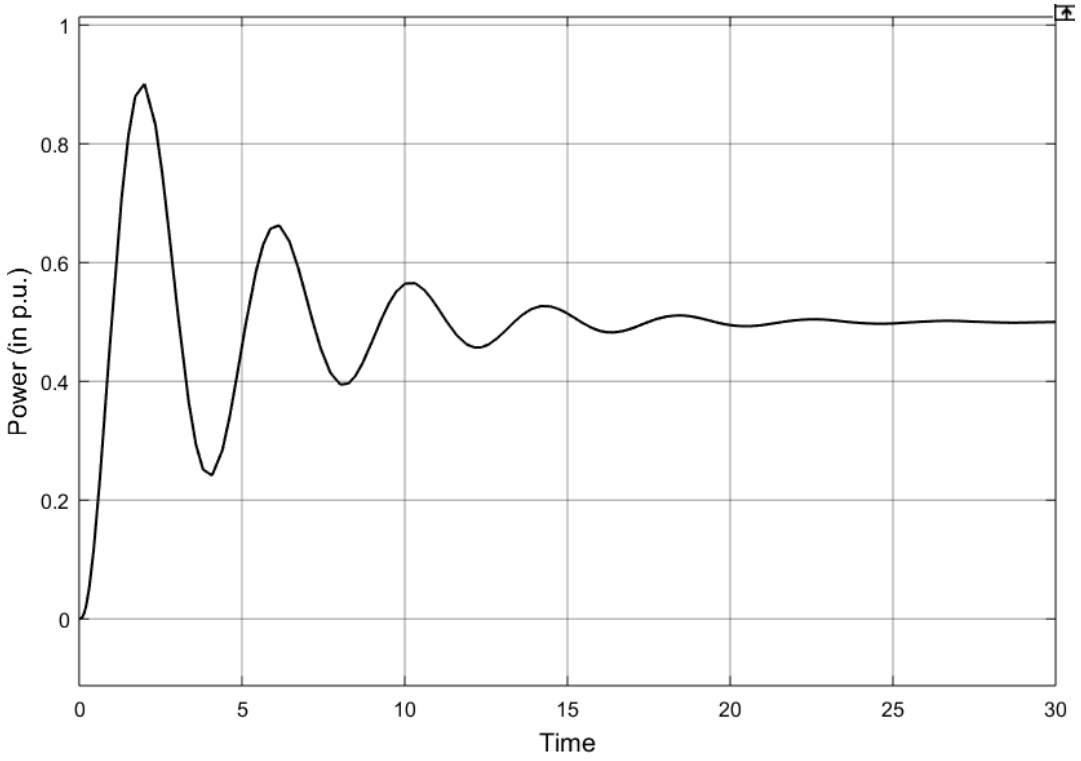

Figure 3.14 Power generated mechanically from the thermal system to match 50% increase of load in the system with integral controller only.

3.3 Model of the PV System Connected to the Single-Area Power Grid

This section presents the connection of both the photovoltaic system and the single-area thermal power system that were previously explained.

First, regarding the units, all the units in the system should be in per unit (p.u.) system, which is why the power in Figure 3.14 for example is given in p.u. MVA. The values in the power system given by the transfer functions automatically gives the p.u. value. Therefore, in order to make the units compatible with each other before connecting both systems, the output power of the photovoltaic system also needs to be converted to per unit. Per unit system is a way of calculation so that all the values obtained from a certain

system can be expressed as a ratio of one common value (which is the base value) [36]. The base value is the reference with which all other values in the system are compared. The base value of this thermal power system is 10MVA which is the rating of the generator [36]. Thus, compared with that scale, a change in load of 1p.u. is equivalent to a change of 10MW and a change of 0.5p.u. is equivalent to a change of 5MW (50% change in load).

The base load of the power system is considered 10MVA in terms of apparent power, however the load is purely resistive as previously explained, which means that all the apparent power is real power, and there is no reactive power. That is why it can be considered that the base value is 10MW. The average output power of the PV system will also be compared to the base value 10MW at all times. For example, an average output power of 4.5MW in the PV system is equivalent to $\frac{4.5MW}{10MW} = 0.45p.u.$ and this is the value at MPP. P_{avg} in the design of the PV system is modified according to this calculation to obtain the final output of the PV system (ΔP_{pv}), which by its turn becomes the second input to the thermal power system, besides the first input which is ΔP_{load}.

Now, the penetration level of PV in the conventional thermal power system also needs to be determined before the connection. PV penetration is defined as the rated PV capacity as a ratio to the total capacity of the grid [35]. The photovoltaic capacity is 4.5MVA=4.5MW (0.45 p.u.) and the total capacity of the system grid is 10MVA (1 p.u.). Therefore, there is a 45% PV penetration level in the system under study.

According to these calculations and the previously explained models of the PV system and single-area thermal power system, Figure 3.15 shows both systems after being connected.

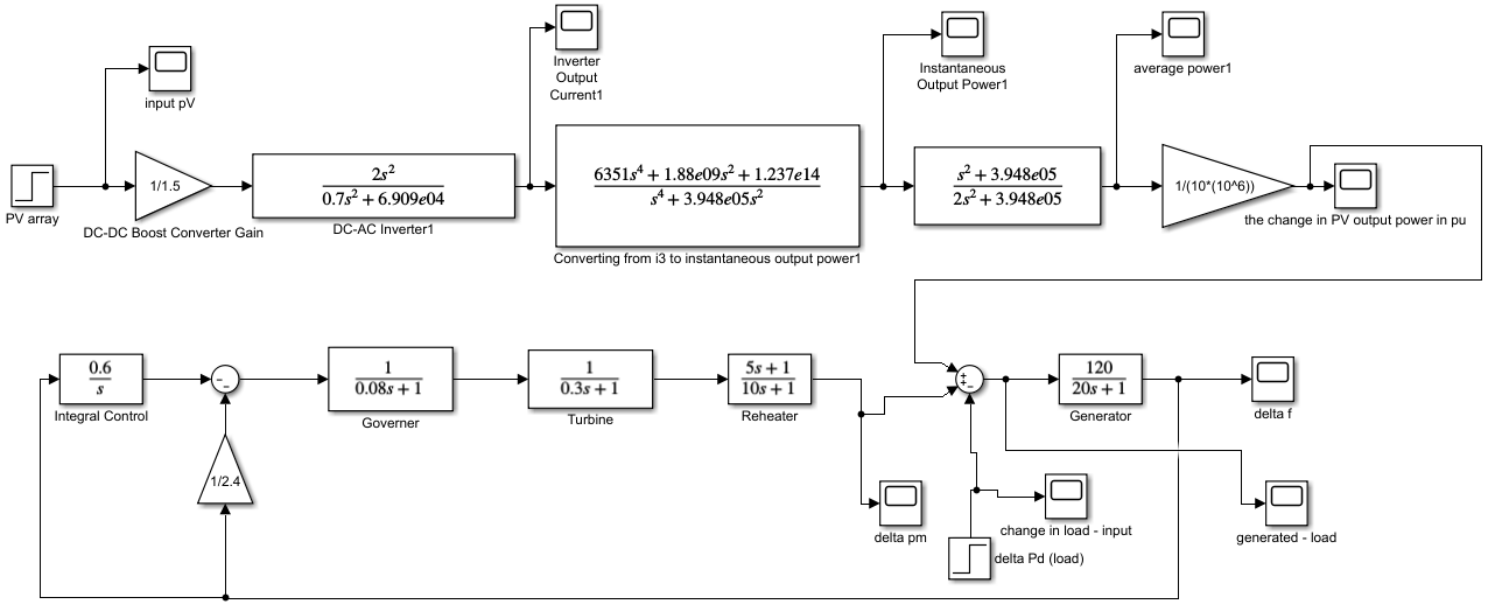

Figure 3.15 The photovoltaic system connected to the grid.

One of the objectives in this thesis is to determine the effect of the connection of a photovoltaic system to a thermal power system on the frequency of the system. This would be helpful in designing a controller that takes this effect into consideration. Figure 3.16 shows the system frequency response of the system before and after connecting it to a PV system with a 100% change in load, Figure 3.17 for 50% change in load and Figure 3.18 for less than 50% load change. Table 3.4 summarizes the responses for the different cases. The steady state error is 0 for all the figures because, as mentioned, the integral controller is part of the model now.

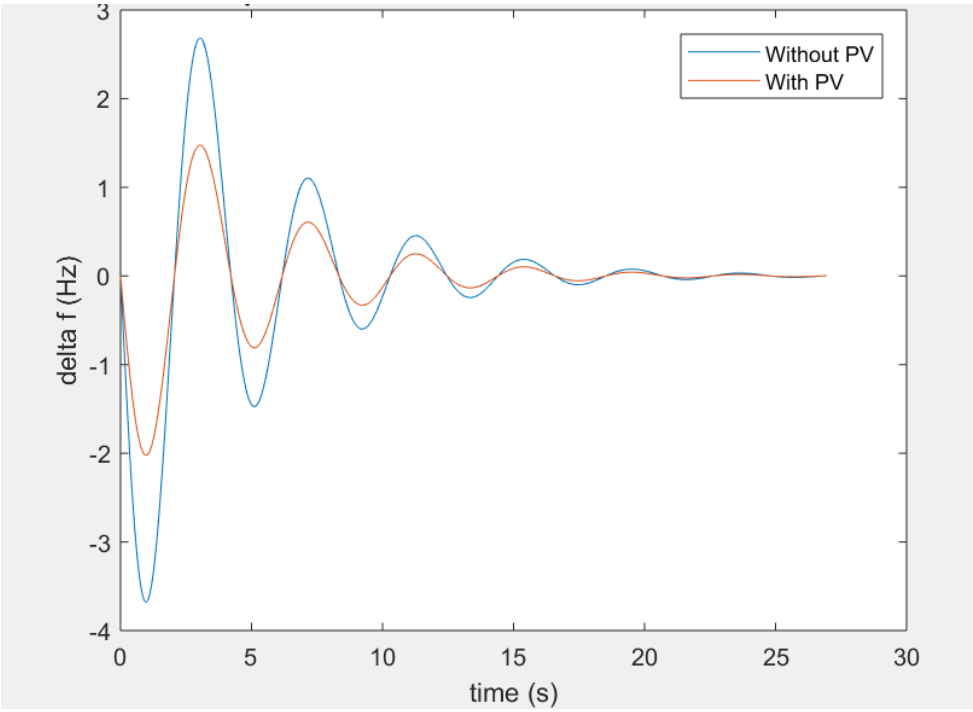

Figure 3.16 Comparison between responses of the system connected and unconnected to the PV system (100% load increase).

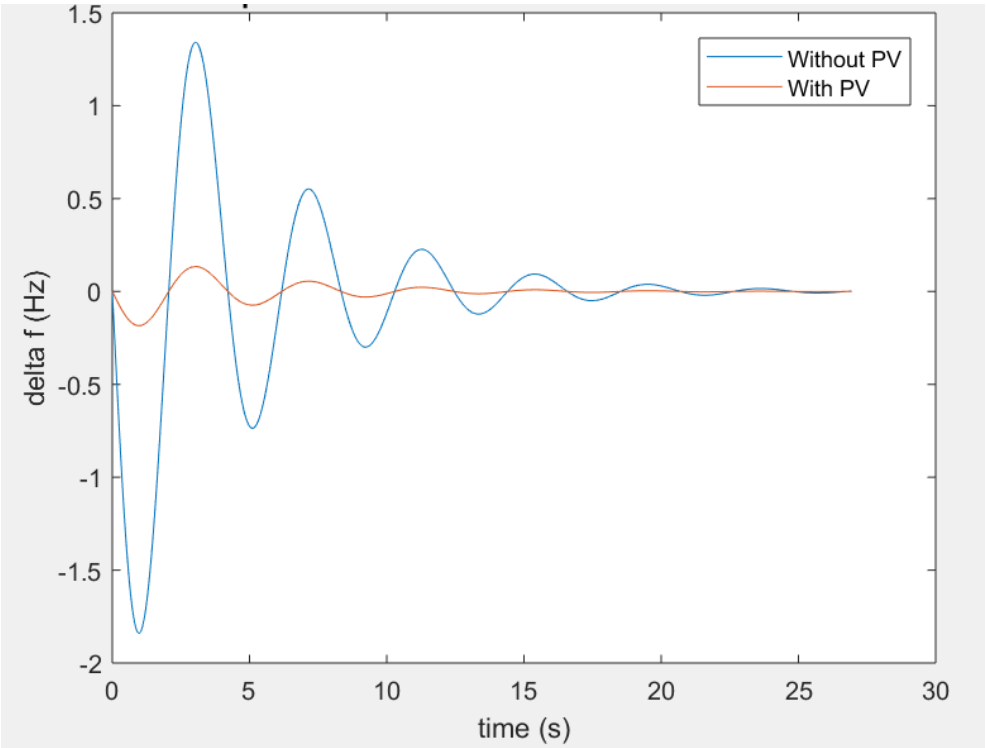

Figure 3.17 Comparison between responses of the system connected and unconnected to the PV system (50% load increase).

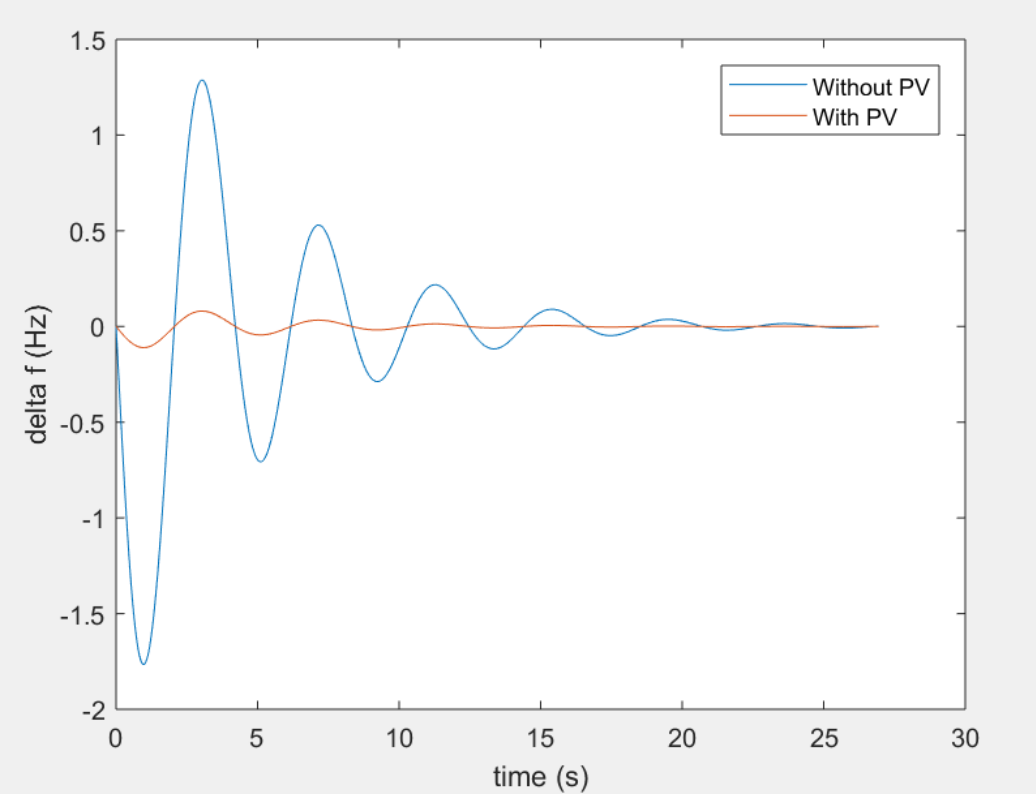

Figure 3.18 Response of the system with and without PV (for a reasonable change in load).

Table 3.4 Comparison for the different responses of the thermal power system connected and unconnected to the PV system.

	Without PV (100% load)	**With PV (100% load)**	**Without PV (50% load)**	**With PV (50% load)**	**Without PV (20% load)**	**With PV (20% load)**
Settling Time (s)	19.7165	19.7165	19.71657	19.7165	19.7165	19.7165
Undershoot (Hz)	-3.679	-2.0239	-1.83992	-0.18398	-0.11039	-1.7663
SSE (Hz)	0	0	0	0	0	0

It can be clearly noticed that the effect of connecting PV to the system is in fact positive, because it helps the power system to match the load demand. It can also be observed that there is no difference in the settling time with the changes in load in the PV-

connected thermal power system. The undershoot with the response has been fairly improved. Thus, the PV system has no effect on the settling time of the deviation of frequency, and only on the system undershoot.

The positive effect on the undershoot could be explained as follows. The mechanical power generated from the thermal system equals the power of the load added to the power loss but subtracted from the power of the photovoltaic system as shown below [1].

$$\Delta P_m = \Delta P_{load} + P_{loss} - \Delta P_{pv} \tag{3.48}$$

Thus, the PV system helps reduce the load pressure on the thermal power system. This is because, in the blue graph (without PV) in Figure 3.18, ΔP_m had to provide the system with the full power demand (1p.u.) which is why it settles down at this value. However, after the connection with PV (non-dispatchable generator), ΔP_m (dispatchable generator, i.e. the one in the thermal power system) is now providing only the remaining part of what the PV could not provide, keeping the power flow unchanged [16]. Therefore, it settles at a value less than 1p.u., i.e., the load is now distributed between the PV system and the thermal power system. ΔP_{pv} is a DC value as explained earlier and does not contribute to more oscillations nor takes time to reach the steady state. And since this makes ΔP_m provide for less load, it has a smaller undershoot. These factors affect the output (Δf) positively by reducing the undershoot of the system, but not affecting the settling time neither positively nor negatively.

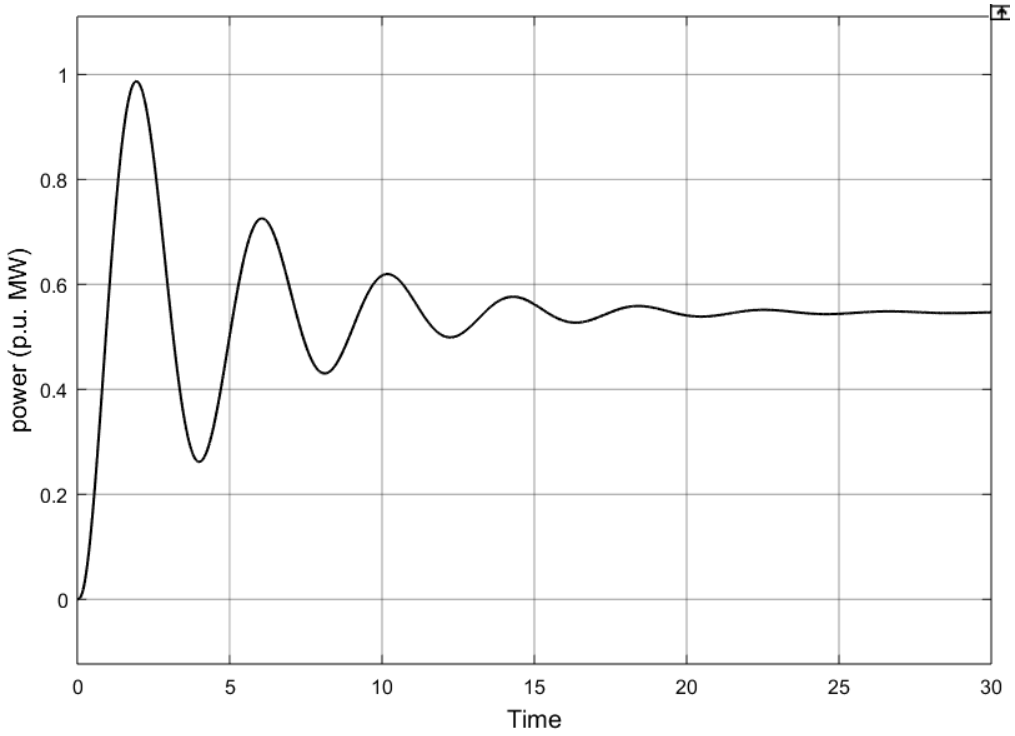

Figure 3.19 thermal power system provides the remaining power that the PV system could not provide.

3.4 Model of the Two-Area Power Grid Connected to the PV System

In this section, the model of the two-area power system that is connected to the PV system is described along with the responses of the system without controllers other than the integral one. Starting with the second area separate from the first area, its block diagram is shown in Figure 3.20 and Table 3.5 shows the parameters used in the modeling.

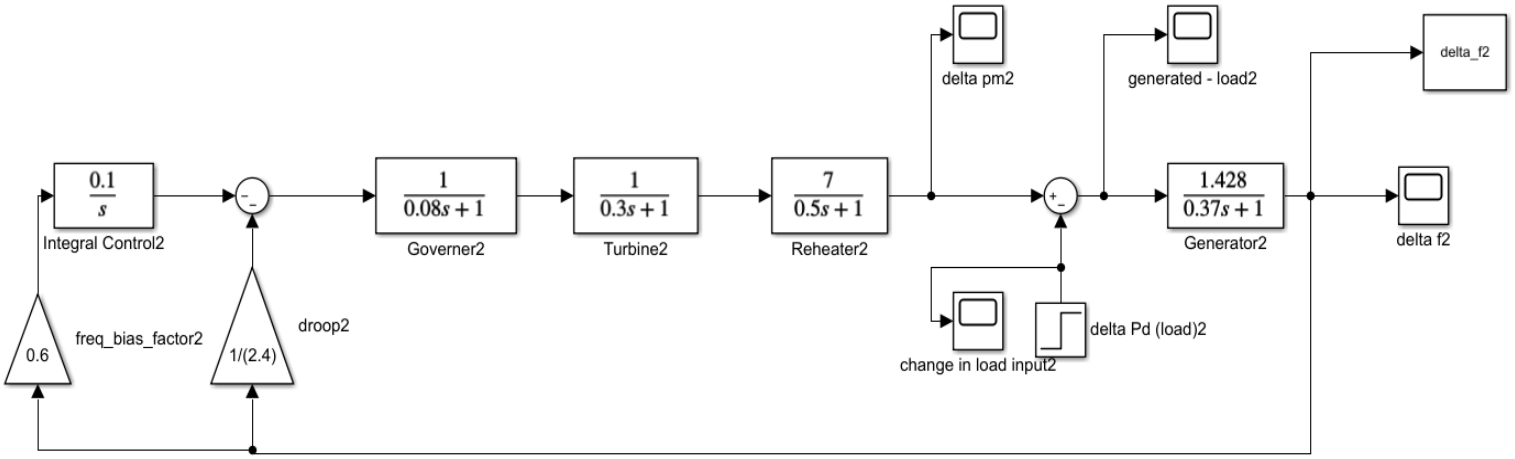

Figure 3.20 Block diagram of the second area.

Table 3.5 Parameters for the modeling of the second area in the thermal power system.

Parameter	Definition	Value
T_{g2}	Governor time constant	0.08
R_2	Droop	2.4
T_{t2}	Turbine time constant	0.3
T_{r2}	Reheater time constant	0.5
K_{r2}	Reheater gain	7
T_{p2}	Generator time constant	0.37
K_{p2}	Gain constant	1.428

The state space model of this power system has been calculated as follows,

$$\dot{x_6} = -2.7027x_6 + 3.859x_7 + 3.859\Delta P_{pv2} - 3.859\Delta P_{load2} \tag{3.49}$$

$$\dot{x_7} = -2x_7 + 14x_8 \tag{3.50}$$

$$\dot{x_8} = -\frac{1}{0.3}x_8 + \frac{1}{0.3}x_9 \tag{3.51}$$

$$\dot{x_9} = -5.208x_6 - 12.5x_9 - 12.5x_{10} \tag{3.52}$$

$$\dot{x_{10}} = fb_2 \times k_{i2}x_6 \tag{3.53}$$

This model includes the integral controller in order to force the steady state error to be 0. In matrix form, we have

$$\begin{bmatrix} \dot{x_6} \\ \dot{x_7} \\ \dot{x_8} \\ \dot{x_9} \\ \dot{x_{10}} \end{bmatrix} = \begin{bmatrix} -2.7027 & 3.85946 & 0 & 0 & 0 \\ 0 & -2 & 14 & 0 & 0 \\ 0 & 0 & \frac{-1}{0.3} & \frac{1}{0.3} & 0 \\ -5.208 & 0 & 0 & -12.5 & -12.5 \\ k_{i2} & 0 & 0 & 0 & 0 \end{bmatrix} \begin{bmatrix} x_6 \\ x_7 \\ x_8 \\ x_9 \\ x_{10} \end{bmatrix} + \begin{bmatrix} -3.86 \\ 0 \\ 0 \\ 0 \\ 0 \end{bmatrix} [\Delta P_{load}] \tag{3.54}$$

$$y = [1 \quad 0 \quad 0 \quad 0 \quad 0] \begin{bmatrix} x_6 \\ x_7 \\ x_8 \\ x_9 \\ x_{10} \end{bmatrix} \tag{3.55}$$

The state variable x_6 is the output change of frequency for this second area, and x_7 is the power generated mechanically in the second area. Based on this model, the responses of the second area only is shown in Figure 3.21 and summarized in Table 3.6.

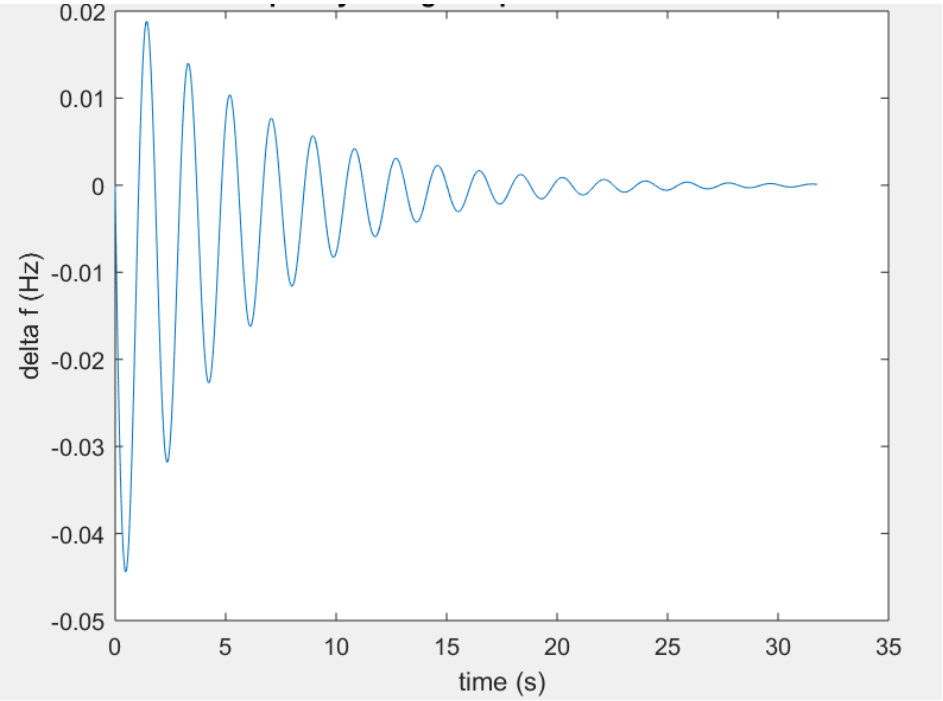

Figure 3.21 The response of the second area only with integral controller.

Table 3.6 Summary of the response of the second area only with integral controller.

Settling Time (s)	21.382
Undershoot (Hz)	-0.0444
SSE (Hz)	0

For the connection of these areas together, there are 5 state variables from the first area and 5 state variables from the second. However, the interconnection adds one more state variable because of the tie-line power change giving a total of 11. For this interconnected system, it has 4 inputs (ΔP_{load1}, ΔP_{pv1}, ΔP_{load2} & ΔP_{pv2}) and 2 outputs which are the change in frequency of area 1 (Δf_1) and the change in frequency of area 2 (Δf_2). The state space model of the PV system connected to this grid is the same as the one mentioned in section 3.1.

As to the full model of the two-area system of the thermal power system, combining Equations 3.42-45 and 3.49-53 along with the following modifications (shown in green in Equations 3.56-3.60) to create the state space model accounting for the interconnected parts between both areas.

$$\dot{x_1} = \frac{-1}{20}x_1 + 6x_2 - 6x_{11} + 6\Delta P_{pv1} - 6\Delta P_{load1} \tag{3.56}$$

$$\dot{x_5} = fb \times k_i x_1 + k_i x_{11} \tag{3.57}$$

$$\dot{x_6} = -2.7027x_6 + 3.859x_7 + 3.859x_{11} + 3.859\Delta P_{pv2} - 3.859\Delta P_{load2} \tag{3.58}$$

$$\dot{x_{10}} = fb_2 \times k_{i2}x_6 - k_{i2}x_{11} \tag{3.59}$$

$$\dot{x_{11}} = 2\pi T x_1 + 2\pi T x_6 \tag{3.60}$$

The system matrices

$$A = \begin{bmatrix} \frac{-1}{20} & 6 & 0 & 0 & 0 & 0 & 0 & 0 & 0 & 0 & -6 \\ 0 & -0.1 & -1.566 & \frac{5}{3} & 0 & 0 & 0 & 0 & 0 & 0 & 0 \\ 0 & 0 & \frac{-1}{0.3} & \frac{1}{0.3} & 0 & 0 & 0 & 0 & 0 & 0 & 0 \\ -5.21 & 0 & 0 & -12.5 & -12.5 & 0 & 0 & 0 & 0 & 0 & 0 \\ fb \times k_i & 0 & 0 & 0 & 0 & 0 & 0 & 0 & 0 & 0 & k_i \\ 0 & 0 & 0 & 0 & 0 & -2.7027 & 3.859 & 0 & 0 & 0 & 3.859 \\ 0 & 0 & 0 & 0 & 0 & 0 & -2 & 14 & 0 & 0 & 0 \\ 0 & 0 & 0 & 0 & 0 & 0 & 0 & \frac{-1}{0.3} & \frac{1}{0.3} & 0 & 0 \\ 0 & 0 & 0 & 0 & 0 & -5.208 & 0 & 0 & -12.5 & -12.5 & 0 \\ 0 & 0 & 0 & 0 & 0 & fb_2 \times k_{i2} & 0 & 0 & 0 & 0 & -k_{i2} \\ 2\pi T & 0 & 0 & 0 & 0 & -2\pi T & 0 & 0 & 0 & 0 & 0 \end{bmatrix} \tag{3.61}$$

$$B = \begin{bmatrix} -6 & 6 & 0 & 0 \\ 0 & 0 & 0 & 0 \\ 0 & 0 & 0 & 0 \\ 0 & 0 & 0 & 0 \\ 0 & 0 & 0 & 0 \\ 0 & 0 & -3.859 & 3.859 \\ 0 & 0 & 0 & 0 \\ 0 & 0 & 0 & 0 \\ 0 & 0 & 0 & 0 \\ 0 & 0 & 0 & 0 \\ 0 & 0 & 0 & 0 \end{bmatrix} \tag{3.62}$$

$$C = \begin{bmatrix} 1 & 0 & 0 & 0 & 0 & 0 & 0 & 0 & 0 & 0 & 0 \\ 0 & 0 & 0 & 0 & 0 & 1 & 0 & 0 & 0 & 0 & 0 \end{bmatrix} \tag{3.63}$$

$$D = [0] \tag{3.64}$$

The controllability and observability of the system have also been checked. The rank of both the controllability matrix and the observability matrix is equal to 11 which is the same as the number of state variables, therefore, the two-area system is controllable and observable.

As to the stability of the two-area system, the eigenvalues are: -12.8774, -11.0897, -8.4731, -0.2412 + 5.7803i, -0.2412 - 5.7803i, -0.2479 + 2.8600i, -0.2479 - 2.8600i, -2.5267, -0.2152 + 0.1814i, -0.2152 - 0.1814i & -0.1439 indicating that the system is stable. Figure 3.22 shows the responses of the two-area system without any controller, and Table 3.7 summarizes the response specifications for the comparison purpose needed later.

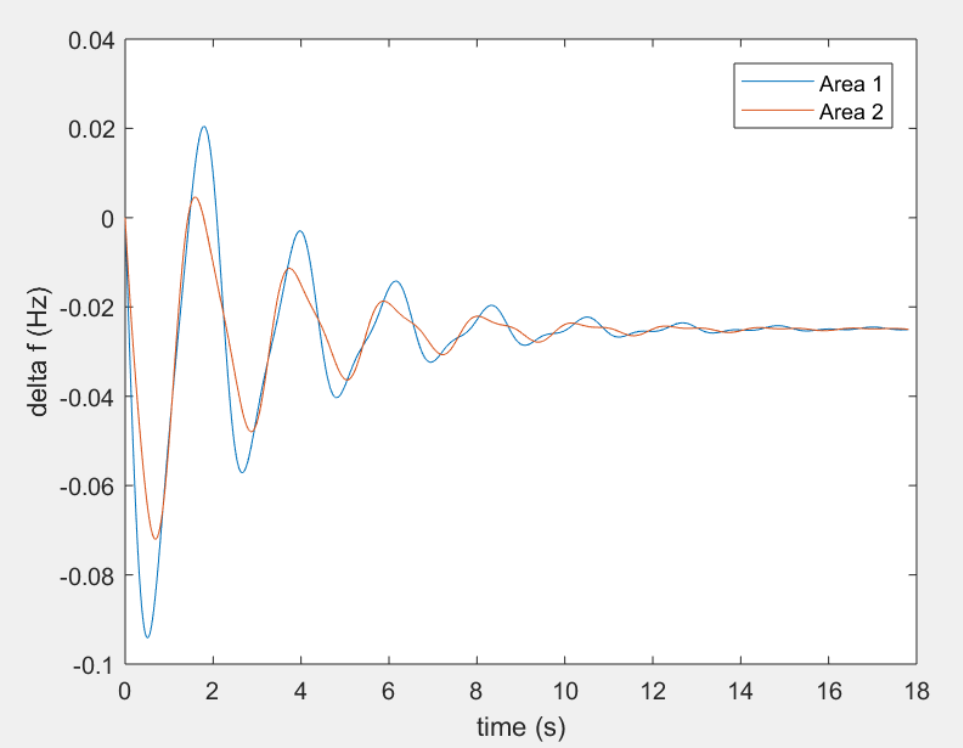

Figure 3.22 Response of the two-area system without any controller due to 50% increase in load.

Table 3.7 Response specifications summary of the two-area system without any controller due to 50% increase in load.

	Area 1	Area 2
Settling Time (s)	23.14	20.61
Undershoot (Hz)	-0.0875	-0.0670
SSE (Hz)	-0.0267	-0.02746

Figure 3.23 shows the block diagram of the interconnected two-area system with PV with integral controllers. ACE is indicated on the same figure too. Figure 3.24 and Figure 3.25 show the responses of both outputs in this system with integral controller for various changes in load. Table 3.8 summarizes the important characteristics of the response.

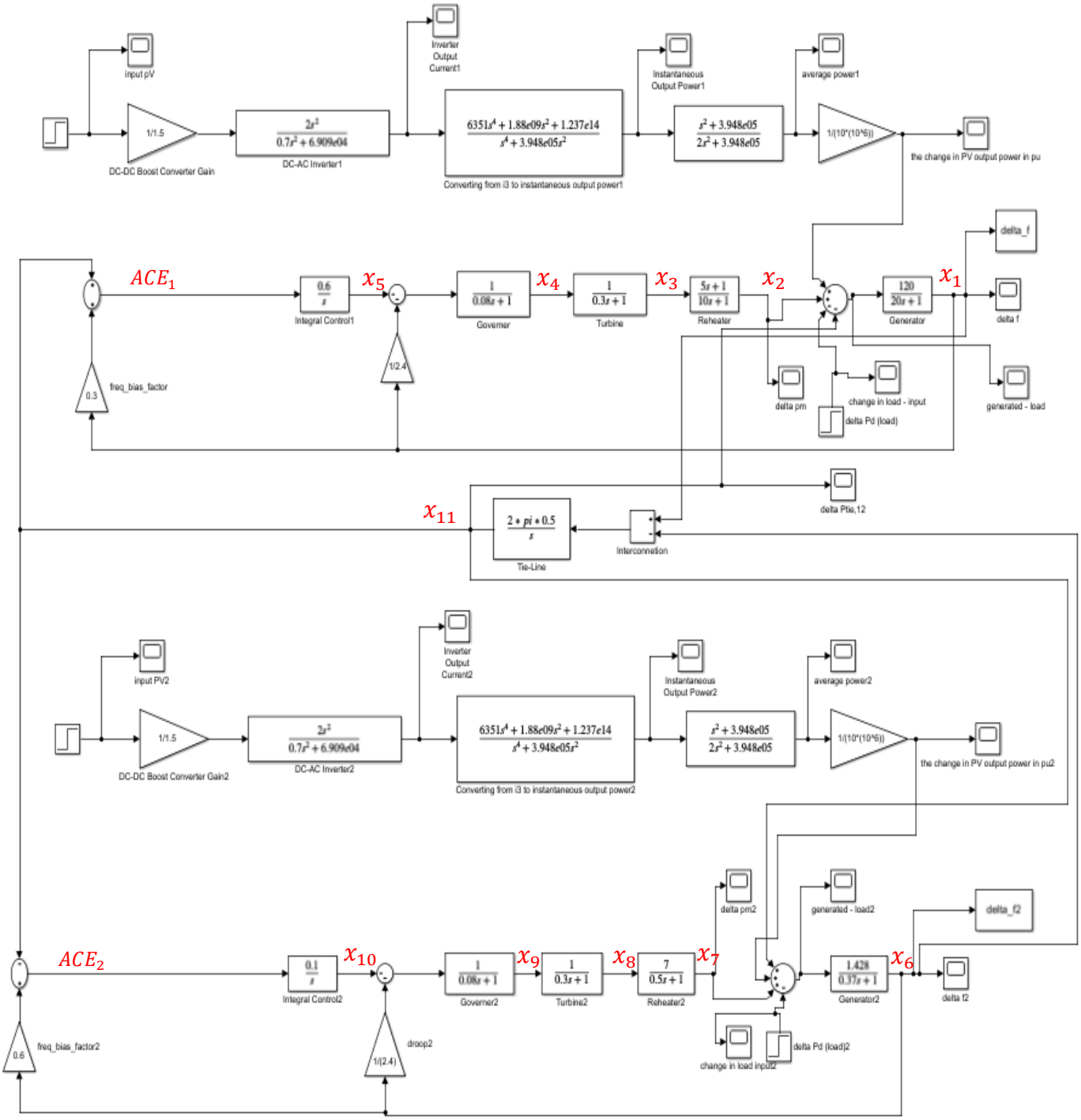

Figure 3.23 Block diagram of the two-area system with PV connected to the grid (I controller only).

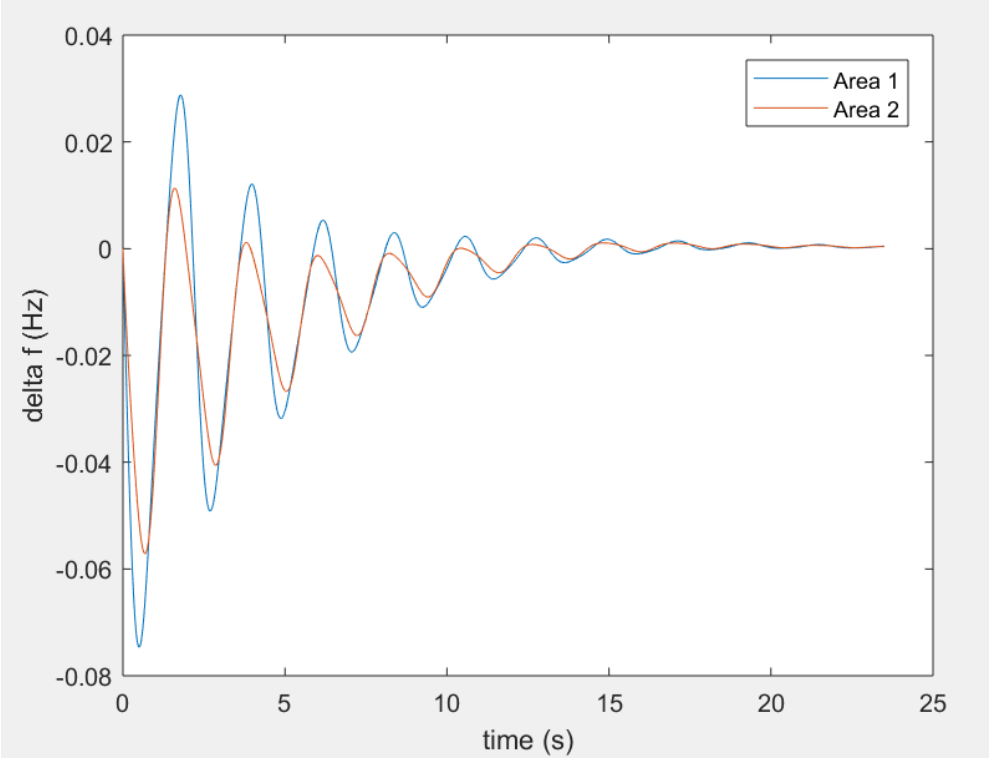

Figure 3.24 Change of frequency from area 1 and area 2 (for the system only with integral controller) for reasonable load.

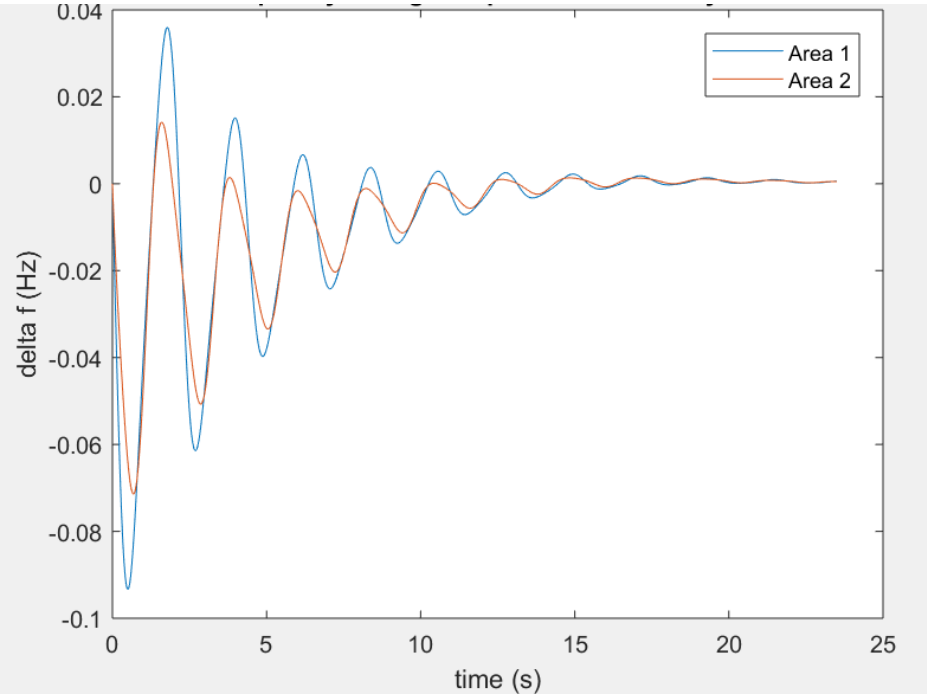

Figure 3.25 Change of frequency from area 1 and area 2 (for the system only with integral controller) for 50% increase in load.

Table 3.8 Summary of the response of both changes in frequency of the two-area system for 50% load.

	Area 1	Area 2
Settling Time (s)	15.106	14.099
Undershoot (Hz)	-0.093343	-0.071406
SSE (Hz)	0	0

Chapter 4: Controller Design and Analysis

In this chapter, controllers design will be explained for single-area and two-area system connected to PV. For each system, three controllers were designed and applied; namely LQR, PI and FL controllers. Each of these controllers will be applied to the system with a reasonable change in load, and also to the case of a sudden increase of load by 50%. It is to be noted that the case of a sudden increase of 50% is an extreme change and is a very unreasonable change to occur. However, even with an extreme case (improbable) load change, the controllers would still enhance the system performance greatly, leaving it with much less undershoot and settling time than the case without any controller.

The same two cases will be studied for the two-area system connected to PV with the addition of two more cases; the case when area 1 endures more load change than area 2, and when area 2 endures more load change than area 1. This helps study the effect of one area on the other with various changes in load.

For each case, a standard set of response specifications, i.e. the undershoot, settling time and steady state error of the response, will be demonstrated. This would allow for a comparison of the responses for all the different cases. It is to be noted that the model of the PV system is the same as explained in section 3.1, assuming it operates at MPP.

4.1 Design of the Linear Quadratic Regulation for PV Grid-Connected Single-Area Power Grid

LQR controller has been designed for the single-area system in this study and the design is presented in this section. The model of the system with the integral controller ($k_i = 0.6$) was used in the design to ensure a zero steady state error.

In order to choose the best possible values for state and control weighting matrices (Q and R) in the LQR controller, an optimization code has been created on MATLAB for this purpose. By creating this optimization code, the optimized Q and R matrices chosen were:

$$Q = \begin{bmatrix} 2.8 & 0 & 0 & 0 & 0 \\ 0 & 19.8 & 0 & 0 & 0 \\ 0 & 0 & 5.8 & 0 & 0 \\ 0 & 0 & 0 & 5.8 & 0 \\ 0 & 0 & 0 & 0 & 1 \end{bmatrix} \quad (4.1)$$

$$R = [0.001] \quad (4.2)$$

The costate matrix (P) is calculated and, accordingly, the best values for state feedback gains (K matrix) are calculated through the Riccati equation of LQR, giving the following values.

$$K = [53.508 \quad -89.7 \quad 15.284 \quad -27.976 \quad 77.02] \quad (4.3)$$

These are the values of the state feedback gains that, when multiplied by the corresponding state variables, gives the optimal system response in terms of settling time and undershoot. The following cases present various load changes and their responses of the system with this designed LQR controller.

4.1.1 Case 1: Acceptable increase in load ($\Delta P_{load} < 10\%$)

Figure 4.1 shows the frequency error response of the single area after applying this LQR controller and Table 4.1 summarizes the response parameters. The three criteria are met since the settling time is less than 3s, undershoot is less than 0.02Hz and the steady state error is zero.

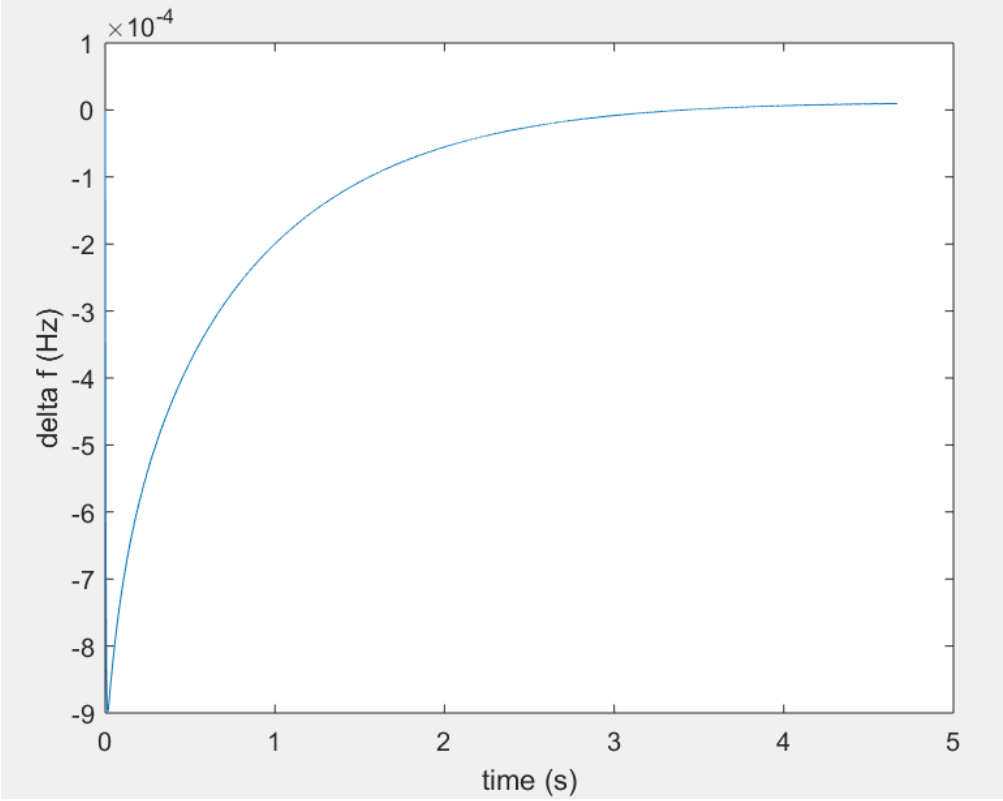

Figure 4.1 Frequency Response of the single-area system connected to PV with LQR controller (for reasonable load change).

Table 4.1 Response characteristics of the single-area system connected to PV with LQR controller (for reasonable load change).

Settling Time (s)	2.68106
Undershoot (Hz)	-8.9809e-04
SSE (Hz)	0

4.1.2 Case 2: 50% increase in load (worst-case scenario)

As explained earlier, the case of 50% sudden increase in load will be studied in all sections in order to observe that even in the extreme case, there is a big improvement in the system response.

The same controller designed in case 1 is proved to be reliable even in the worst-case scenario, when 50% increase in load occurs at the same second. Figure 4.2 and Table 4.2 show that the response still meets the required criteria. The LQR controller is efficient

in that it forced the system to meet all the required criteria even in the worst case of a sudden 50% increase in load.

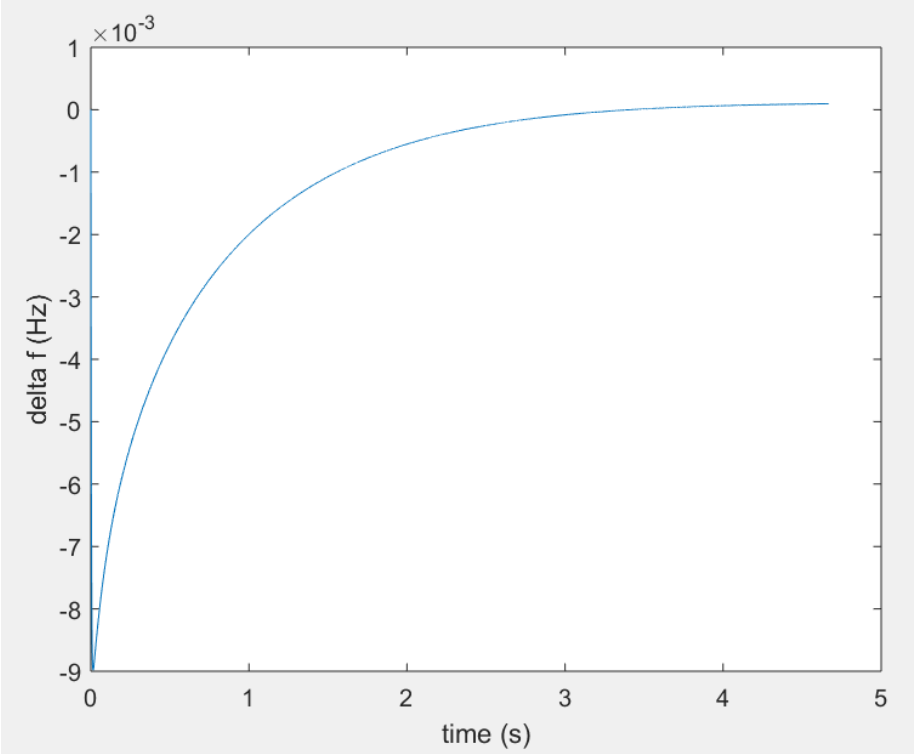

Figure 4.2 Response of PV-connected single-area system with LQR controller (50% increase in load).

Table 4.2 Response characteristics of PV-connected single-area system with LQR controller (50% increase in load).

Settling Time (s)	2.68106
Undershoot (Hz)	-0.009879
SSE (Hz)	0

It is to be noticed that the settling time does not change with changes in the load or changes in the solar input. The same controller gave the same settling time in all cases (2.6s). Only the undershoot is affected. Moreover, a big advantage of the LQR is that it stabilizes the system automatically. The eigenvalues of the closed loop system are checked after the applying the designed values of the LQR (*K*) to the state variables. All eigenvalues (poles) are negative, therefore, the system is stable.

4.2 Design of PI Controller for PV Grid-Connected Single-Area Power Grid

PI controller has been designed for the single-area system with PV. As mentioned earlier, in the design of LQR, the integral controller was already included. Thus, what is added in this section is the proportional controller. Figure 4.3 shows the block diagram of the system with PI. Optimization using MATLAB has been carried out in order to find the K_p and K_i values that would give the best response (i.e. the least undershoot possible with the least settling time). The value of $K_p = 2.1$, and $K_i = 0.6$ were the result of the optimization and the following are the results for each case with these values of K_p and K_i.

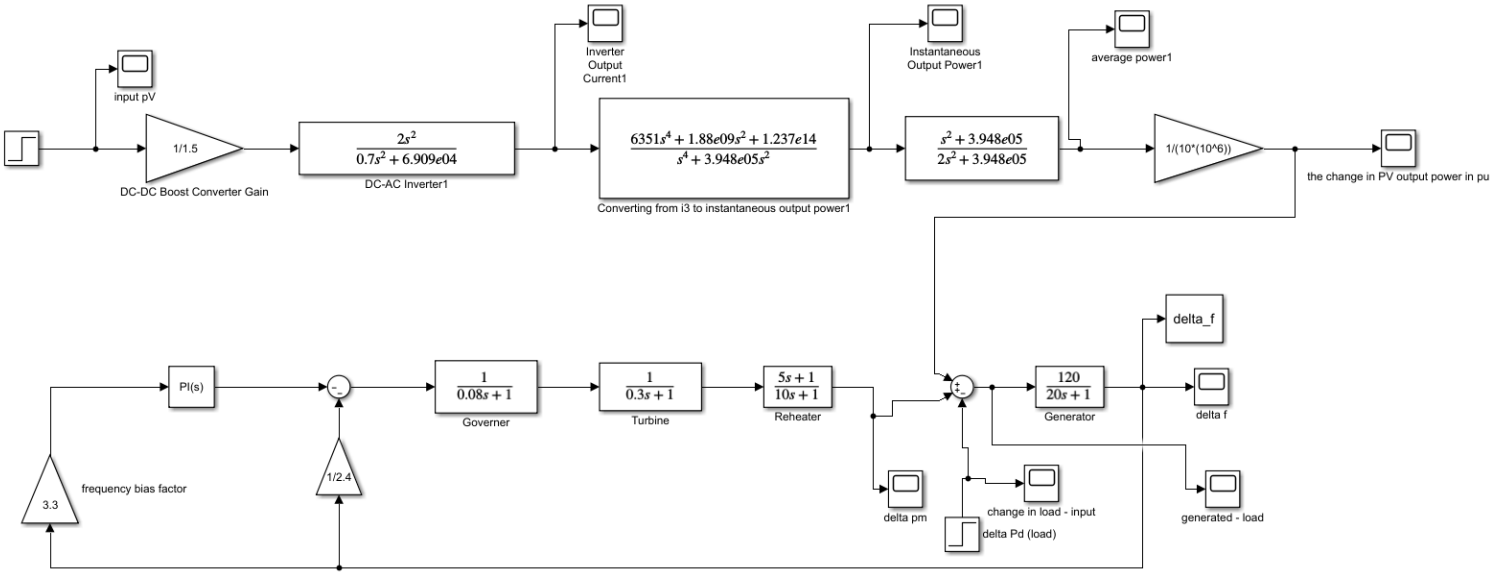

Figure 4.3 PI controller integrated to the single-area system with PV.

4.2.1 Case 1: Acceptable increase in load ($\Delta P_{load} < 10\%$)

With an increase of load less than 50%, Figure 4.4 and Table 4.3 describe the response of the system with PI controller. It can be noticed that the undershoot and settling time have been improved from the case without any controller. However, the response is still not meeting the criteria even with the best (optimized) values of K_p and K_i after many iterations.

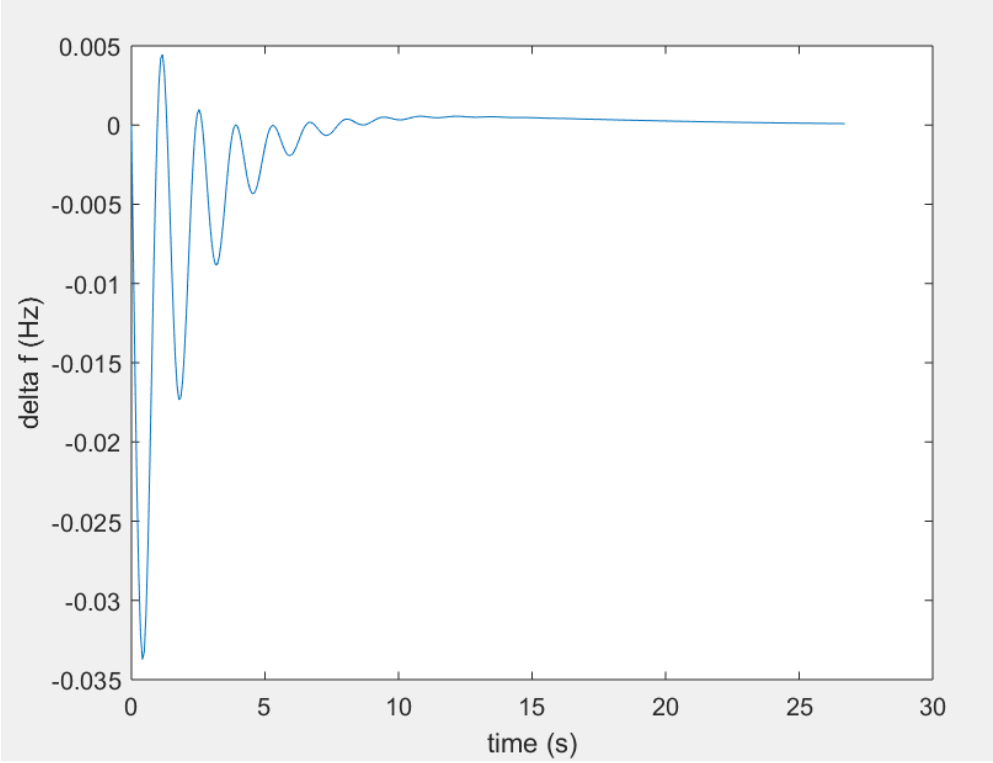

Figure 4.4 Response of PV-connected single-area with PI controller for reasonable change in load.

Table 4.3 Response parameters of the single-area grid connected to PV with PI controller.

Settling Time (s)	6.3335
Undershoot (Hz)	-0.033733
SSE (Hz)	0

4.2.2 Case 2: 50% increase in load (worst-case scenario)

This extreme increase in load affected the undershoot and increased it more as expected. None of the requirements is met except the steady state error due to the integral controller. Figure 4.5 and Table 4.4 show the response under the worst-case scenario.

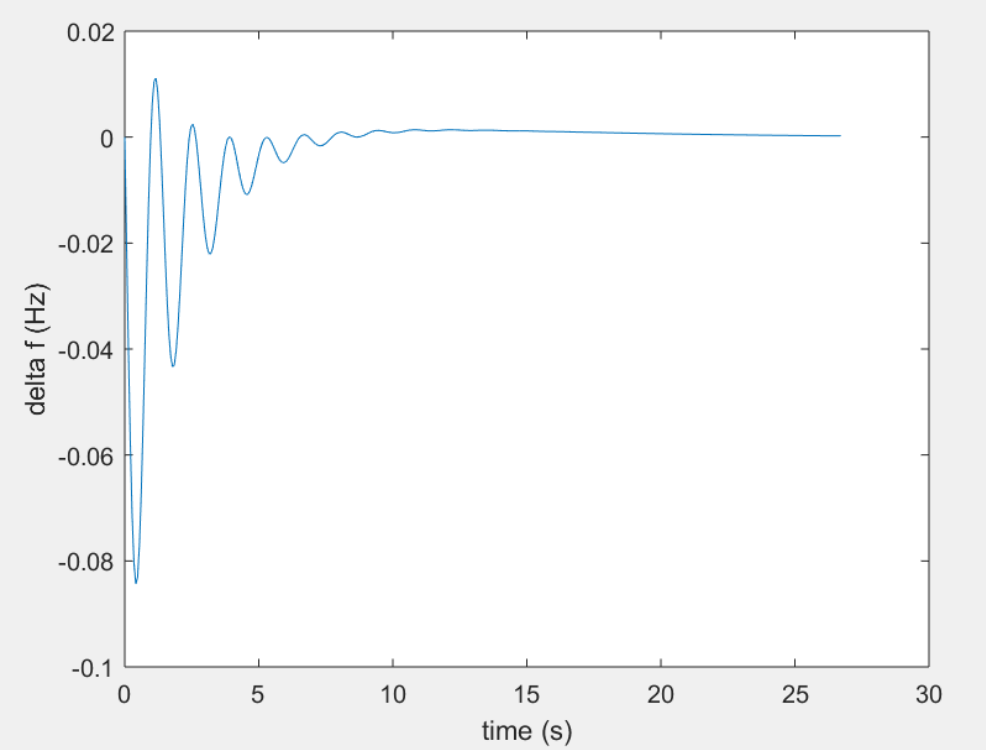

Figure 4.5 Response of the PV-connected single-area under high sudden increase in load (50%).

Table 4.4 Response parameters of the PV-connected single-area under high sudden increase in load (50%).

Settling Time (s)	6.3335
Undershoot (Hz)	-0.08433
SSE (Hz)	0

4.3 Design of Fuzzy Logic Controller for PV Grid-Connected Single-Area Power Grid

As noticed in section 4.2, the PI controller alone could not achieve the required system performance. Therefore, it is necessary to add a new efficient controller; fuzzy logic controller, to enhance the output response.

Two inputs were chosen for the fuzzy logic controller; the system frequency error and the derivative of the error [37]. In control systems, usually the error derivative is chosen as a second input to the FL controller because the derivative of a curve is the slope, which indicates the direction of the curve at each point. This is crucial in determining what the

controller output should be based on whether the error is decreasing or increasing at that point [30].

The range of both these inputs should cover all the possible values of the error and the rate of change of the error. Thus, the ranges of error and its derivative have been checked for various loads, and the values never exceeded -3 and 3. Thus, this is the range chosen for both.

As to the output of the controller, there is only one output and it is negatively fedback to the system. The range of this output has been chosen to be -0.5 and 0.5. This is the range that produced the best response.

As for the first stage of fuzzy logic controller design which is the fuzzification, the membership functions chosen are 7. First, 3 and 5 membership functions were tried but did not give the required specifications. Also, 9 membership functions have been studied but did not have any noticeable enhancement on the response than with only 7 membership functions. Therefore, the best number for this application was 7 and they are the following: Negative Big (NB), Negative Medium (NM), Negative Small (NS), ZZ (Zero Change), Positive Small (PS), Positive Medium (PM) and Positive Big (PB).

Figure 4.6 shows these membership functions with their ranges that have been distributed equally among all membership functions from the original range (between -3 and 3 for the inputs and -0.5 to 0.5 for the output). Narrower ranges at some points are only required when fine tuning and very accurate control is necessary at a certain small range [30]. For the current application, narrower ranges were tried but did not give much difference. Thus, the equal ranges were implemented. As to the shape of these functions, triangular shape was chosen because it the standard shape to begin with in FLC for the purpose of simplicity in the calculations purposes. Since it gave the required results, there was no need to implement the other shapes which have more complicated calculations. Moreover, there is no noticeable difference in the response with various shapes of membership functions, thus, the choice of the range and the number of these membership functions is what matters most, rather than the shape. [30]

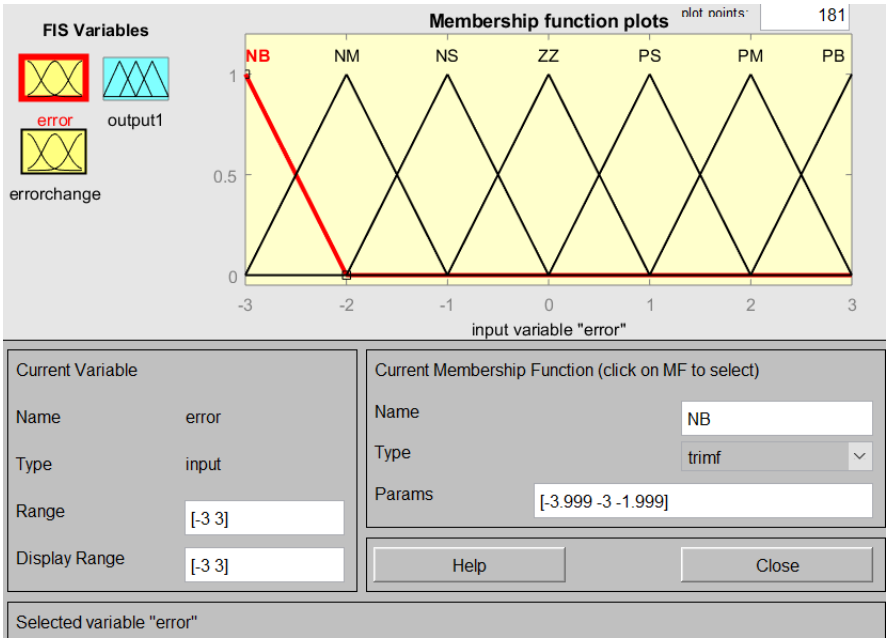

Figure 4.6 Membership functions in the fuzzy controller design.

The next stage in the design is creating the rules from which the inference procedure will take place. The general rules to start with in the design of FLC are shown in Table 4.5 for 7 membership functions, i.e. 49 rules. These rules are in the form of (if e is a and $\dot{e}$ is b then fuzzy controller output is c). The design of these rules is based on trial and error and human experience [31], however, there are some general characteristics to these rules that help with the initial trials. The more experience one has in the behavior of FL controllers, the more accurate these rules can be designed.

Table 4.5 The general rules of designing a fuzzy logic controller.

e | $\dot{e}$	**NB**	**NM**	**NS**	**ZZ**	**PS**	**PM**	**PB**
NB	NB	NB	NB	NB	NM	NS	ZZ
NM	NB	NB	NB	NM	NS	ZZ	PS
NS	NB	NB	NM	NS	ZZ	PS	PM
ZZ	NB	NM	NS	ZZ	PS	PM	PB
PS	NM	NS	ZZ	PS	PM	PB	PB
PM	NS	ZZ	PS	PM	PB	PB	PB
PB	ZZ	PS	PM	PB	PB	PB	PB

For example, the initial table of rules is logically symmetric as shown in Table 4.5. This is because for example if error is a big negative number (NB) and the derivative of error is also increasing rapidly in the negative side (NB), then the controller needs to produce a big negative value of the controller in order to correct this effect. Keeping in mind that the value of the controller (whether it is negative or positive) is inserted to the system as a negative value, which means with the opposite sign. Thus, a big negative controller output will be feedback to the system as a big positive value which will correct the effect of a negative big error increasing rapidly in the negative direction.

Another reason for this symmetry is that the error and the derivative of error can go in both directions. Thus, tuning the rules is limited to the negative output in the negative side of inputs and the positive output in the positive side of inputs. This also helps limit the possible tuning changes during trial and error.

However, further tuning in Table 4.5 was required in order to meet the specifications. This is because the logical method of choosing the FL controller output values still leaves some undetermined output values for certain inputs. After the further tuning, Table 4.6 and Figure 4.7 show the final rules that gave the best response for the system.

Table 4.6 Chosen rules for the fuzzy logic controller.

e | $\dot{e}$	**NB**	**NM**	**NS**	**ZZ**	**PS**	**PM**	**PB**
NB	NB	NB	NB	NB	NS	NS	ZZ
NM	NB	NM	NM	NM	NS	ZZ	PS
NS	NB	NB	NM	NS	PS	PM	PB
ZZ	NB	NM	NS	ZZ	PS	PM	PB
PS	NM	NS	ZZ	PS	PS	PM	PM
PM	NS	ZZ	PS	PM	PM	PM	PM
PB	ZZ	PS	PM	PB	PB	PB	PB

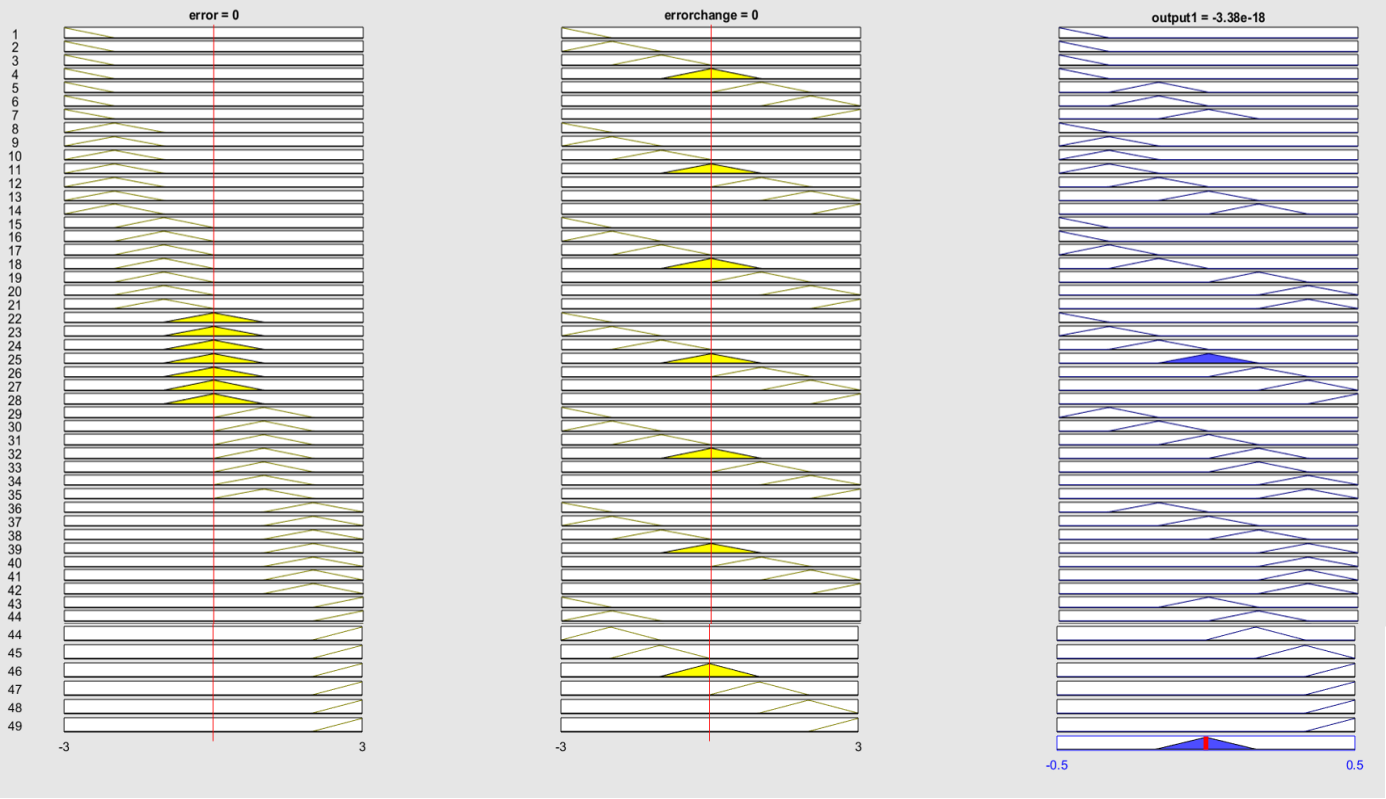

Figure 4.7 The 49 rules of the fuzzy logic controller designed.

The last stage in the fuzzy controller design is defuzzification, i.e. changing the fuzzy value of the controller output into a numerical value that could be feedback to the system. There are several methods for defuzzification and the one applied in this controller is the centroid (center of gravity) method as it is the most commonly used.

The equation mentioned in the literature review for this method is applied to an example in this application to illustrate the concept. Assume at one point the error has a value of -3, this means that we are 100% certain that the error is NB at this point according to the triangular shapes of the membership functions shown in Figure 4.6. Thus, it has a membership value of 1. Assume at the same point that the derivative of the error is -2.5. This means we are 50% certain that it is NB and 50% certain that it is NM. This produces two possible rules to be applied:

Rule 1: if e is NB and $\dot{e}$ is NB then fuzzy controller output is NB

Rule 2: if e is NB and $\dot{e}$ is NM then fuzzy controller output is NB

Applying the inference method of minimum for both these rules:

$$\mu_{rule1} = \min(\mu_e, \mu_{\dot{e}}) = \min(1,0.5) = 0.5 \tag{4.4}$$

$$\mu_{rule2} = \min(\mu_e, \mu_{\dot{e}}) = \min(1,0.5) = 0.5 \tag{4.5}$$

Thus, both rules have a probability of 0.5. They are equally likely in this example. To do the defuzzification based on weighing each rule, the center of NB is $b_1 = -3$, and the center of NM is $b_2 = -2$. Calculating the shaded area of the triangle for the derivative of the error:

$$For\ Rule\ 1: A_1 = w\left(h - \frac{h^2}{2}\right) = 2\left(0.5 - \frac{0.5^2}{2}\right) = 0.75 \tag{4.6}$$

$$For\ Rule\ 2: A_2 = w\left(h - \frac{h^2}{2}\right) = 2\left(0.5 - \frac{0.5^2}{2}\right) = 0.75 \tag{4.7}$$

According to these values, the controller output can be calculated as in Equation 4.8:

$$u = \frac{\sum b_i \times membership\ value}{\sum membership\ values} = \frac{(-3 \times 0.75) + (-2 \times 0.75)}{(0.75 + 0.75)} = -2.5 \tag{4.8}$$

The value -2.5 on the scale of the inputs (-3 to 3) refers to a Negative Big value which is why the output is NB. The exact value of the output would be the value that matches -2.5 on the output scale which is (-0.5 and 0.5). This value would be:

$$-2.5 \times \frac{0.5}{3} = -0.42 \tag{4.9}$$

By checking the output on MATLAB for the same input values using, the value obtained was almost the same (-0.43).

After applying this designed FLC, the full system is shown in Figure 4.8. After several modifications by trial and error, the best new values of the PI controller that coordinate well with the fuzzy logic controller were $K_p = 0.6$ and $K_i = 0.9$. The responses of each case with PI and FL controllers is described in the following subsections.

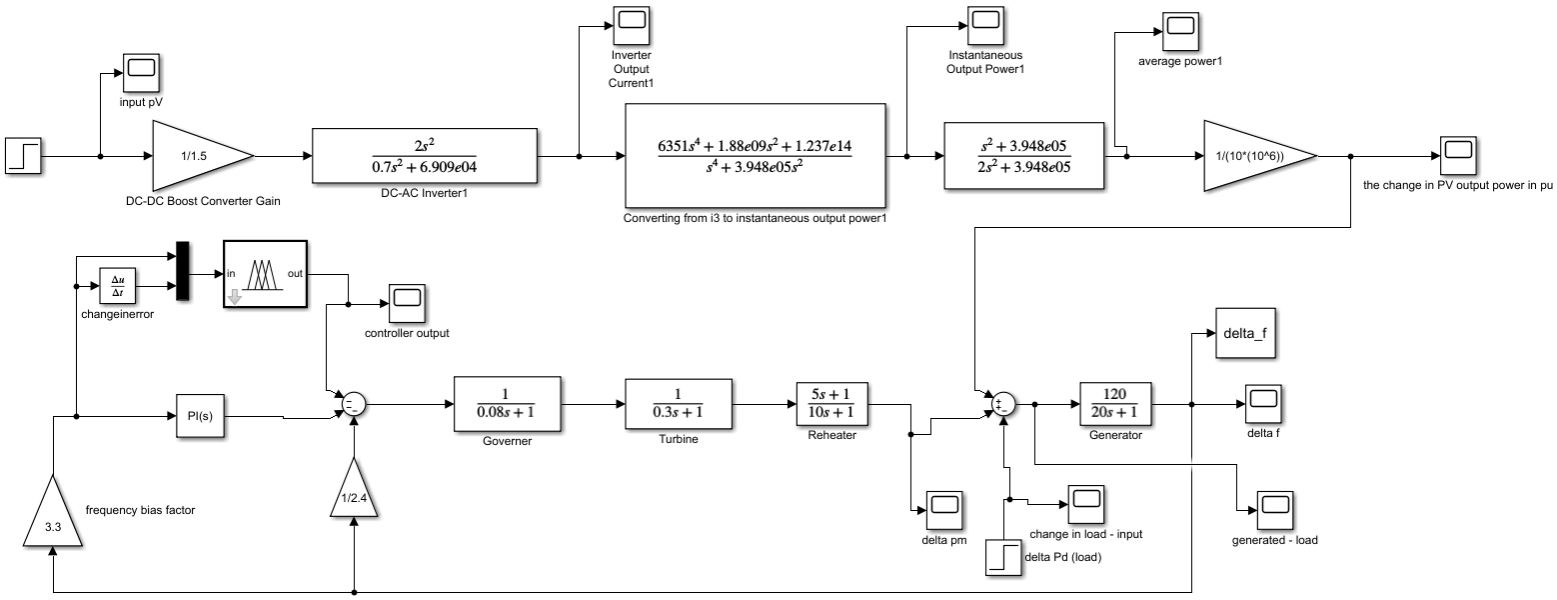

Figure 4.8 Block diagram of the single-area grid connected to PV with PI and fuzzy logic controllers.

4.3.1 Case 1: Acceptable increase in load ($\Delta P_{load} < 10\%$)

As can be noticed from Figure 4.9 and Table 4.7 for the case of having a power load change of less than 50%, the undershoot meets the criteria (<0.02) and the oscillations were reduced tremendously from the case of PI controller only. This proves the significant enhancement that FL controller added to the system.

On the other hand, the settling time is almost the same as the one with PI controller. Fuzzy controllers also have limitations in their structure that they can only enhance the system to a certain level. At this level, the tradeoff between undershoot and settling time becomes quite inevitable. After many attempts, this limitation was obvious in that the settling time could not be improved to less than 7s as it affected the undershoot negatively.

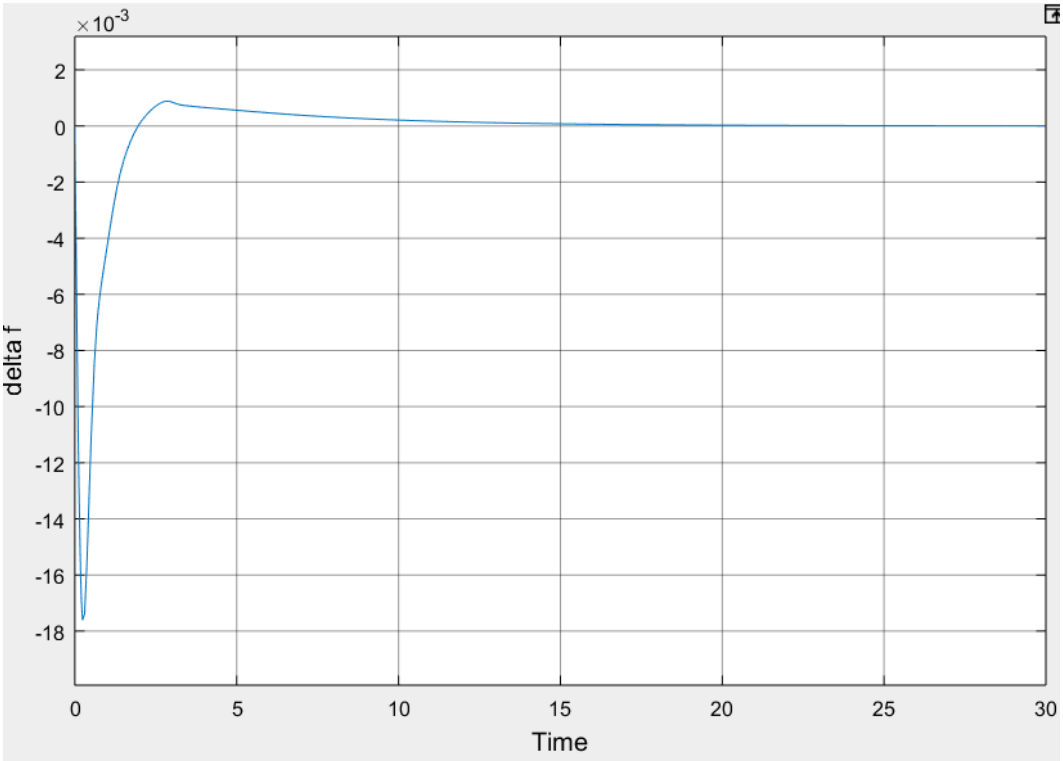

Figure 4.9 Response of the PV-connected single-area system with PI and fuzzy logic controller (for a load less than 50%).

Table 4.7 Response characteristics of the PV-connected single-area system with PI and fuzzy logic controller (for a load less than 50%).

Settling Time (s)	7.4217
Undershoot (Hz)	-0.01761
SSE (Hz)	0

4.3.2 Case 2: 50% increase in load (worst-case scenario)

For the improbable case of having a sudden increase of 50% in the load, FL controller still greatly enhances the system performance than the response with PI controller only making the undershoot very close to the required value as shown in Figure 4.10 and Table 4.8. However, even if the undershoot criteria is not absolutely met in case 2, this case has a rather low probability of happening, thus, it cannot be considered as a disadvantage of FLC. It is to be noticed that in FLC, the settling time changed slightly between both cases with the changes in load.

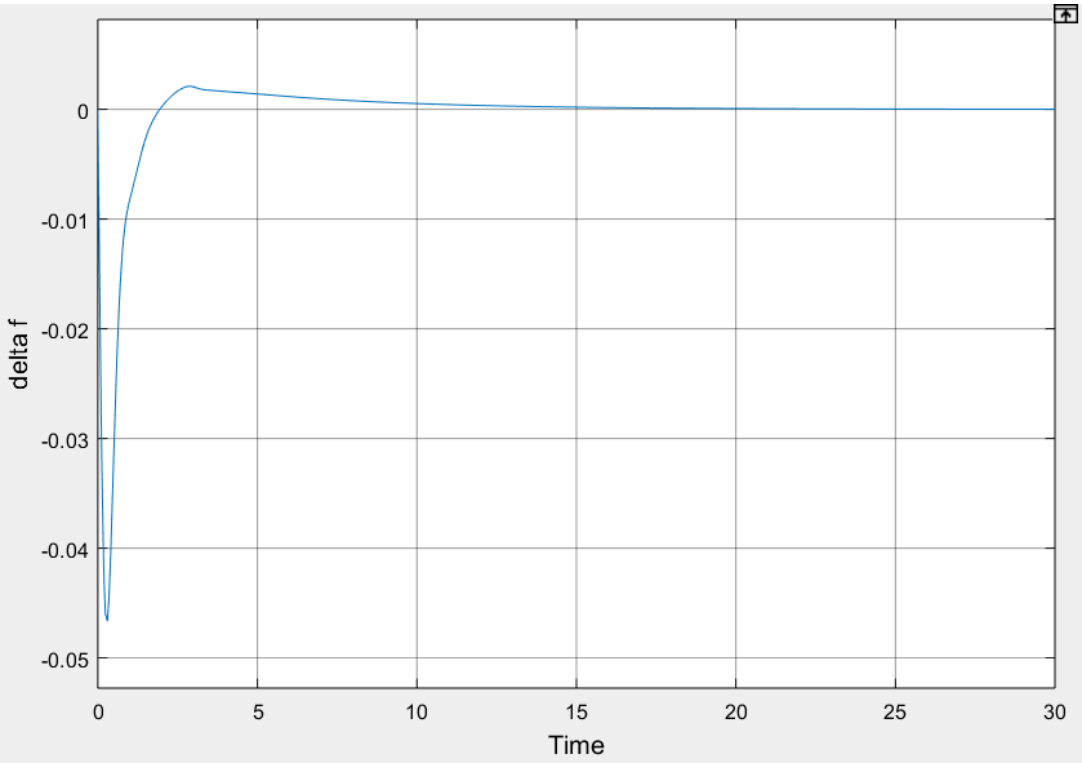

Figure 4.10 Response of the PV-connected single-area system with PI and fuzzy logic controller (for a 50% increase in load).

Table 4.8 Response parameters of the PV-connected single-area system with PI and fuzzy logic controller (for a 50% increase in load).

Settling Time (s)	7.13032
Undershoot (Hz)	-0.0466
SSE (Hz)	0

The original response of the system with integral controller is compared with that after applying the fuzzy logic controller along with the PI controller in Figure 4.11 for this worst-case scenario. PI controller produced many oscillations that the FLC was able to eliminate, while also reducing the undershoot tremendously.

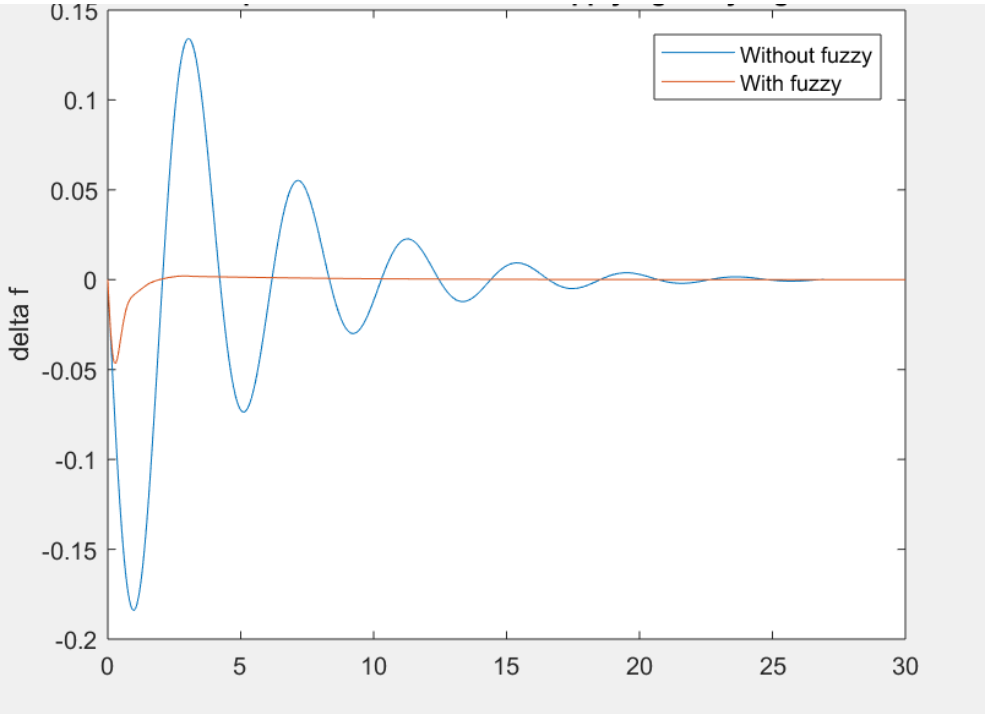

Figure 4.11 Comparison between the PV-connected single-area system response with and without fuzzy logic for the case of 50% increase in load.

4.4 Design of the Linear Quadratic Regulation for PV Grid-Connected Two-Area Power Grid

LQR was designed for the second area separately first and optimized, then designed for the two-area system. The optimized state and control weighting matrices (Q and R) for the two-area system are shown in (4.10) and (4.11) and along with the designed K values (state gain feedback) for each state variable in (4.12).

$$Q = \begin{bmatrix} 0.3 & 0 & 0 & 0 & 0 & 0 & 0 & 0 & 0 & 0 & 0 \\ 0 & 19.9 & 0 & 0 & 0 & 0 & 0 & 0 & 0 & 0 & 0 \\ 0 & 0 & 1 & 0 & 0 & 0 & 0 & 0 & 0 & 0 & 0 \\ 0 & 0 & 0 & 1 & 0 & 0 & 0 & 0 & 0 & 0 & 0 \\ 0 & 0 & 0 & 0 & 1 & 0 & 0 & 0 & 0 & 0 & 0 \\ 0 & 0 & 0 & 0 & 0 & 0.3 & 0 & 0 & 0 & 0 & 0 \\ 0 & 0 & 0 & 0 & 0 & 0 & 15.5 & 0 & 0 & 0 & 0 \\ 0 & 0 & 0 & 0 & 0 & 0 & 0 & 5.8 & 0 & 0 & 0 \\ 0 & 0 & 0 & 0 & 0 & 0 & 0 & 0 & 5.8 & 0 & 0 \\ 0 & 0 & 0 & 0 & 0 & 0 & 0 & 0 & 0 & 5.8 & 0 \\ 0 & 0 & 0 & 0 & 0 & 0 & 0 & 0 & 0 & 0 & 5.8 \end{bmatrix} \quad (4.10)$$

$$R = [0.001] \quad (4.11)$$

$$K = [-1.6946 \quad -84.0166 \quad 19.1327 \quad -8.9603 \quad 48.5421 \quad 38.0034 \quad -37.1264$$
$$-184.8331 \quad -61.8141 \quad 8.8978 \quad 74.554] \tag{4.12}$$

With this designed LQR controller, the four cases of various loads are studied and summarized in the following sub-sections. SSE is zero in all cases because of the integral controller.

4.4.1 Case 1: Acceptable increase in load ($\Delta P_{load1} = \Delta P_{load2}$)

In this case, both the loads in area 1 and area 2 increased by the same percentage. Figure 4.12 and Table 4.9 summarize the response for case 1. Settling time requirement is far from the desired specification, however, the undershoot and steady state error requirements are met.

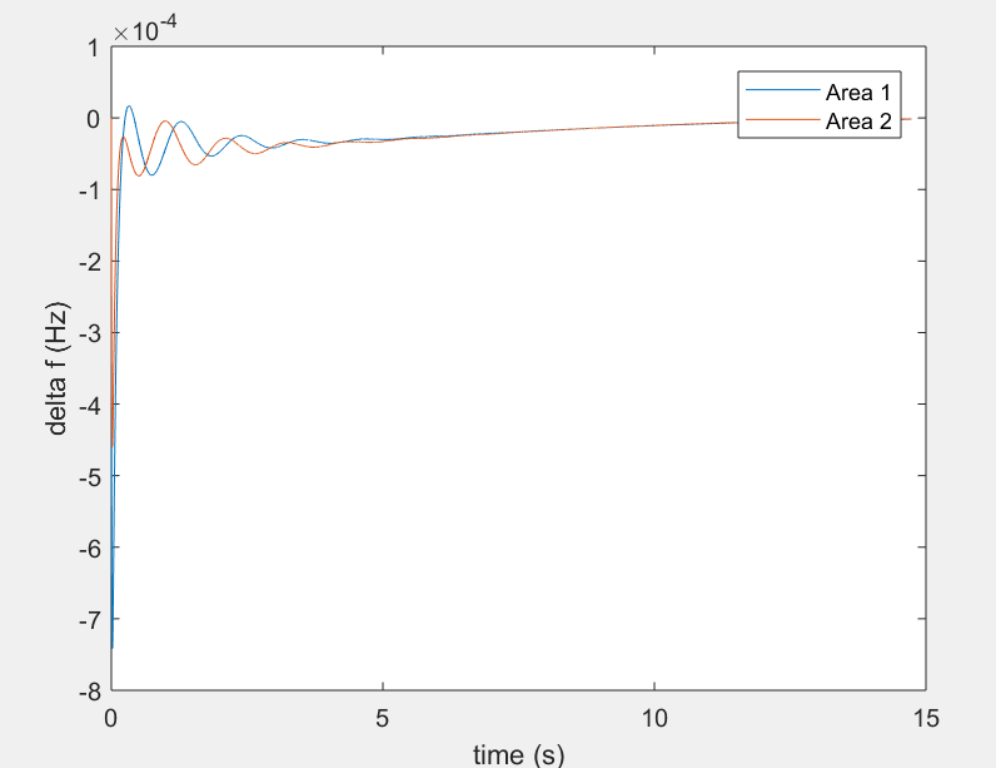

Figure 4.12 Response of both areas with LQR controller for equal and reasonable change in load.

Table 4.9 Response summary for both areas with LQR (equal and reasonable change in load).

	Area 1	Area 2
Settling Time (s)	8.74751	10.442
Undershoot (Hz)	-0.00074147	-0.00045986
SSE (Hz)	0	0

4.4.2 Case 2: $\Delta P_{load1} > \Delta P_{load2}$

Figure 4.13, Figure 4.14 and Table 4.10 show the response for case 2 in which more change occurs on the load connected to area 1 than in area 2. The settling time did not change from case 1, thus, still does not meet the required specification. The undershoot and steady state error are within the required range.

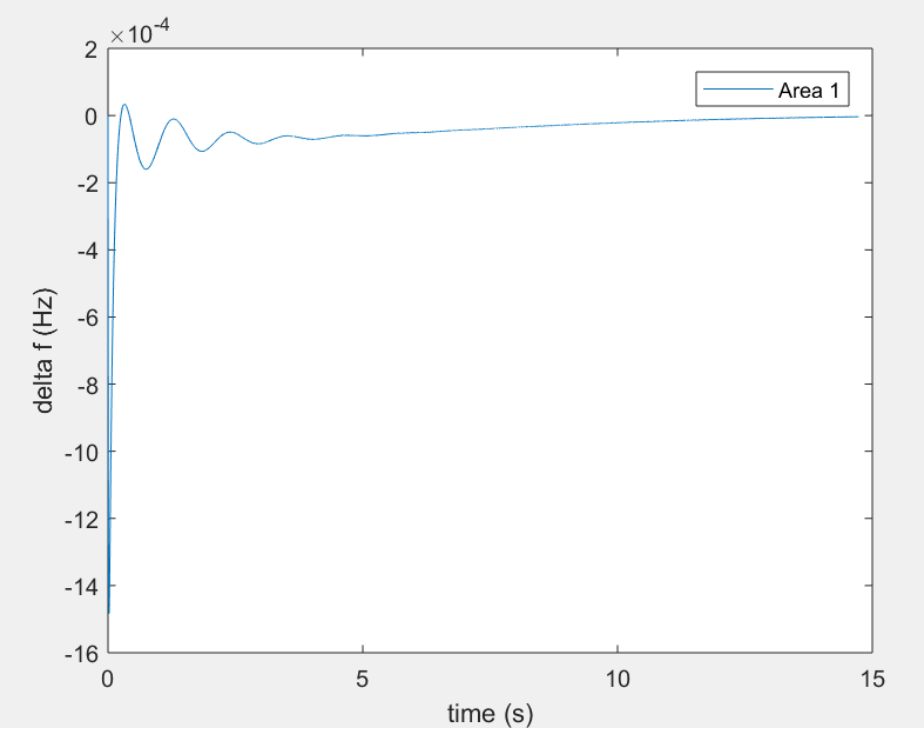

Figure 4.13 Response of area 1 in the two-area system with LQR controller and with more load at area 1.

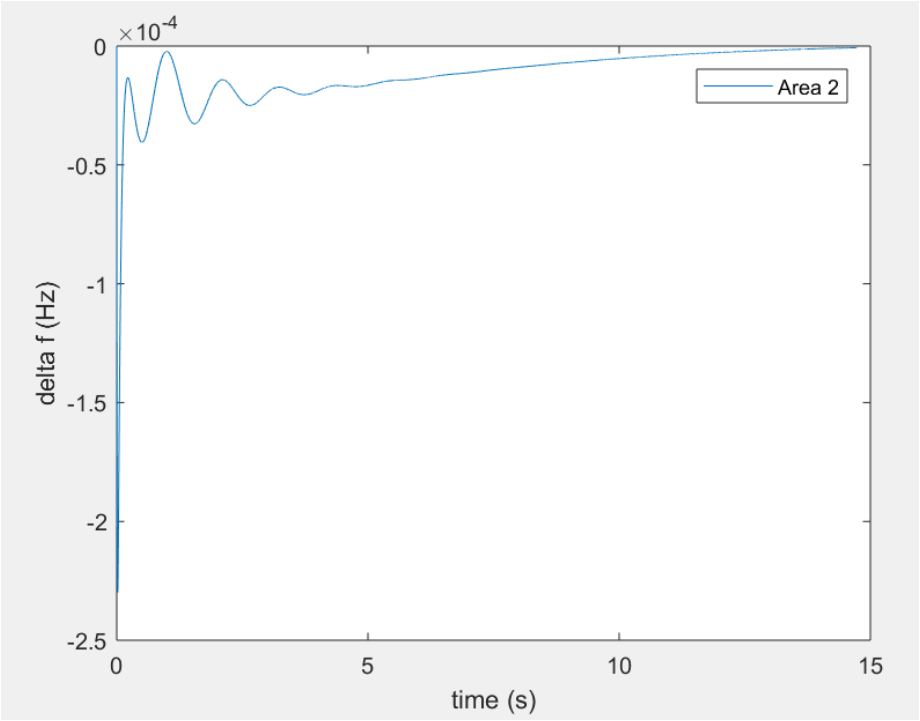

Figure 4.14 Response of area 2 in the two-area system with LQR controller and with more load at area 1.

Table 4.10 Response summary of the two-area system with LQR and with more load at area 1.

	Area 1	Area 2
Settling Time (s)	8.747515	10.44206
Undershoot (Hz)	-0.001483	-0.0002299
SSE (Hz)	0	0

4.4.3 Case 3: $\Delta P_{load2} > \Delta P_{load1}$

Figure 4.15, Figure 4.16 and Table 4.11 show the response for case 3 in which more change occurs on the load connected to area 2 than in area 1. The responses of both areas are similar to case 2 in terms of meeting the required specifications. It is observed that the changes of the load affect the undershoot more than the settling time when the LQR controller is applied to the system.

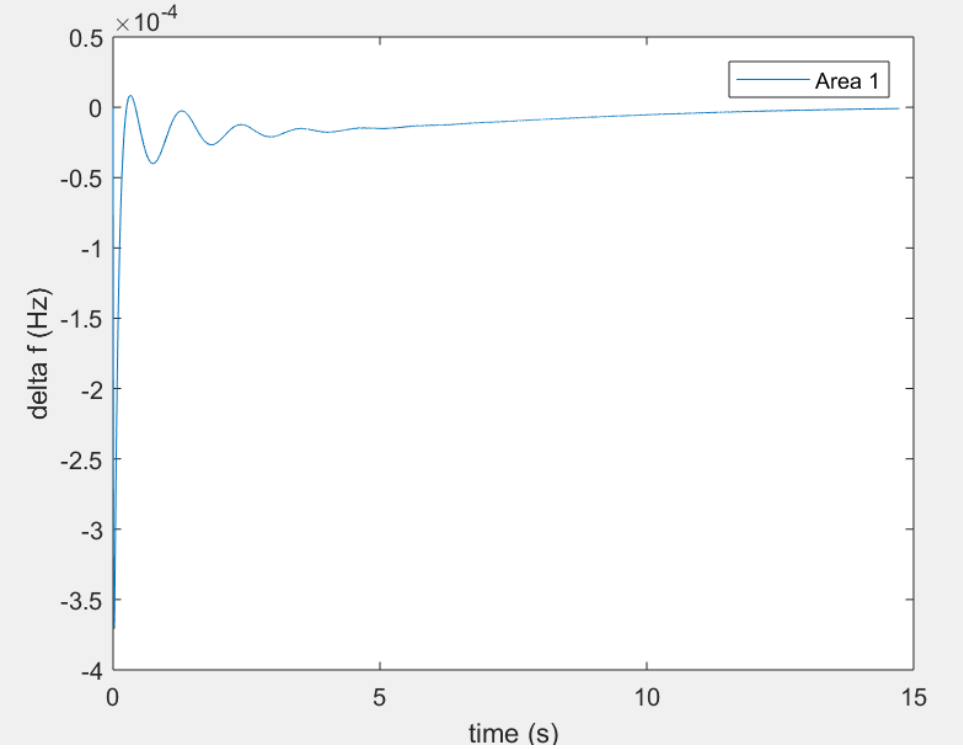

Figure 4.15 Response of area 1 in the two-area system with LQR controller and with more load at area 2.

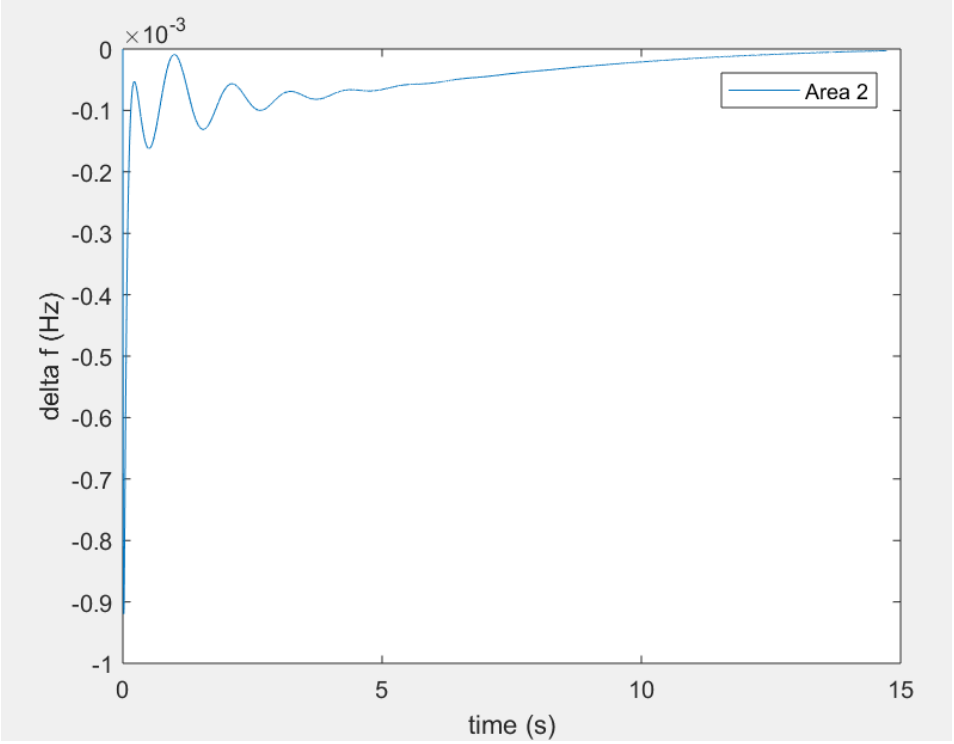

Figure 4.16 Response of area 2 in the two-area system with LQR controller and with more load at area 2.

Table 4.11 Response summary of the two-area system with LQR controller (more load at area 2.)

	Area 1	Area 2
Settling Time (s)	8.74751	10.44205
Undershoot (Hz)	-0.000371	-0.0009197
SSE (Hz)	0	0

4.4.4 Case 4: $\Delta P_{load1} = \Delta P_{load2} = 50\%$ (worst-case scenario)

Figure 4.17 and Table 4.12 show the response for case 4 in which both loads change simultaneously with the same amount (50%). It can be noted that even under this worst-case scenario the undershoot and the steady state error requirements are met by the LQR controller designed. It is noticed that the settling time in all cases did not change with the changes in the load.

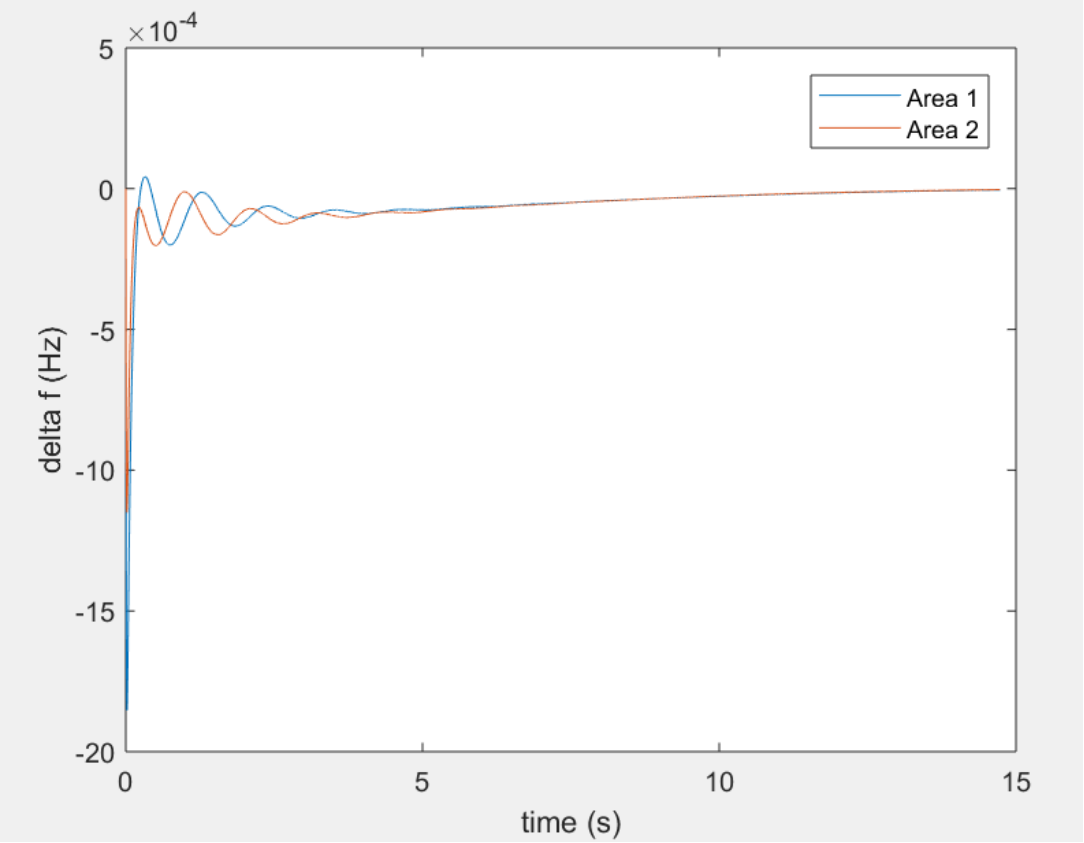

Figure 4.17 Response of both areas with LQR controller for equal change in load of 50%.

Table 4.12 Response summary of both areas with LQR controller for equal change in load of 50%.

	Area 1	Area 2
Settling Time (s)	8.7475	10.442
Undershoot (Hz)	-0.0018537	-0.0011496
SSE (Hz)	0	0

4.5 Design of PI Controller for PV Grid-Connected Two-Area Power Grid

By optimizing the system to get the best values of K_p and K_i before applying the FL controller, the optimization gave no values for K_p and only K_i values were obtained. Any K_p value added to area 2 made it worse in terms of undershoot and oscillations. Therefore, only integral controller was added with the value of $K_i = 0.1$ to the second area. Figure 4.18 shows the two-area system with PI controller.

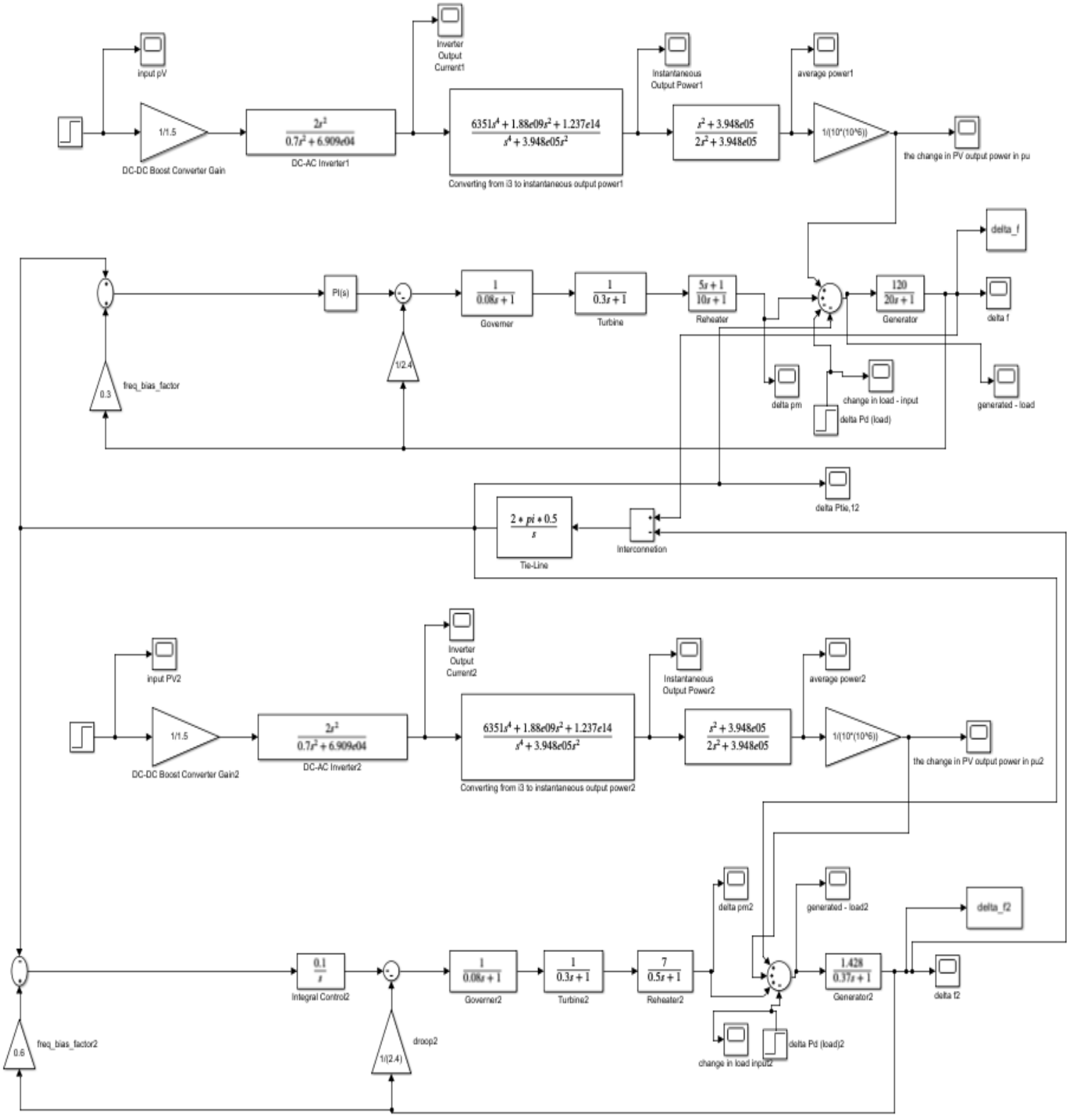

Figure 4.18 Two-area system with PI controller.

4.5.1 Case 1: Acceptable increase in load ($\Delta P_{load1} = \Delta P_{load2}$)

For the case of a reasonable equal increase in load that is equal in both areas, Figure 4.19, Figure 4.20 and Table 4.13 describe the responses and Figure 4.21 shows the tie-line power change. This tie-line power change represents the power transferred between these two areas with a zero steady state value. Area 2 satisfies the criteria of undershoot and steady state error, however, area 1 only satisfies the steady state error limit. Both of them have a long settling time.

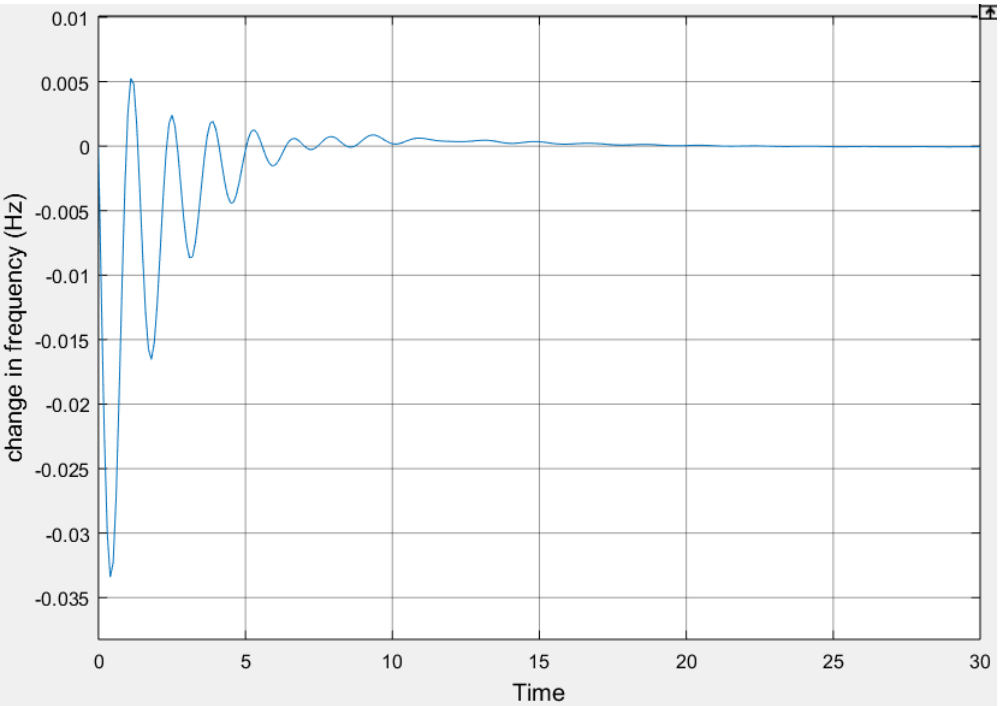

Figure 4.19 Response of area 1 in the two-area system for a reasonable increase in load.

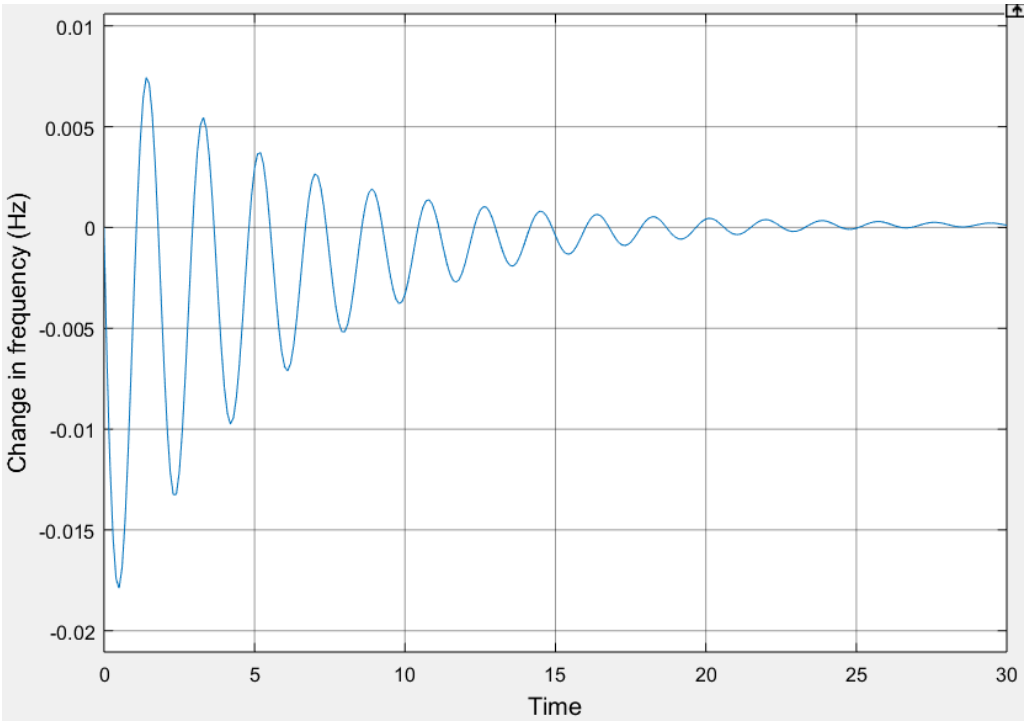

Figure 4.20 Response of area 2 in the two-area system for a reasonable increase in load.

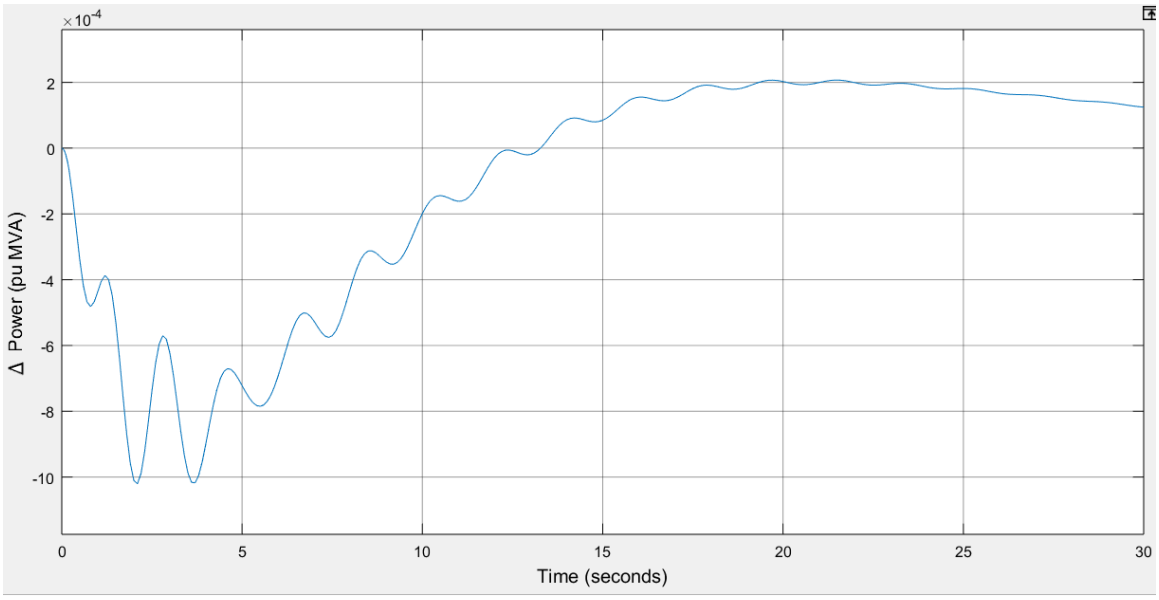

Figure 4.21 Tie-line power change response due to a reasonable increase in load.

Table 4.13 Response summary of the two-area system for a reasonable increase in load.

	Area 1	Area 2
Settling Time (s)	9.59875	22.1189
Undershoot (Hz)	-0.03340	-0.01788
SSE (Hz)	0	0

4.5.2 Case 2: $\Delta P_{load1} > \Delta P_{load2}$

In this case, area 1 still does not meet the undershoot criteria, but area 2 does. Figure 4.22, Figure 4.23 and Table 4.14 describe the response, while Figure 4.24 shows the tie-line power change between both areas.

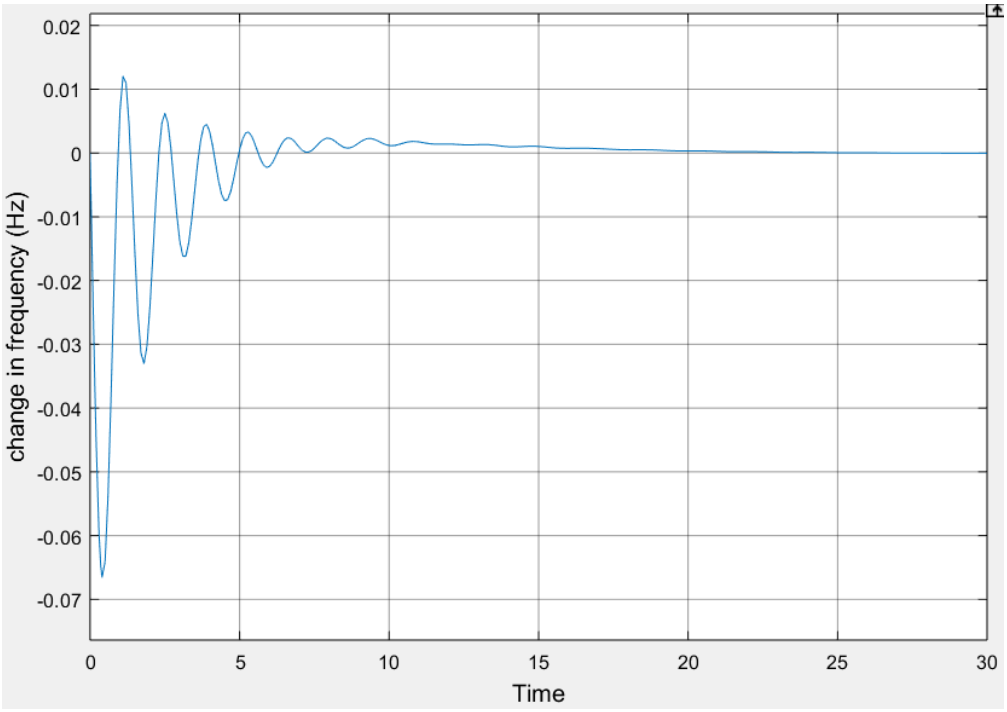

Figure 4.22 Response of area 1 in the two-area system due to more increase in load in area 1 than in area 2.

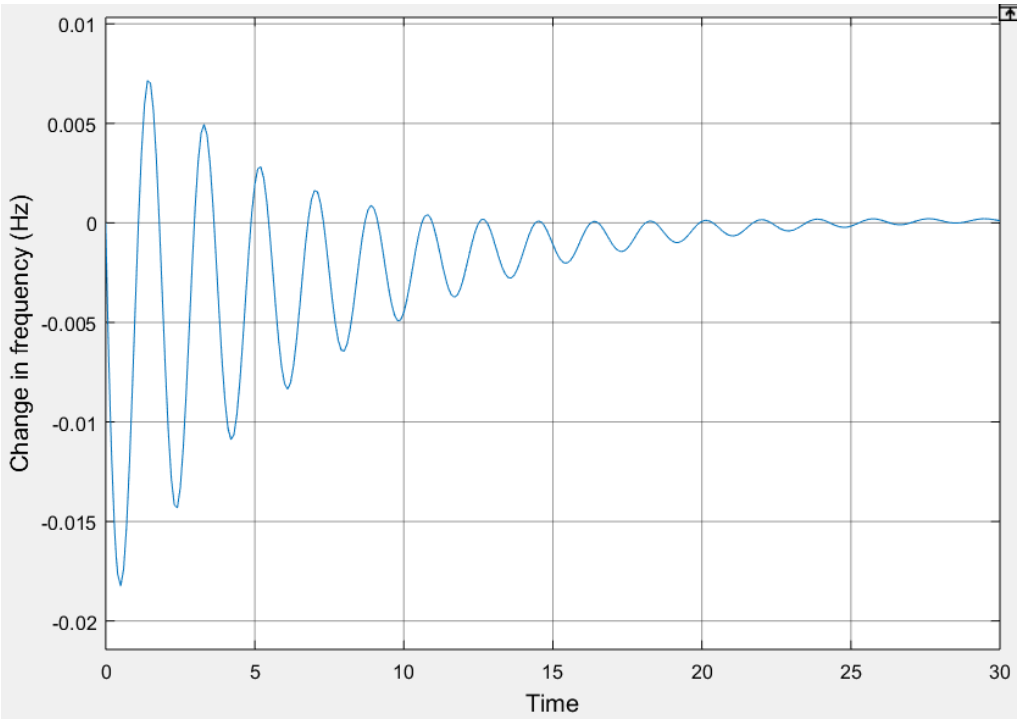

Figure 4.23 Response of area 2 in the two-area system due to more increase in load in area 1 than in area 2.

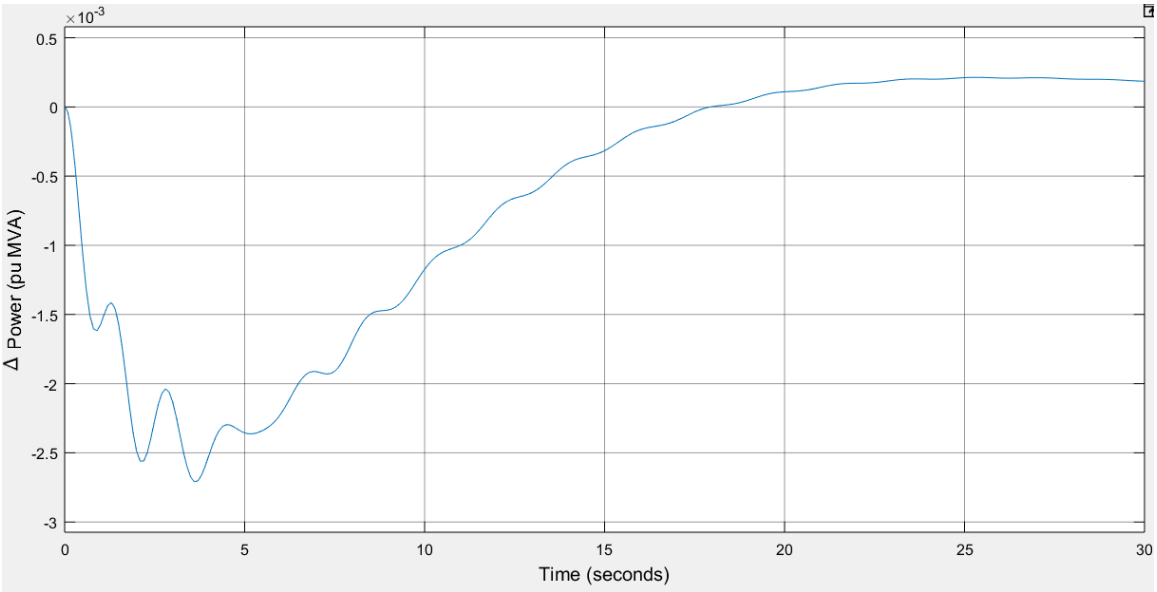

Figure 4.24 Tie-line power change between area 1 and 2 area 2 for more increase in load in area 1 than in area 2.

Table 4.14 Response summary of both areas for more increase in load in area 1 than in area 2.

	Area 1	Area 2
Settling Time (s)	12.32081	23.05033
Undershoot (Hz)	-0.06656	-0.018254
SSE (Hz)	0	0

4.5.3 Case 3: $\Delta P_{load2} > \Delta P_{load1}$

For case 3, neither area 1 nor area 2 satisfy the criteria of undershoot, and there are still some oscillations (resulting in a long and unacceptable settling time). Figure 4.25, Figure 4.26 and Table 4.15 show the response of the system for case 3 of the two-area system with PI controllers. Figure 4.27 shows the tie-line power change between both areas.

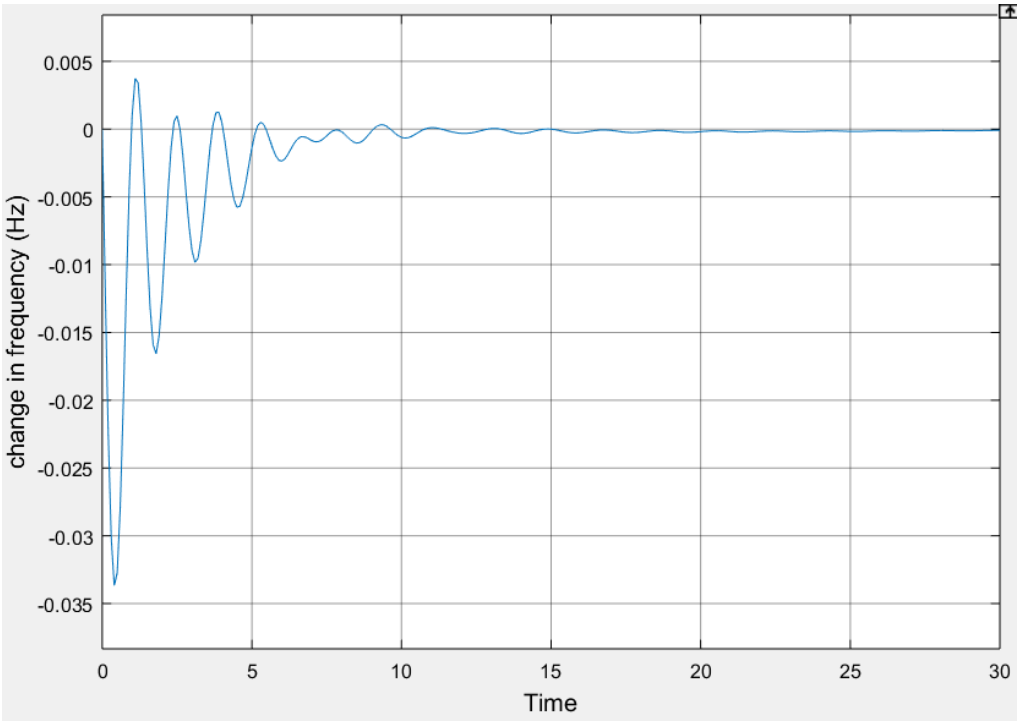

Figure 4.25 Response of area 1 in the two-area system due to more increase in load in area 2 than in area 1.

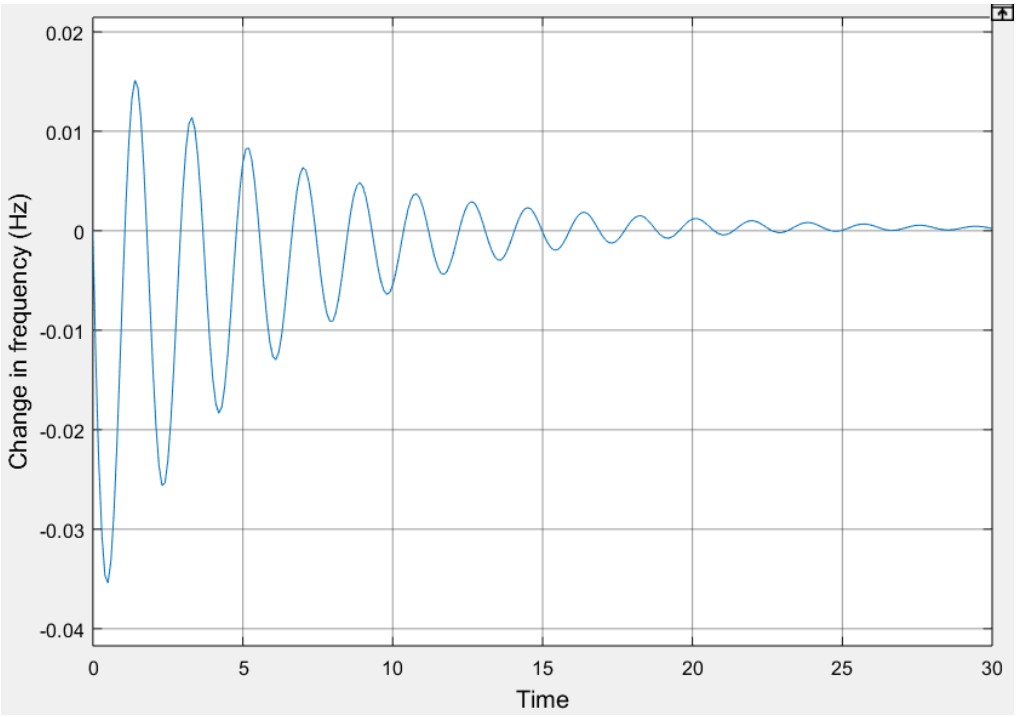

Figure 4.26 Response of area 2 in the two-area system due to more increase in load in area 2 than in area 1.

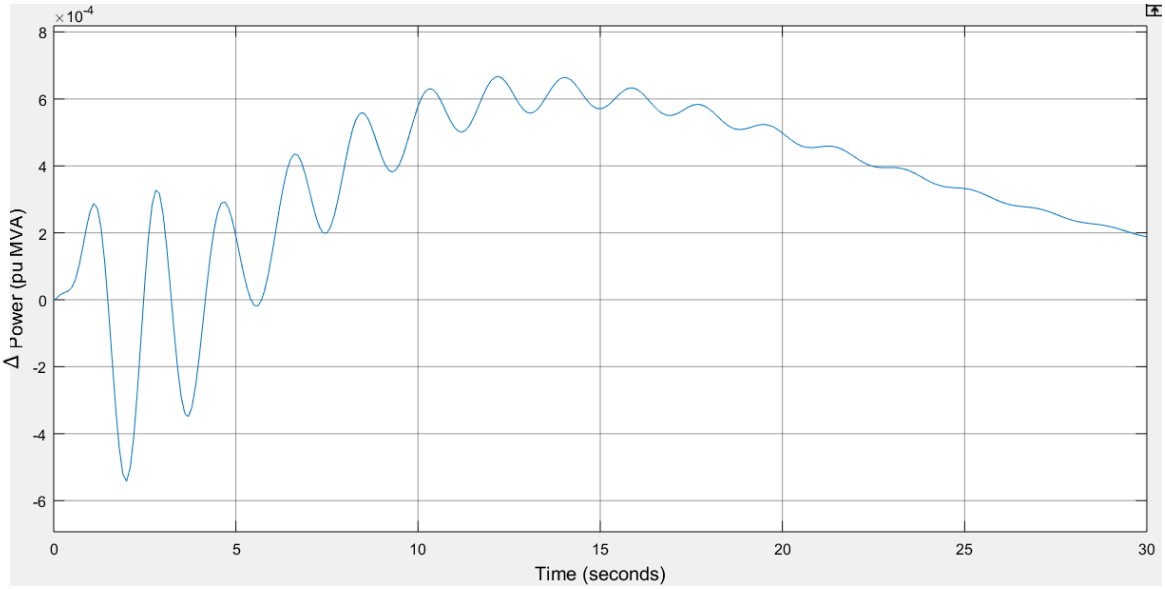

Figure 4.27 Tie-line power change between area 1 and area 2 due to more increase in load in area 1 than in area 2.

Table 4.15 Response summary of both areas due to more increase in load in area 2 than in area 1.

	Area 1	Area 2
Settling Time (s)	8.7972	24.0620
Undershoot (Hz)	-0.0336	-0.03541
SSE (Hz)	0	0

4.5.4 Case 4: $\Delta P_{load1} = \Delta P_{load2} = 50\%$ (worst-case scenario)

Figure 4.28, Figure 4.29 and Table 4.16 show the response of both areas in case 4 with PI controller. Also, the criteria required are not met. The responses are slightly enhanced than the case without any controller but with unacceptable limits. Figure 4.30 shows the tie-line power change between both areas.

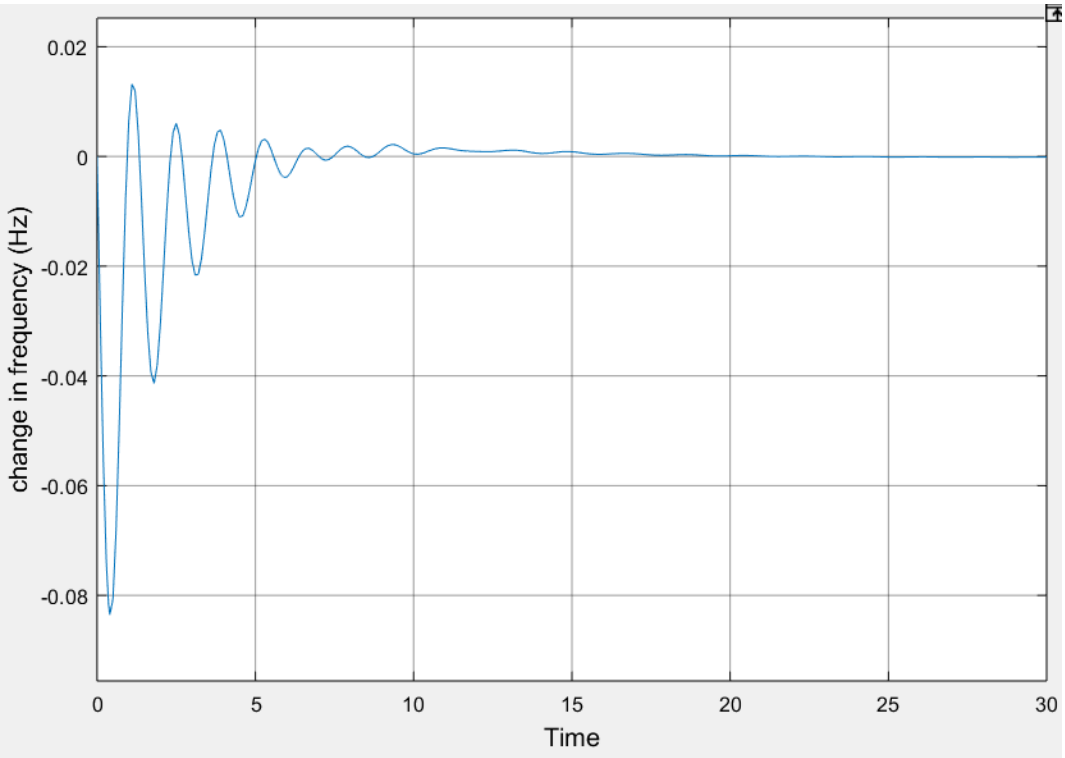

Figure 4.28 Response of area 1 in the two-area system for a 50% increase in load.

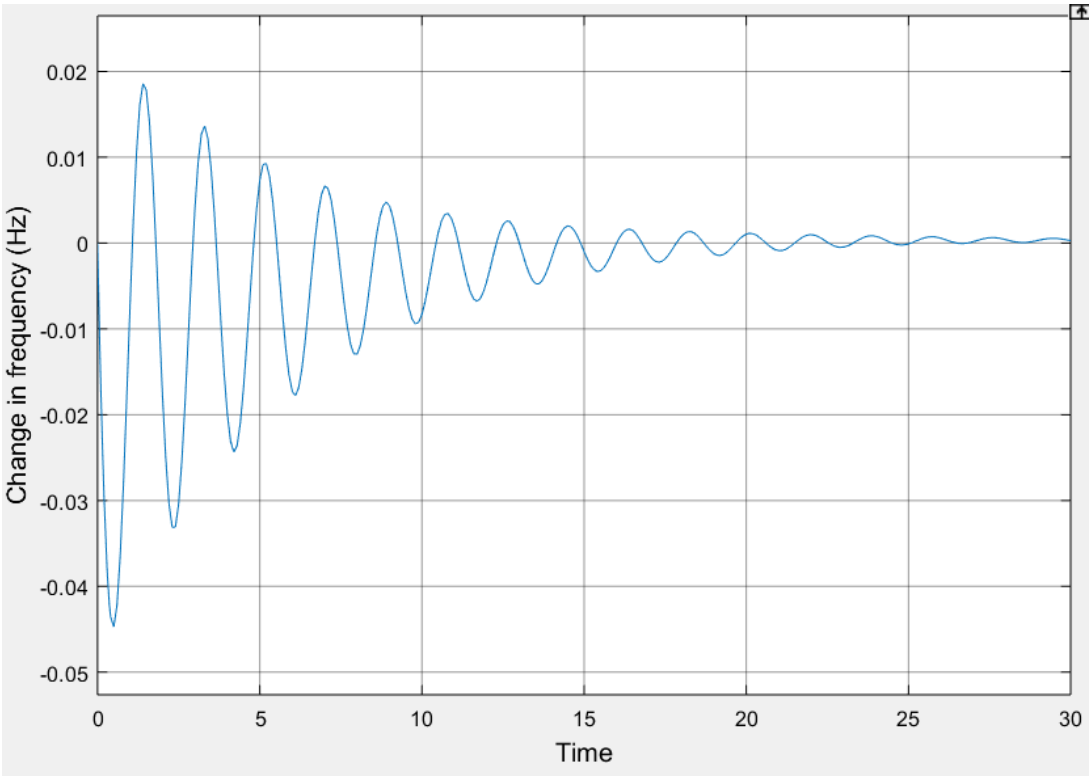

Figure 4.29 Response of area 2 in the two-area system for a 50% increase in load.

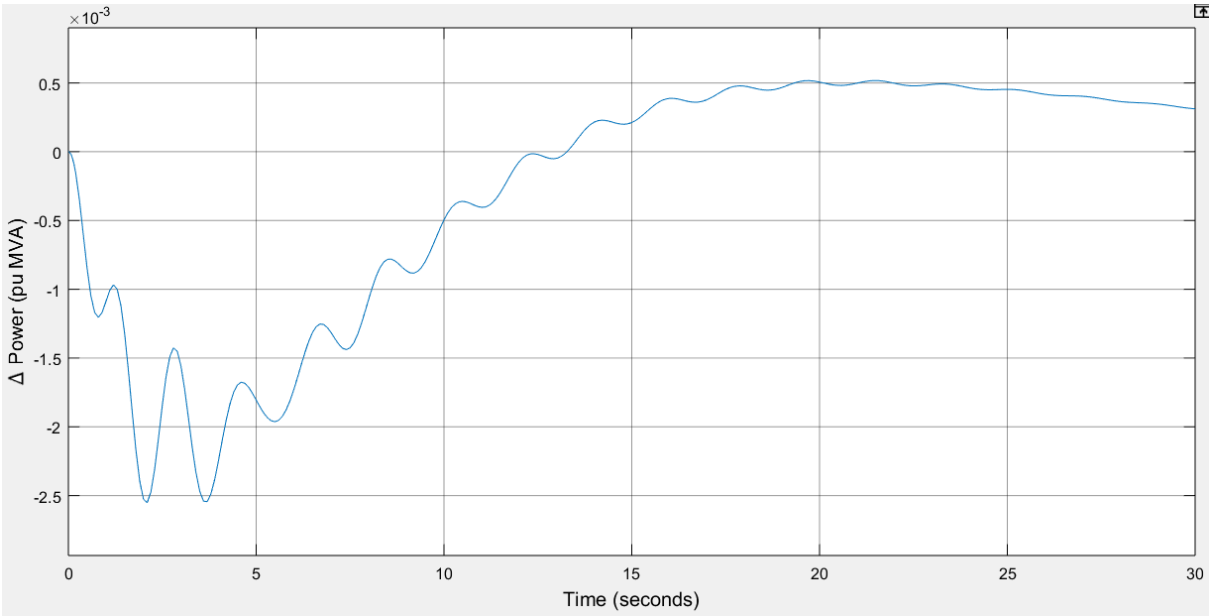

Figure 4.30 Tie-line power change between area 1 and area 2 for a 50% increase in load.

Table 4.16 Response summary for both areas due to an increase in load of 50%.

	Area 1	Area 2
Settling Time (s)	9.5987	22.11898
Undershoot (Hz)	-0.0835	-0.04472
SSE (Hz)	0	0

4.6 Design of Fuzzy Logic Controller for PV Grid-Connected Two-Area Power Grid

Figure 4.31 shows the two-area system with both PI and FLC. The K_p and K_i values in the PI controller of area 1 were modified to $K_p = 0.6$ and $K_i = 0.9$ and for the second area $K_i = 1.1$ because they gave the best response in the two-area system. The fuzzy rules designed for the two-area are the same as the ones designed in section 4.3.

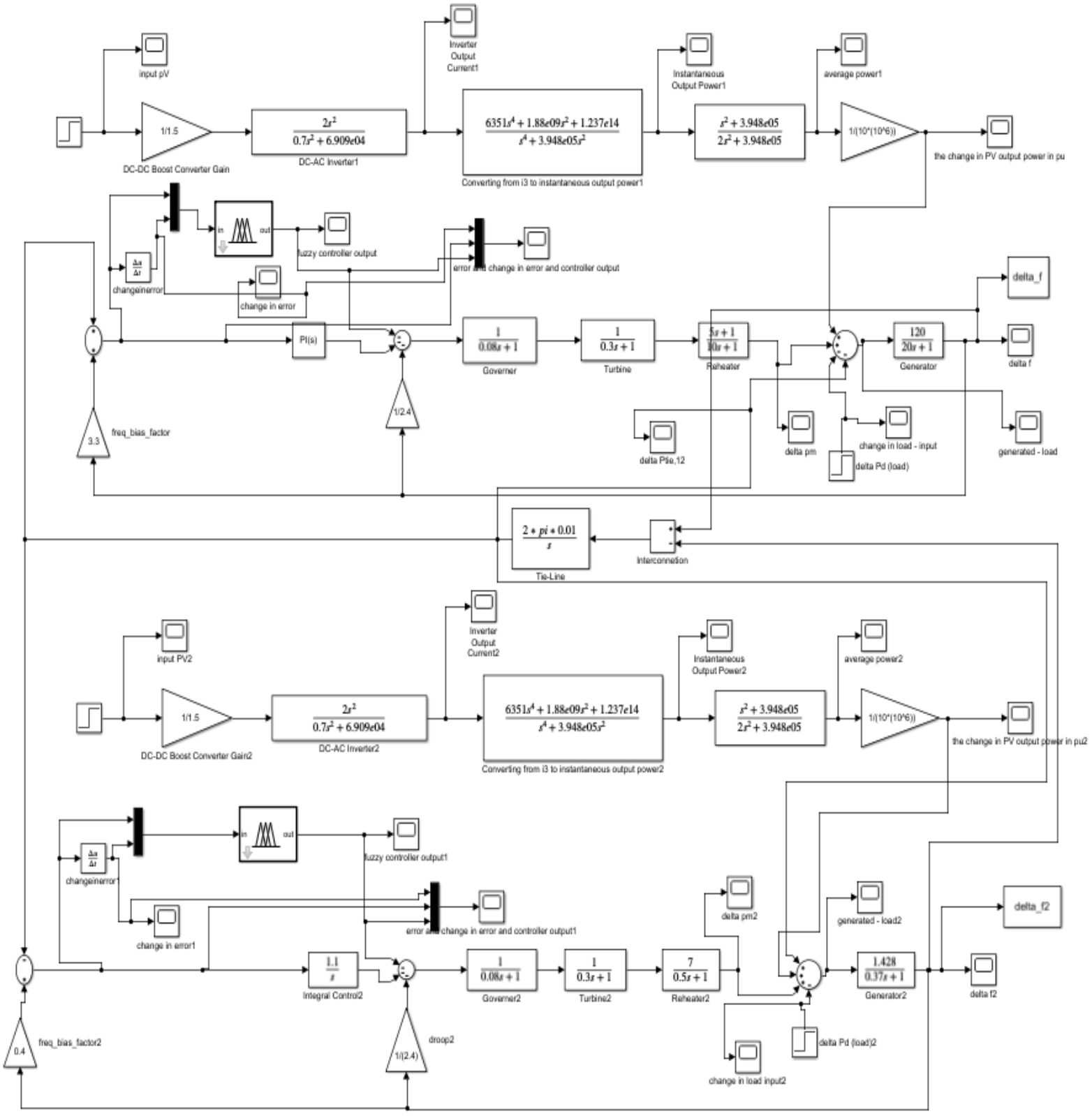

Figure 4.31 Two-area system with PI and FLC.

4.6.1 Case 1: Acceptable increase in load ($\Delta P_{load1} = \Delta P_{load2}$)

Figure 4.32, Figure 4.33 and Table 4.17 show the response of both areas due to a reasonable change in load that is equal between both systems. The tie-line power change between both areas is shown in Figure 4.34. For this case, the response is within the required criteria for the undershoot, the settling time and the steady state error. The settling time is close to the required range due to the limitation of the fuzzy logic controller as there is a maximum improvement that could occur after the application of the controller. Even with the PI case it has been shown that neither the undershoot nor the settling time could be met even with many iterations in the optimization process. This is because the nature of the controller itself can only help improve a certain system to a certain extent. However, the enhancement that the FL controller provided to the system is obvious in comparison with PI controllers.

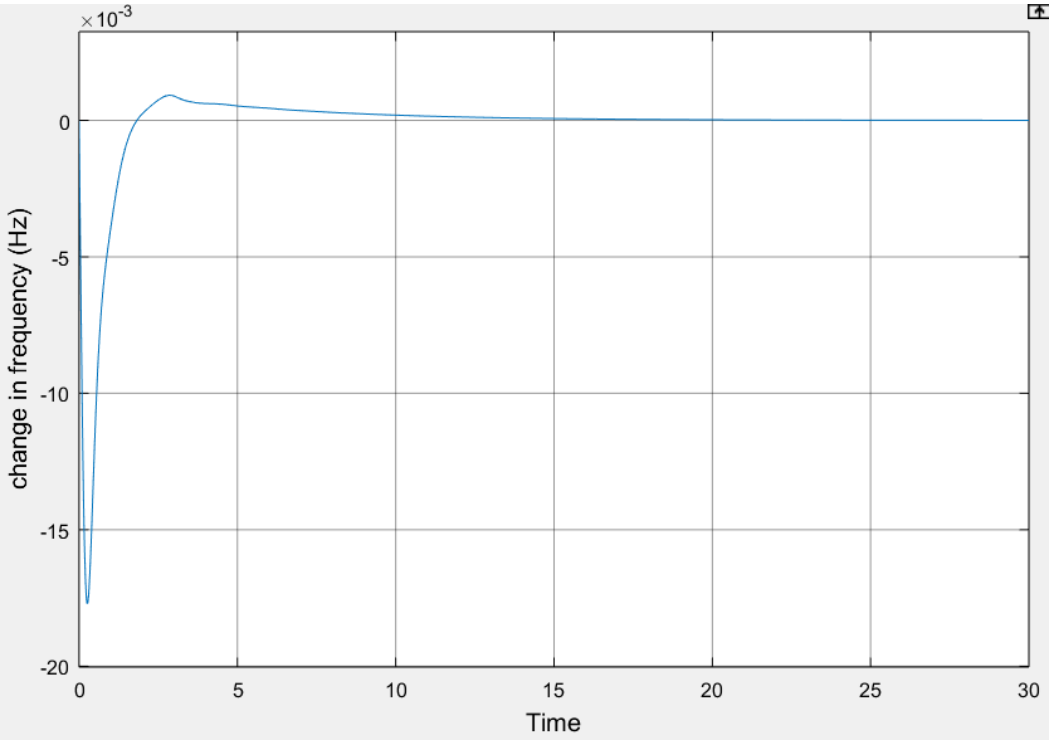

Figure 4.32 Response of area 1 with PI and fuzzy logic controllers for equal and reasonable change in load.

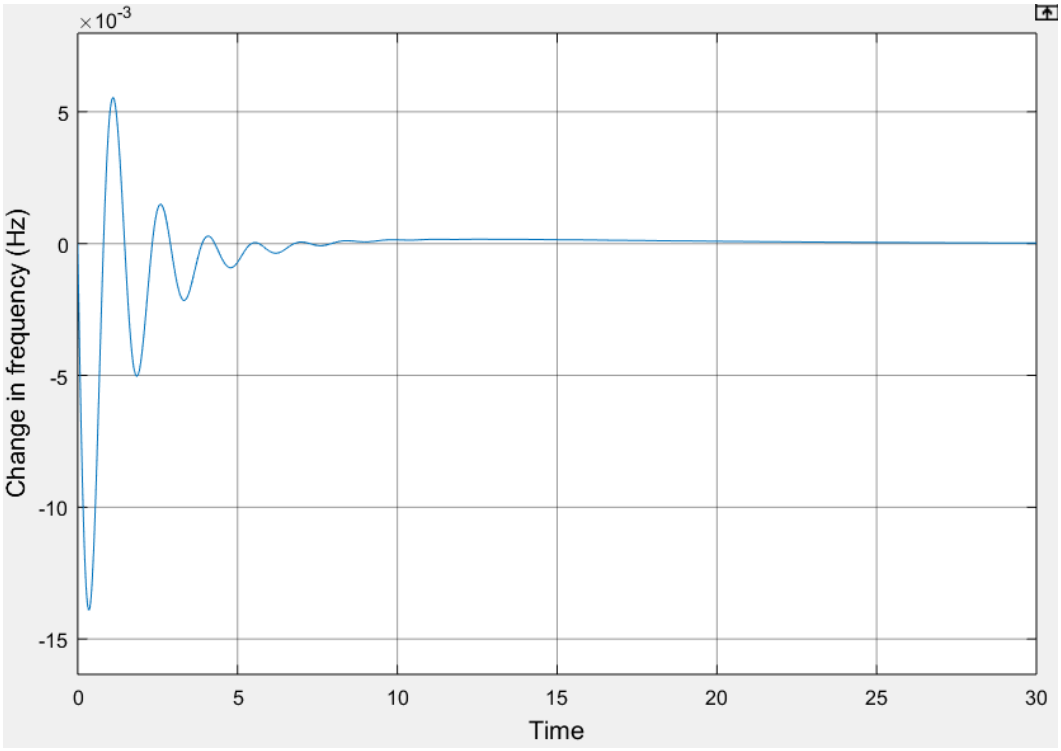

Figure 4.33 Response of area 2 with PI and fuzzy logic controllers for equal and reasonable change in load.

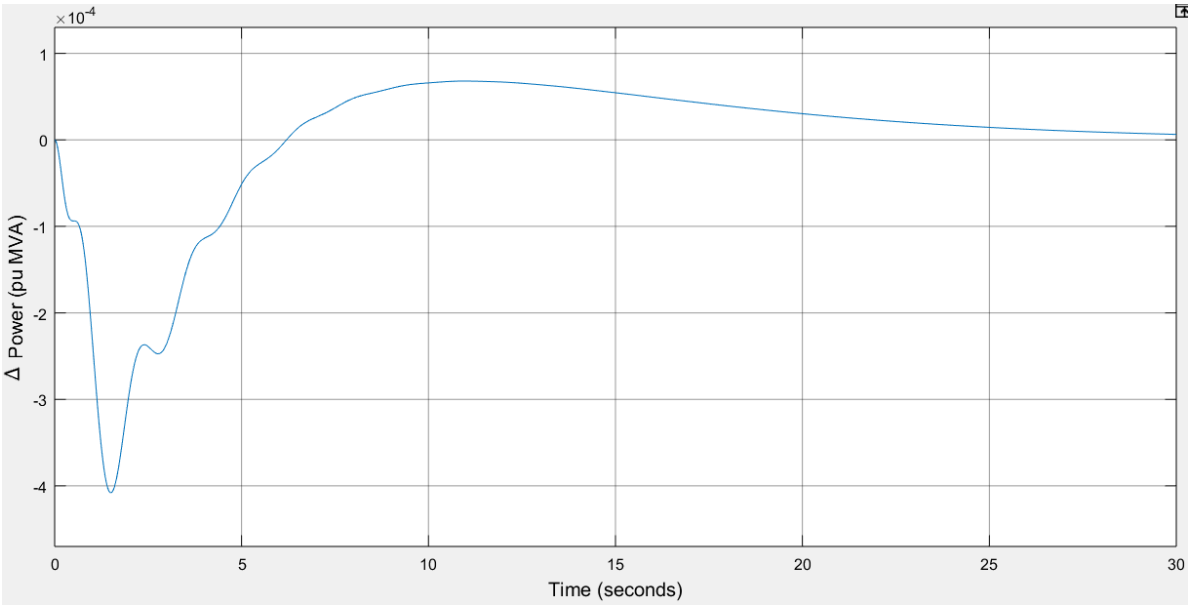

Figure 4.34 Tie-line power change between area 1 and 2 for the system with PI and FLC (reasonable change in load).

Table 4.17 Response summary of both areas with PI and FLC for equal and reasonable change in load.

	Area 1	Area 2
Settling Time (s)	7.4	6.4828
Undershoot (Hz)	-0.0177	-0.01390
SSE (Hz)	0	0

4.6.2 Case 2: $\Delta P_{load1} > \Delta P_{load2}$

Figure 4.35, Figure 4.36 and Table 4.18 show the response of the two-area system with the load increase in area 1 being more than that of area 2. Figure 4.37 shows the tie-line power change between both areas for this case. The criteria are met for both areas, which shows the big advantage of adding FLC to the system rather than the conventional controllers (PI).

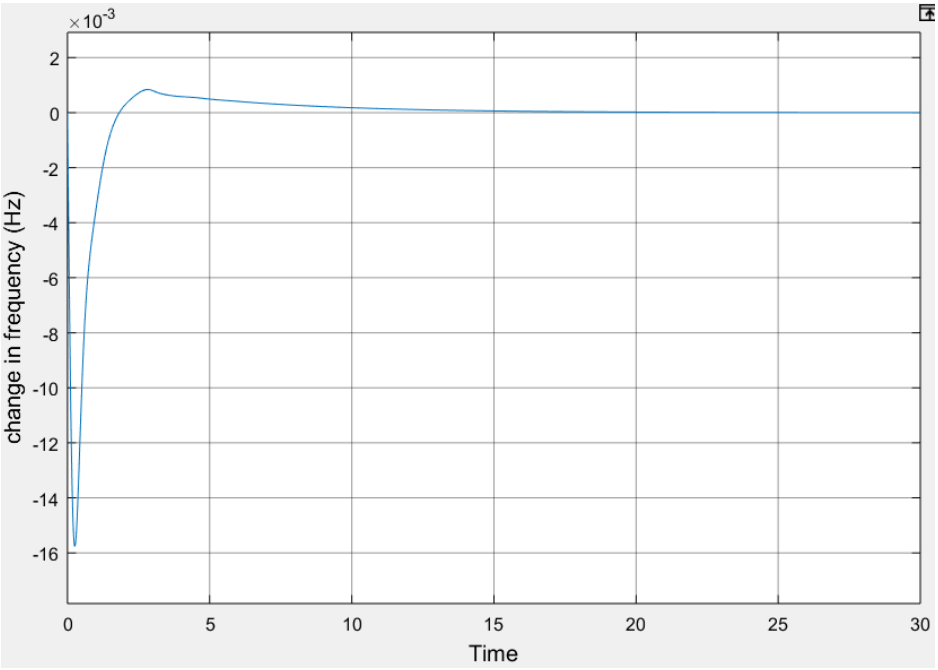

Figure 4.35 Response of area 1 in the two-area system with PI and fuzzy logic controllers (more load in area 1 than 2).

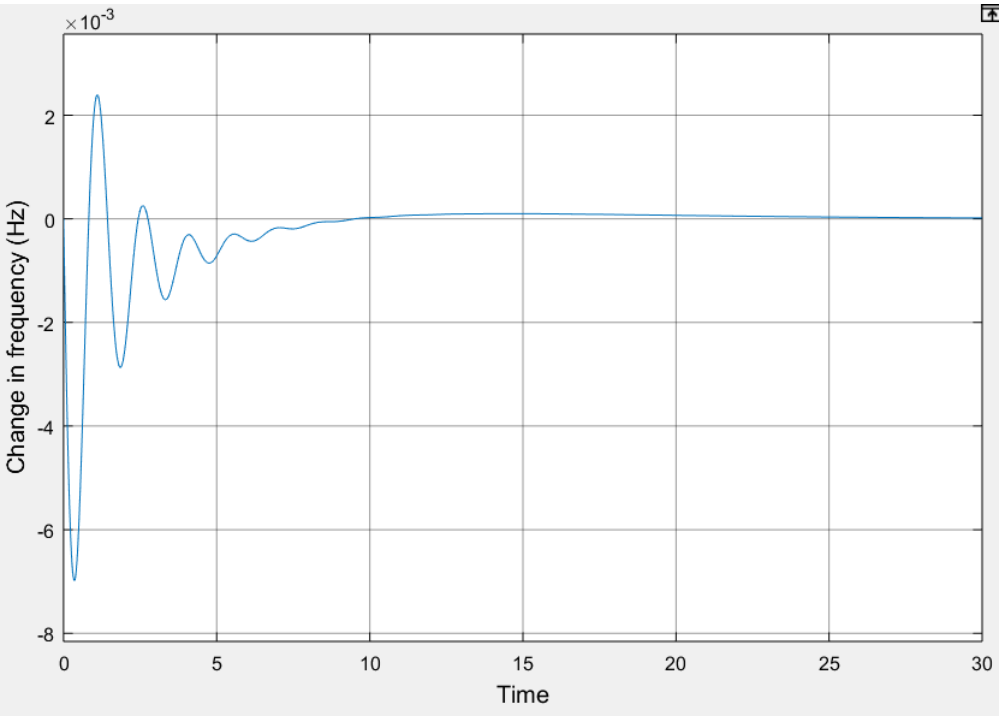

Figure 4.36 Response of area 2 in the two-area system with PI and fuzzy logic controllers (more load in area 1 than 2).

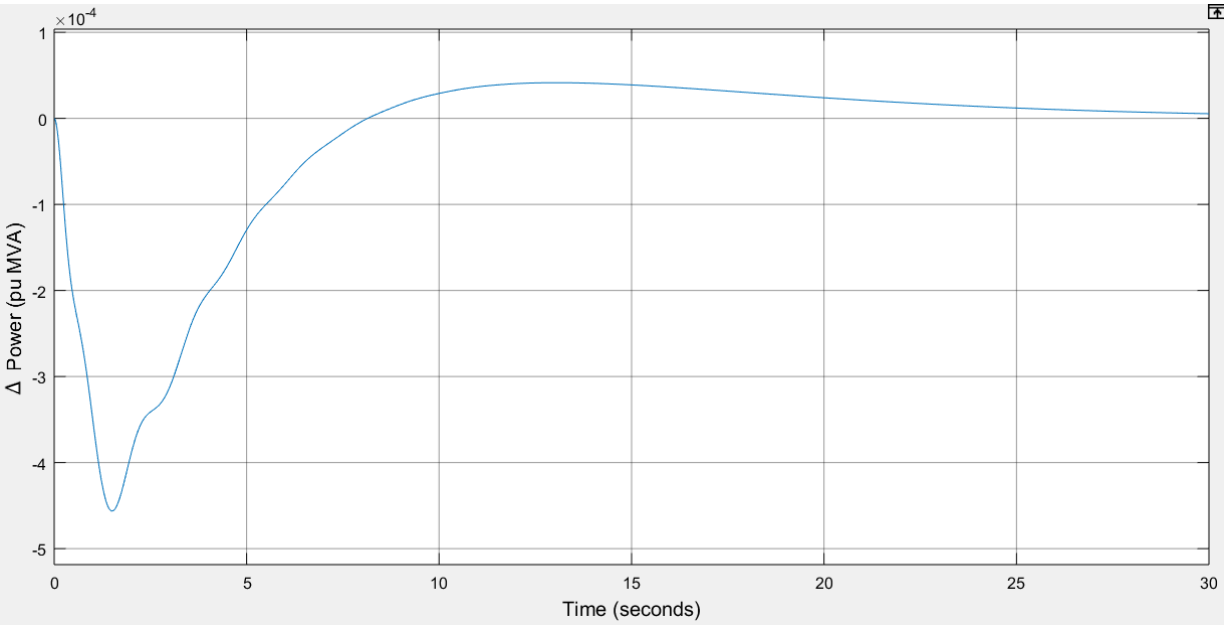

Figure 4.37 Tie-line power change between area 1 and 2 for the system with PI and fuzzy logic controllers (more load in area 1 than 2).

Table 4.18 Response summary of both areas with PI and FLC (more load in area 1 than 2).

	Area 1	Area 2
Settling Time (s)	7.2646	7.88814
Undershoot (Hz)	-0.01576	-0.006985
SSE (Hz)	0	0

4.6.3 Case 3: $\Delta P_{load2} > \Delta P_{load1}$

Figure 4.38, Figure 4.39 and Table 4.19 show the response of the two-area system with the load increase in area 2 more than that of area 1. Figure 4.40 shows the tie-line power change between both areas for this case. Also, the responses of both areas meet the criteria.

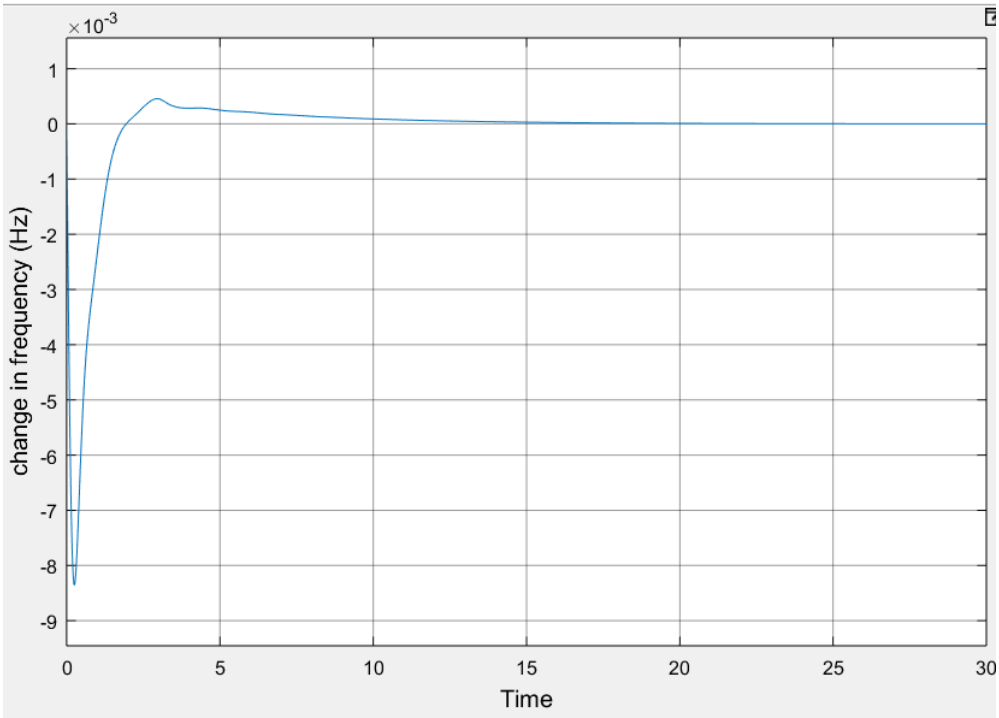

Figure 4.38 Response of area 1 in the two-area system with PI and FLC (more load in area 2 than 1).

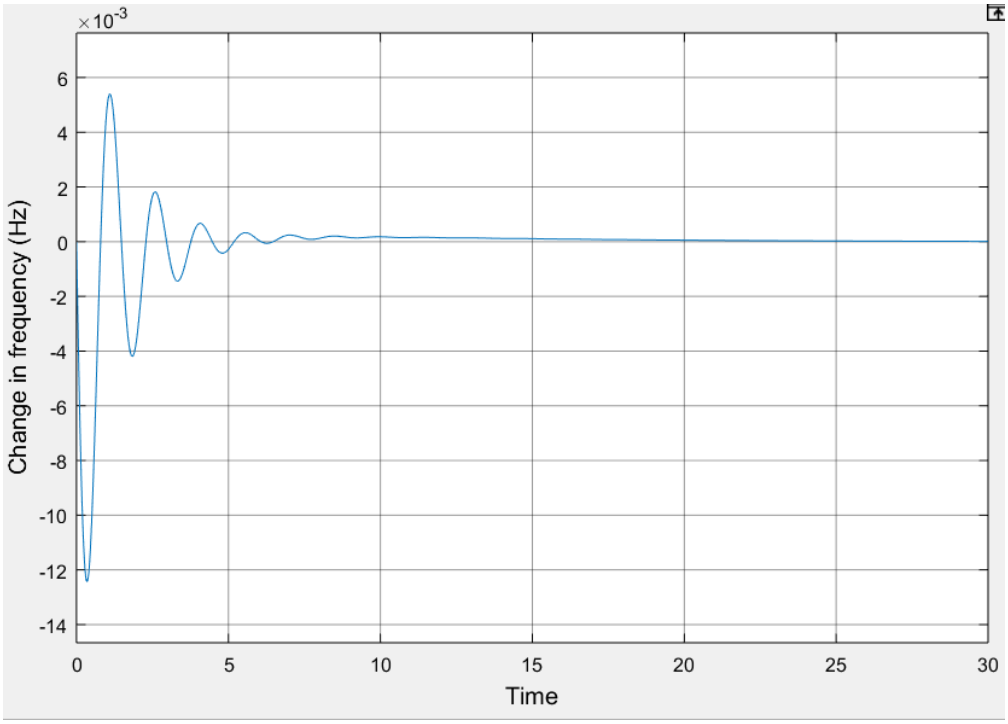

Figure 4.39 Response of area 2 in the two-area system with PI and FLC (more load in area 2 than 1).

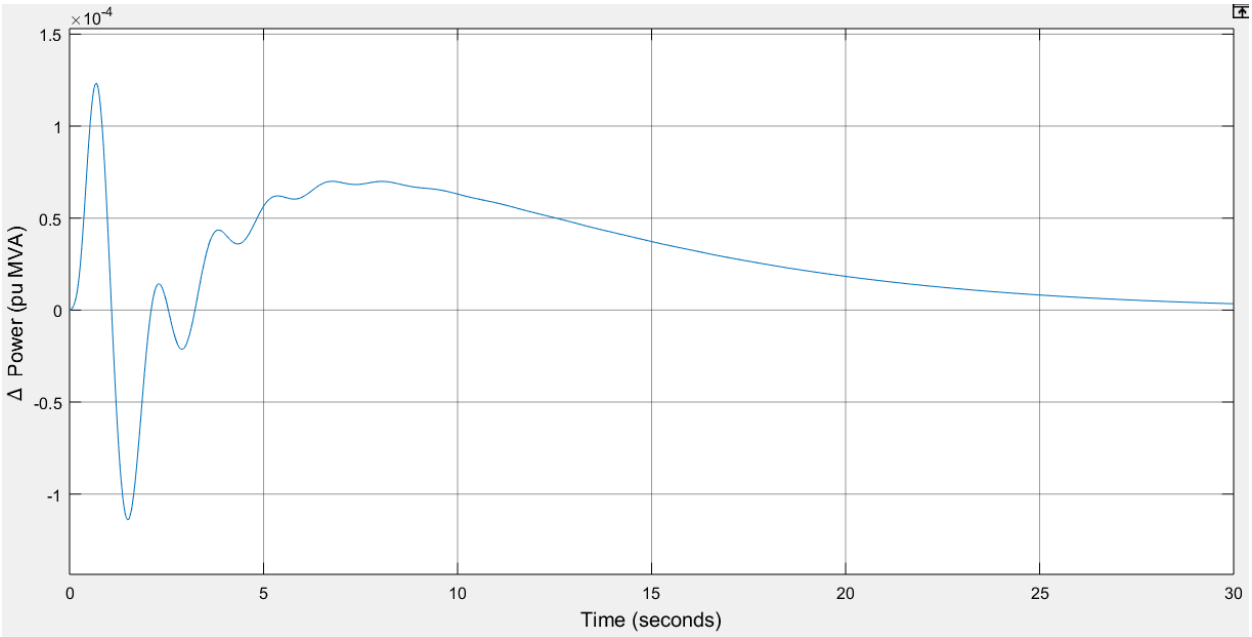

Figure 4.40 Tie-line power change between area 1 and 2 for the system with PI and fuzzy logic controllers (more load in area 2 than 1).

Table 4.19 Response summary of both areas with PI and FLC (more load in area 2 than 1).

	Area 1	Area 2
Settling Time (s)	7.0742	5.75177
Undershoot (Hz)	-0.0083	-0.0124
SSE (Hz)	0	0

4.6.4 Case 4: $\Delta P_{load1} = \Delta P_{load2} = 50\%$ (worst-case scenario)

Figure 4.41, Figure 4.42 and Table 4.20 show the response of the two-area system with a sudden 50% increase in load. Figure 4.43 shows the tie-line power change between both areas for this case. The criteria of undershoot and settling time are not exactly met, but they are fairly acceptable since this is the assumed worst-case scenario. A big improvement of the system response can still be observed from the uncontrolled case or the controlled with PI and even the LQR for two-area. The best settling time in the two-area system was achieved by the FL controller even in the worst-case scenario.

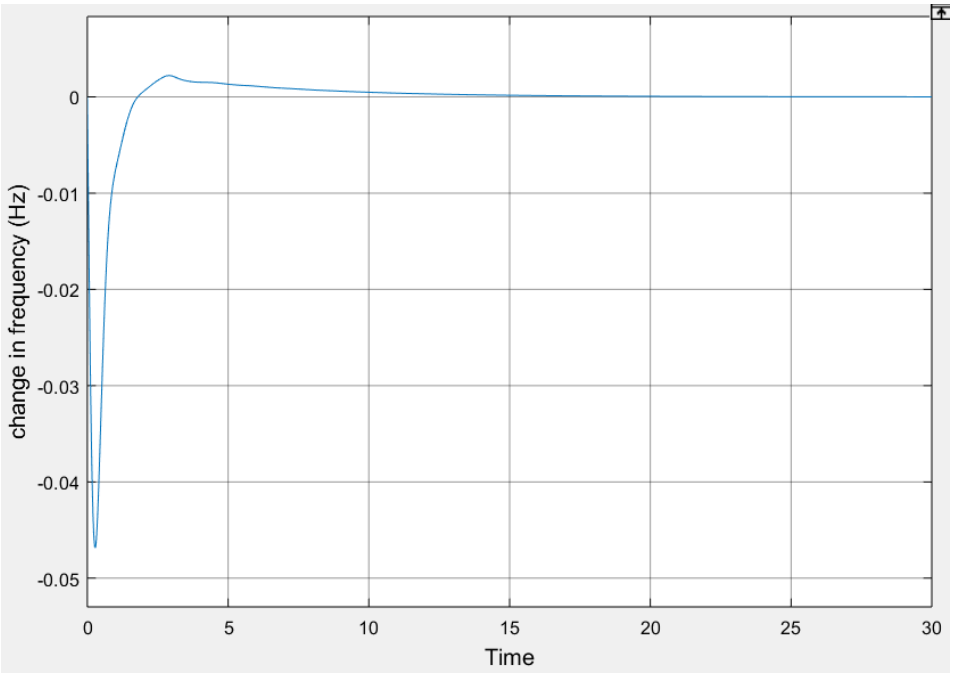

Figure 4.41 Response of area 1 with PI and FLC for 50% increase in load.

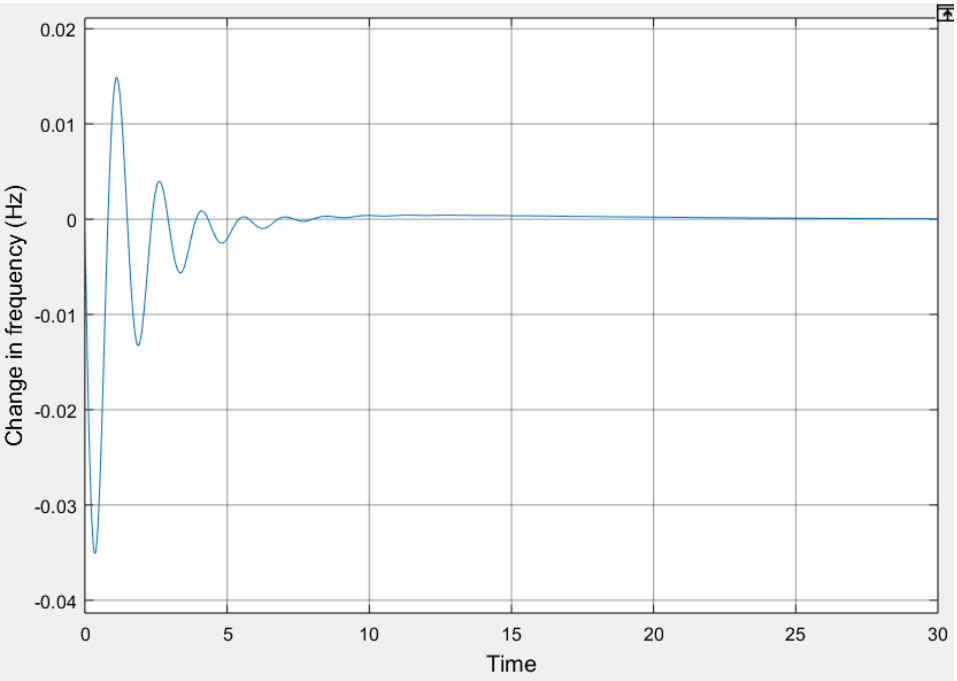

Figure 4.42 Response of area 2 with PI and FLC for 50% increase in load.

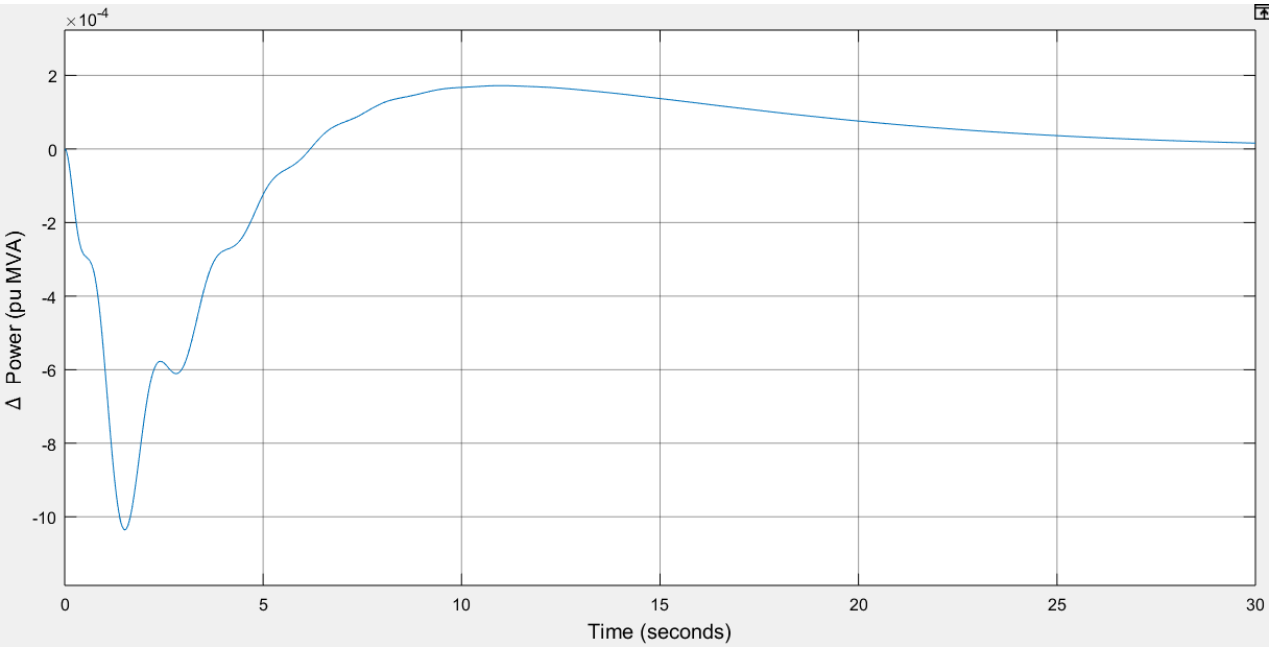

Figure 4.43 Tie-line power change between area 1 and 2 for the system with PI and fuzzy logic controllers (for 50% increase in load).

Table 4.20 Response summary of both areas with PI and FLC for 50% increase in load.

	Area 1	Area 2
Settling Time (s)	6.734636	6.4828
Undershoot (Hz)	-0.046853	-0.03509
SSE (Hz)	0	0

Chapter 5: Analysis & Conclusion

In this chapter, the frequency and power exchange errors after the implementation of the three controllers (LQR, PI and FLC) are compared for the single-area and the two-area systems, along with observations regarding the responses that will lead to the final conclusion. The uncontrolled system response summary is re-written for the worst-case scenario (case 2 in single area and case 4 in two-area) for the comparison purposes. All the comparisons are for the grid with the PV system connected to it and operating at MPP. The best response that meets all the criteria in each comparison is highlighted in green in the comparison tables, keeping in mind that the criteria to be met are settling time less than 3s, undershoot less than 0.02 and steady state error equals to 0.

As mentioned from the beginning, the integral controller forced the system to have a zero steady state error, thus, even with LQR and FL controllers designed, the integral controller was already part of the model. Since K_i controller adds one state variable to the system, it had to be taken into consideration in the mathematical models used to design the controllers. Therefore, all the controlled systems in this thesis, no matter what method is used for the control, has a steady state error of 0.

5.1 PV Grid Connected Single-Area Analysis

Figure 5.1 shows the comparison between the responses due to the three different controllers for the single-area system connected to PV operating at MPP for case 1 and Table 5.1 summarizes the comparison for both cases.

In terms of meeting the system response specifications, the LQR controller gave better response in both cases (case 1 and case 2) for the single-area system connected to PV. As for the PI controller, it did not meet the specifications (of undershoot and settling time) even for the reasonable increase in load. The PI controller also added oscillations to the system as shown in Figure 5.1.

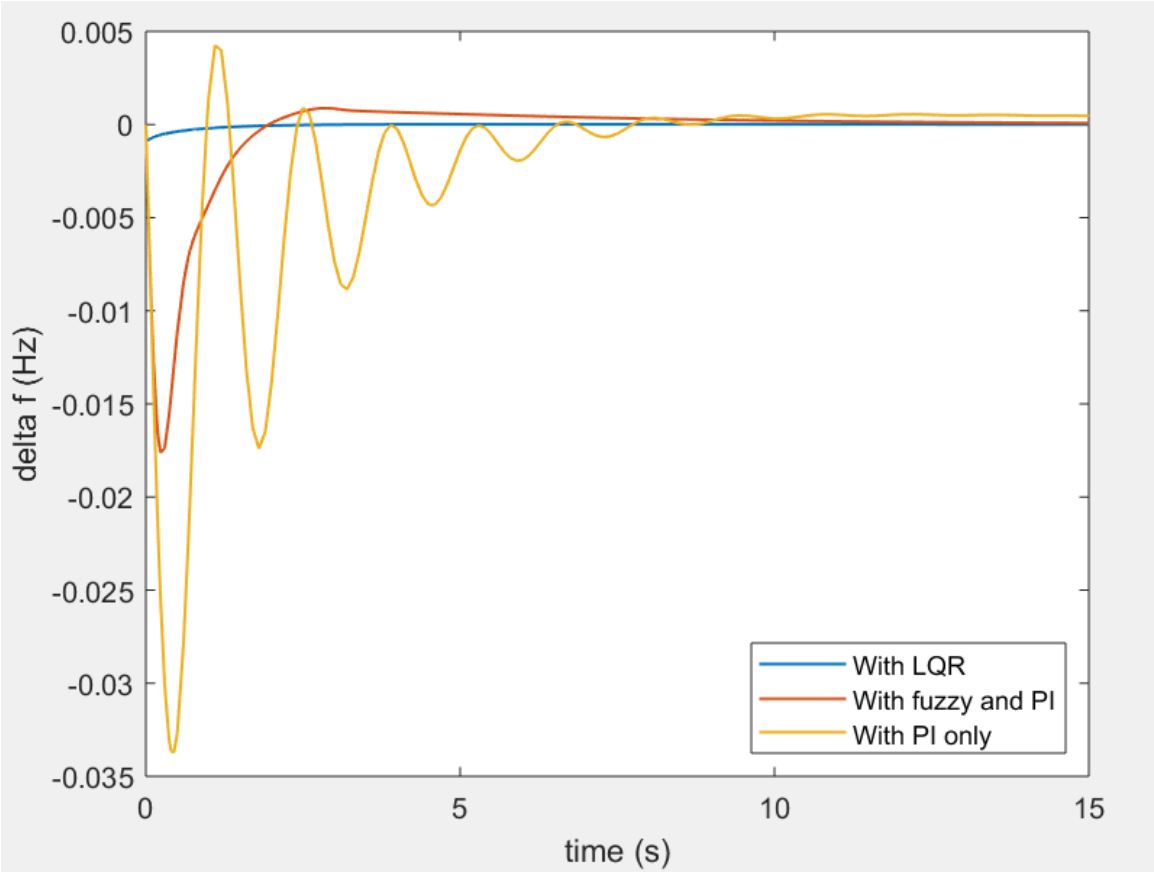

Figure 5.1 Comparison between LQR, PI and FLC for the single-area system connected to PV due to a reasonable change in load.

Table 5.1 Summary of comparisons between all controllers for the single-area system connected to PV.

		Settling Time	Undershoot	SSE
Case 1 (reasonable increase in load)	**LQR**	2.68106	-8.9809e-04	0
	PI	6.3335	-0.033733	0
	FLC	7.4217	-0.01761	0
Case 2 ($\Delta P_{load} = 50\%$)	**Uncontrolled**	18.2	-2.33299	-1.175
	I	19.7	-1.8399269	0
	LQR	2.68106	-0.009879	0
	PI	6.3335	-0.08433	0
	FLC	7.13032	-0.0466	0

The FLC almost met all criteria for case 1 (reasonable load) with the settling time a little bit off the range. Although the FLC did not meet the undershoot specification for case 2, there are two points to be considered. First, that this is the improbable case which is unlikely to occur. Second, that it enhanced the system greatly in terms of undershoot and oscillations compared to the system with PI controller only as shown in Figure 5.2 which demonstrates a comparison between PI and FL controllers for the single-area system (case 2).

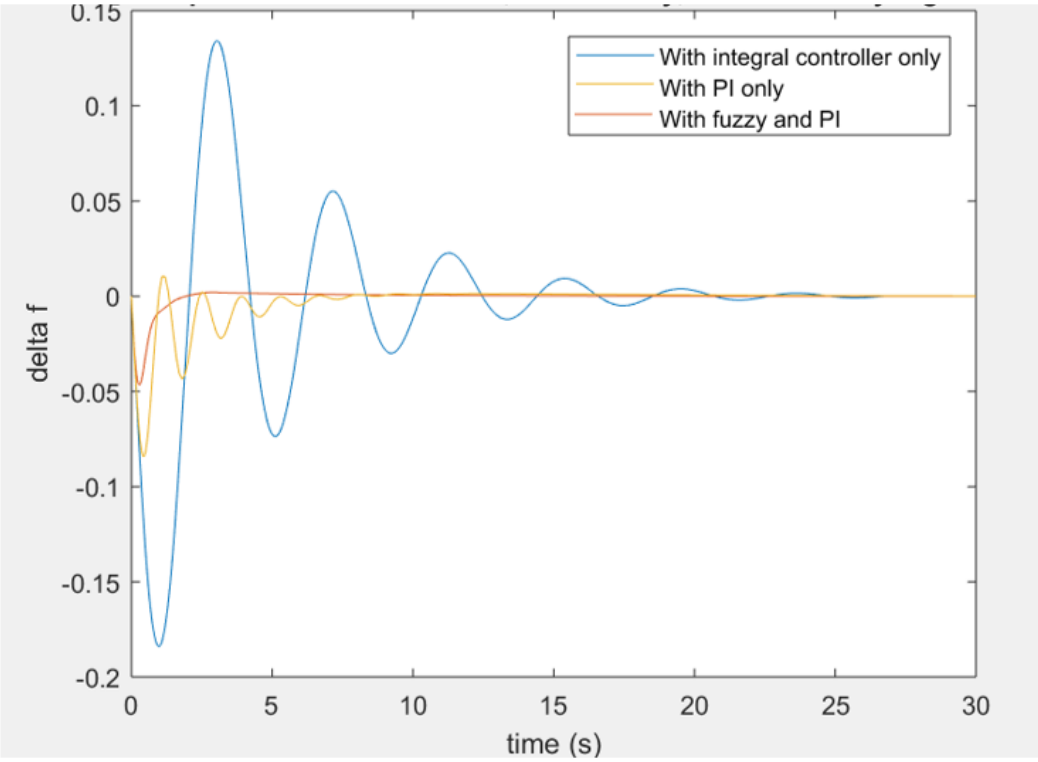

Figure 5.2 Comparison between I, PI and FLC for the single-area system connected to PV (due to 50% increase in load).

5.2 PV Grid Connected Two-Area Analysis

Figures 5.3 and 5.4 shows the comparison between the responses due to the three different controllers for the two-area system connected to PV operating at MPP for case 1 and Table 5.2 summarizes the comparison for all cases.

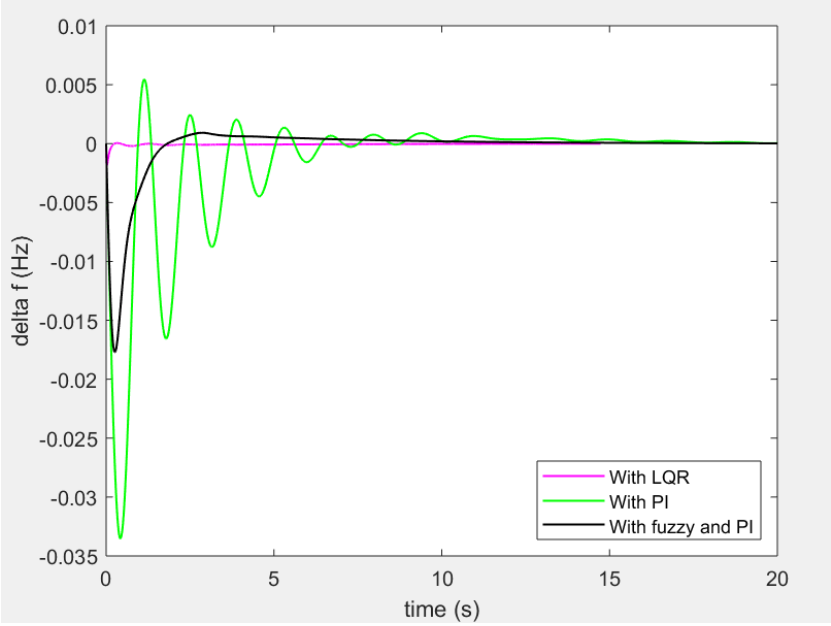

Figure 5.3 Comparison between LQR, PI and FLC for area 1 in the two-area system connected to PV due to a reasonable change in load.

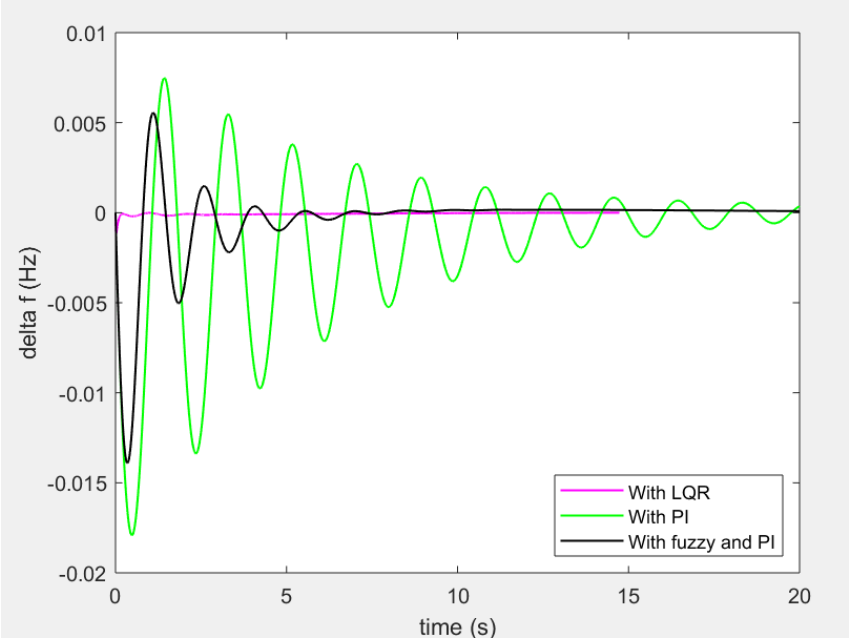

Figure 5.4 Comparison between LQR, PI and FLC for area 2 in the two-area system connected to PV due to a reasonable change in load.

Table 5.2 Summary of comparisons between the three controllers for the PV connected two-area system.

		Settling Time		Undershoot		Steady State Error	
		Area 1	**Area 2**	**Area 1**	**Area 2**	**Area 1**	**Area 2**
Case 1 (reasonable increase in load)	**LQR**	8.74751	10.422	-0.0007414	-0.0004598	0	0
	PI	9.59875	22.11898	-0.0334	-0.01788	0	0
	FLC	7.4	6.4828	-0.0177	-0.0139	0	0
Case 2 ($\Delta P_{load1} > \Delta P_{load2}$)	**LQR**	8.74751	10.44206	-0.001483	-0.0002299	0	0
	PI	12.3208	23.0503	-0.06656	-0.018254	0	0
	FLC	7.2646	7.8814	-0.01576	-0.006985	0	0
Case 3 ($\Delta P_{load2} > \Delta P_{load1}$)	**LQR**	8.74751	10.44206	-0.0003707	-0.0009197	0	0
	PI	8.7972	24.062	-0.0336	-0.03541	0	0
	FLC	7.0742	5.75177	-0.0083	-0.0124	0	0
Case 4 ($\Delta P_{load1} = \Delta P_{load2} = 50\%$)	**Uncontrolled**	23.14	20.61	-0.0875	-0.067	-0.0267	-0.02746
	I	15.1076	14.099	-0.093343	-0.071406	0	0
	LQR	8.7475	10.442	-0.0018537	-0.0011496	0	0
	PI	9.5987	22.11898	-0.0835	-0.04472	0	0
	FLC	6.7346	6.4828	-0.046853	-0.03509	0	0

For the LQR controlled two-area system, although the settling time did not meet the specification unlike the case of LQR controlled single-area, but the undershoot is already extremely small. For example, an undershoot of -0.001 like in case 4 means that the worst value of the frequency reached is 49.999Hz which is a negligible undershoot. However, this also shows a limitation of LQR controller when the system becomes more complicated. Since the two-area model is more complex than the single-area, even optimization is very difficult to implement like in the single-area case. Thus, a response that satisfies all the criteria with LQR controller is difficult to attain.

With the PI controller, the system had more oscillations and worse undershoot and settling time than in the single-area case. It did improve the system compared to the response of the uncontrolled system, however, even with the optimized values of K_p and K_i, neither the settling time nor the undershoot specifications were met.

For cases 1, 2 and 3, FLC is the only one that satisfied all conditions (as to the settling time, it is the closest to the required value (3s)), the LQR and PI controllers gave higher settling time. This shows the biggest advantage of FLC which is the ability to force the system to meet the specifications even when the model of the system becomes very complicated. As to case 4, FLC did not satisfy the undershoot criteria, and LQR controller is the only controller that did that in case 4. However, this is the worst-case scenario. Moreover, the response of the system with LQR in case 4 has a large settling time, so even though the undershoot specification is met, there is another trade-off with the settling time. FLC gave much better settling time for two-area system in case 4 compared to the LQR controller.

Therefore, for the two-area system, the best controller is the fuzzy logic controller (FLC). The undershoot and error criteria are met, and the settling time is the smallest compared to the two other controllers. This shows the big advantage of FLC in that it does not depend on the mathematical model of the system. Thus, even with complex models, an enhanced response can be achieved using FLC and it can also deal with nonlinear systems [32].

In addition, just as in the case of single-area, it can be observed in the two-area system that FLC improved the oscillations and undershoot greatly compared to the system with the conventional controller (PI) only. In Figures 5.3 and Figure 5.4 earlier, this enhancement due to fuzzy logic controller in comparison to PI is observed clearly for both areas.

As a final note in the analysis, it is observed from all the cases in single-area and two-area system that once the load changes, it usually only affects undershoot and not the settling time especially in the case of applying LQR controller to the system. For single-area system the changes in the load does not affect the settling time at all, while in two-

area, changes in load cause slight changes in the settling time for FLC. In the case of PI controller in the two-area system, the settling time changes significantly with the changes in the load.

5.3 Conclusions and Further Works

In this thesis, PV-connected single-area and two-area power systems have been studied. The model of the PV system and that of each area were presented separately and then connected together. The effect of this connection on the frequency deviation of the system was studied. The connection to PV operating at MPP led to less frequency deviation in the thermal power system because of the nature of its DC output.

Three controllers were designed for the PV grid-connected single-area and two-area systems, namely: LQR, PI and FL controllers. Each controller has been applied to the system and the response was checked accordingly for various cases; each case representing a certain increase in load. The power exchange has also been studied for the PV grid-connected two area power system, and in all cases, this change in tie-line power has a value of zero at steady state and a very small undershoot at the beginning. This implies that, when a load disturbance occurs, there is still minimal excess exchange of power between the areas than the amount agreed on in this specific power system.

According to the results of the single-area system connected to PV, the LQR controller gave the best response. It improved the system response and met all the specifications. The FLC met only two specifications. However, compared to the PI controller, the FLC improved the system significantly decreasing the oscillations and improving the undershoot, while the PI controller alone could only meet the SSE specification.

As to the results of the two-area system connected to PV, the FLC gave the best response and was the only controller that could meet all specifications, taking into consideration the physical limitations of the system that prevented the settling time specification from being strictly met. The LQR controller could not meet the specifications which proves the big advantage of using FLC in systems with complex mathematical models. Moreover, for the LQR controller, it is worth mentioning that, with a small change

in the system, it would collapse and the LQR would need to be redesigned. However, FLC provides a solid tool that would still operate even if the system is changed. The PI controller, as in the case of single-area, did not meet most of the specifications, and had oscillations that FLC was able to reduce significantly.

In both the single-area and two-area systems, the worst-case scenario has been studied for all controllers. This case implies a sudden increase of 50% in the load demand. For this case in single-area (case 2), the LQR controller was still able to meet all the specifications, while PI and FLC did not. As to the two-area system in the worst-case scenario (case 4), the FLC demonstrated the best response compared to the LQR and PI controllers in terms of the settling time. The undershoot was slightly above the specified range in case 4. However, this demonstrates that even under such extreme (and improbable) load changes, the FLC has improved the system response significantly.

It is also observed from both the single-area and two-area systems that, even under normal load changes, the PI controller alone has failed to meet system specifications and added many oscillations to the system. Therefore, advanced controllers such as LQR and FL controllers have much better impact on the system and are required in power systems with a high penetration level of PV. It is true, however, that the integral controller specifically was required alongside with the LQR and FL controllers to meet the third specification required which is a steady state error of zero.

As to the future work recommended, the effects of changes in the PV input could be studied at different times of the day or when it is not operating at the MPP. Also, the rules and the ranges in FLC design for single-area and two-area could be further modified in order to improve the system response. Last but not least, more detailed mathematical models could be considered for the thermal power system and the photovoltaic system.

References

[1] H. Bevrani, A. Ghosh, G. Ledwich, "Renewable energy sources and frequency regulation: survey and new perspectives," *IET Renewable Power Generation*, vol. 4, issue 5, pp. 438–457, February 2010. DOI: 10.1049/iet-rpg.2009.0049

[2] P. Loganthurai, G. Manikandan, "Modeling Of Grid Connected Hybrid System With Fuzzy Logic Controller For Voltage Regulation", *International Journal of Innovative Research in Science Engineering and Technology*, vol. 3, Special Issue 3, March 2014.

[3] K. Arulkumar, K. Palanisamy & D.Vijayakumar, "Recent Advances and Control Techniques in Grid Connected Pv System – A Review", *International Journal of Renewable Energy Research*, Vol.6, No.3, 2016.

[4] A. Samadia, M. Ghandharia, and L. Södera, "Reactive Power Dynamic Assessment of a PV System in a Distribution Grid", Technoport RERC Research, 2012.

[5] R. Rajbongshi, L. C. Saikia, "Combined control of voltage and frequency of multi-area multisource system incorporating solar thermal power plant using LSA optimized classical controllers", *IET Generation Transmission & Distribution*, January 2017.

[6] A. Gupta, S. Chanana, and T. Thakur, "Power quality assessment of a solar photovoltaic two-stage grid connected system: Using fuzzy and proportional integral controlled dynamic voltage restorer approach", *AIP Publishing Journal of Renewable and Sustainable Energy*, 2015.

[7] V. Kumar, P. Rai, and Ghanshyam, "Frequency Control of Smart Grid - A MATLAB/SIMULINK Approach", *International Journal of Engineering Research & Technology (IJERT)*, Vol. 2, Issue 10, October 2013.

[8] Z. Kamaruzzaman, A. Mohamed, H. Shareef, "Effect of grid-connected photovoltaic systems on static and dynamic voltage stability with analysis techniques – a review," in Przeglad Elektrotechniczny, June 2015.

[9] S. A. Pourmousavi, A.S. Cifala, and M.H. Nehrir, “Impact of High Penetration of PV Generation on Frequency and Voltage in a Distribution Feeder”, IEEE North American Power Symposium (NAPS), 2012.

[10] S. Yang, “Solar energy control system design,” Master of Science thesis, KTH Information and Communication Technology, Stockholm, Sweden, 2013.

[11] P. Tielens, D. Hertem, “Grid inertia and frequency control in power systems with high penetration of renewables,” *Semantic Scholar*, 2012.

[12] K. Krishna, B. Mohan, M. Lalitha, “Dynamic modeling and control of grid connected hybrid wind-PV generation system,” *International Journal of Engineering Research and Development,* e-ISSN: 2278-067X, p-ISSN: 2278-800X, vol. 10, issue 5, pp. 01-12, May 2014.

[13] X. Liu, P. Wang, P. Loh, “A hybrid AC-DC microgrid and its coordination control,” *IEEE Transactions on Smart Grid*, vol. 2, no. 2, June 2011.

[14] M. Alam and F. Khan, “Transfer function mapping for a grid connected PV system using reverse synthesis technique,” in 14th Workshop on Control and Modeling for Power Electronics (COMPEL)-IEEE, 2013.

[15] J. Qian, K. Li, H. Wu, J. Yang, X. Li, “Synergetic control of grid-connected photovoltaic systems,” *International Journal of Photoenergy*, pp. 11, March 2017.

https://doi.org/10.1155/2017/5051489

[16] Y. Liu, L. Zhu, L. Zhan, J. Gracia, T. King, Y. Liu, “Active power control of solar PV generation for large interconnection frequency regulation and oscillation damping,” *International Journal of Energy Research*, vol. 40, pp. 353–361, June 2015. [online]

Available: Wiley Online Library (wileyonlinelibrary.com) DOI: 10.1002/er.3362

[17] A. Abdlrahem, G. Venayagamoorthy, K. Corzine, “Frequency stability and control of a power system with large PV plants using PMU information,” in North American Power Symposium (NAPS) IEEE, September 2013.

[18] E.F. Camacho, M. Berenguel, F.R. Rubio, *Advanced Control of Solar Plants*, London: Verlag London Springer, 1997.

[19] N. Cao, Y. Cao, J. Liu, "Modeling and analysis of grid connected inverter for PV generation," in proceedings of the 2nd International Conference on Computer Science and Electronics Engineering (ICCSEE), Paris, 2013.

[20] "Solar Energy Grid Integration Systems (SEGIS)," Energy Efficiency and Renewable Energy, U.S. Department of Energy, October 2007.

[21] A. Monti and F. Ponci, "Electric power systems", *Intelligent Monitoring, Control, and Security of Critical Infrastructure Systems Springer*, 2015. DOI 10.1007/978-3-662-44160-2_2)

[22] N. Naghshineh and A. Ismail, "Advanced Optimization of Single Area Power Generation System Using Adaptive Fuzzy Logic and PI Control," *International Research Journal of Engineering and Technology (IRJET),* vol. 04, issue: 08, August 2017.

[23] Dr. Abdulla Ismail, Professor of Electrical Engineering at RIT Dubai. Advances in Power Generation System Lecture Notes.

[24] S. Pandey, S. Mohanty, N. Kishor, "A literature survey on load-frequency control for conventional and distribution generation power systems," *Renewable and Sustainable Energy Reviews Elsevier*, April 2013.

[25] A. Ikhe, A. Kulkarni, D. Veeresh, "Load frequency control using fuzzy logic controller of two-area thermal-thermal power plant," *International Journal of Emerging Technology and Advanced Engineering,* ISSN 2250-2459, vol. 2, issue 10, October 2012.

[26] D. Kirk, *Optimal Control Theory an Introduction*, Mineola NY: Dover Publications, 1998.

[27] B.D. Anderson and J.B. Moore, *Optimal Control Linear Quadratic Methods*, New Jersey: Prentice Hall, 1989.

[28] V. Kumar, J. Jerome, K. Srikanth. "Algebraic approach for selecting the weighting matrices of linear quadratic regulator," in Conf. on Green Computing Communication and

Electrical Engineering (ICGCCEE), Coimbatore, India, March 2014. DOI: 10.1109/ICGCCEE.2014.6922382

[29] M. Cavazzutti, "Fuzzy gain scheduling," Control Engineering Laboratory, Helsinki University of Technology, Sci Rep. 62, 2000.

[30] G. Chen and T. Pham, *Introduction to Fuzzy Sets, Fuzzy Logic, and Fuzzy Control Systems*, New York: CRC Press LLC 2001.

[31] K. Tomsovic, "Fuzzy systems applications to power systems", short course Proc. of international conference on intelligent system application to power systems. Brazil Rio de Janeiro; 1999. pp. 1-13.

[32] J. Godjevac, "Comparison between PID and fuzzy control," Département d'Informatique, Ecole Polytechnique Fédérale de Lausanne, Switzerland.

[33] K. Butler, G L. Torres, O.P. Malik, D. Niebur. Hiyama, Chapters 2 and 3 in *Tutorial on Fuzzy Systems Applications to Power Systems*, K. Tomsovic, M.Y. Chow, IEEE-PES, Singapore, January 2000, pp. 87.

[34] K.M. Passino, S. Yurkovich, *Fuzzy Control*, California: Addison-Wesley, 1998.

[35] S. Pourmousavi, A. Cifala, and M. Nehrir, "Impact of high penetration of PV generation on frequency and voltage in a distribution feeder," in North American Power Symposium (NAPS)-IEEE, September 2012. DOI 10.1109/NAPS.2012.6336320

[36] "The utility edge," Power System Engineering Inc., USA, 2015.

[37] P. Dabur, N. Yadav and R. Avtar, "MATLAB Design and Simulation of AGC and AVR For Single Area Power System with Fuzzy Logic Control.," *International Journal of Soft Computing and Engineering (IJSCE)*, ISSN: 2231-2307, vol. 1, Issue-6, January 2012.

Appendix

Sample Codes

Optimization code for LQR single-area:

```
close all
clear all
clc

%%%%Uncontrolled system

%The conventional power part of the state space
model
ki=0.6 %gain of the integral controller added,
it should be a small value for the system to be
stable
freq_bias=1
%for open loop
A_conv_1=[-1/20 6 0 0 0; 0 -0.1 -1.566 5/3 0; 0
0 -1/0.3 1/0.3 0; -5.21 0 0 -12.5 -12.5;
ki*(freq_bias) 0 0 0 0]
openloopEV= eig(A_conv_1)
B_conv_1=[6;0;0;0;0] %u input is considered to
be 0
C_conv_1=[1 0 0 0 0] %because the output is the
state variable x1

conventional_1=ss(A_conv_1,B_conv_1,C_conv_1,0)

%State space model obtained from MATLAB for PV
system
A=[0,-690857.142857143,0,-136357142857.143,0,-
7.692857142857l4e+15,0,0;1,0,0,0,0,0,0,0;0,1,0,
0,0,0,0,0;0,0,1,0,0,0,0,0;0,0,0,1,0,0,0,0;0,0,0
,0,1,0,0,0;0,0,0,0,0,1,0,0;0,0,0,0,0,0,1,0]
B=[1;0;0;0;0;0;0;0]
```

```
C=[0,298775.510203838,0,233775510204.000,0,-
1.09897959183647e+16,0,0]
D=[6001.42857142857]

open_PV_sys=ss(A,B,C,D)

Input_current_PV=750;
%Getting the PV output
opt1 =
stepDataOptions('InputOffset',0,'StepAmplitude'
,Input_current_PV);
[y1,t1] = step(open_PV_sys,opt1); %to put the
average power values in a matrix
avg_PV_power=[y1,t1];
figure
plot(avg_PV_power) %with all the samples taken
V =mean(avg_PV_power)
PV_output=V(1)/(10*(10^6)) %to get it in per
unit
P_load=1; %step change in the power of the load
by 10MW
P_input=PV_output-P_load

opt=stepDataOptions('InputOffset',0,'StepAmplit
ude',P_input);
[y,t4] = step(conventional_1,opt);
conventional_response=[15];
figure
plot(conventional_response)
title('response due to both inputs directly')
ylabel('delta f')

%%%controller - iterations to get best Q and R

syms Q1 Q2 Q3 Q4 Q5 r Q1_req Q2_req Q3_req
Q4_req Q5_req Q_req R_req
settling_t=100; %starting with a big value just
for the first iteration of the loop
undershoot=20;
```

```
%initialization so that the comparison does not
happen with variables
Q1=1;
Q2=1;
Q3=1;
Q4=1;
Q5=1;

for Q1=1:0.3:20
      for Q2=1:0.3:20
          for Q3=1:0.3:6
               for Q4=1:0.3:6
                   for r=0.001:0.005:0.08

         if (Q1<=Q2)
              continue
          end
          if (Q2<=Q3)
              continue
          end
          if (Q2<=Q4)
              continue
          end
          if (Q2<=Q5)
              continue
          end
          if (Q1<=Q3)
              continue
          end
          if (Q1<=Q4)
              continue
          end
          if (Q1<=Q5)
              continue
          end
```

```
   Q=[Q1 0 0 0 0; 0 Q2 0 0 0; 0 0 Q3 0 0; 0 0 0
Q4 0; 0 0 0 0 Q5]
   R=[r]
 %POS_DEF_EIG=eig(R); %to check that R is a
positive definite matrix
[K,P,EV]=lqr(A_conv_1,B_conv_1,Q,R);
Acl=(A_conv_1)-((B_conv_1)*K);
closed=ss(Acl,B_conv_1,C_conv_1,0);
ClosedLoopEV=eig(Acl);

opt_cl=stepDataOptions('InputOffset',0,'StepAmp
litude',P_input);
[y_cl,t5] = step(closed,opt_cl);
controller_response=[y_cl];
Inform=lsiminfo(y_cl,t5);
if (getfield(Inform, 'SettlingTime'))< 3 &
abs((getfield(Inform, 'Min')))< 0.02 &
((getfield(Inform, 'SettlingTime'))< settling_t
| abs((getfield(Inform, 'Min')))<undershoot)
%if (getfield(Inform, 'SettlingTime'))< 3 &
abs((getfield(Inform, 'Min')))< 0.02
settling_t = getfield(Inform, 'SettlingTime');
undershoot= abs(getfield(Inform, 'Min'));
Q1_req=Q1
Q2_req=Q2
Q3_req=Q3
Q4_req=Q4
Q5_req=Q5
Q_req=[Q1_req 0 0 0 0; 0 Q2_req 0 0 0; 0 0
Q3_req 0 0; 0 0 0 Q4_req 0; 0 0 0 0 Q5_req]
R_req=[r]
end

                    end
                end
            end
        end
 end
```

```
Q_req=[Q1_req 0 0 0 0; 0 Q2_req 0 0 0; 0 0
Q3_req 0 0; 0 0 0 Q4_req 0; 0 0 0 0 Q5_req]

Q_req
R_req
[K,P,EV]=lqr(A_conv_1,B_conv_1,Q_req,R_req);
Acl_des=(A_conv_1)-((B_conv_1)*K);
closed_des=ss(Acl_des,B_conv_1,C_conv_1,0);
ClosedLoopEV=eig(Acl_des); %the desired closed
loop

opt_cl=stepDataOptions('InputOffset',0,'StepAmp
litude',P_input);
%opt_cl=stepDataOptions('InputOffset',0,'StepAm
plitude',1);
[y_cl,t5] = step(closed_des,opt_cl);
controller_response=[y_cl];
Inform=lsiminfo(y_cl,t5)
%t6=0:(20/18573):(20-(20/18573)); %number
chosen to be of the same vector length of the
controller response
figure
plot(controller_response)
title('response after LQR controller')
ylabel('delta f')

Inform=lsiminfo(y_cl,t5)

%the cost
xi=[0; 0; 0; 0; 1];
Jo= (1/2)*xi'*P*xi %optimal cost
```

To get comparison figures for two-area system (after running Simulink files for PI and fuzzy and transferring the information to MATLAB):

```
%%Run Simulink two-area files first
```

```
%LQR
ki1=0.6;
ki2=0.1;
fb1=0.3;
fb2=0.6;
T=0.5;

A=[(-1/20) 6 0 0 0 0 0 0 0 0 -6; 0 -0.1 -1.566
(5/3) 0 0 0 0 0 0 0; 0 0 -(1/0.3) (1/0.3) 0 0 0
0 0 0 0; -5.21 0 0 -12.5 -12.5 0 0 0 0 0 0;
(fb1)*(ki1) 0 0 0 0 0 0 0 0 0 (ki1); 0 0 0 0 0
-2.7027 3.85946 0 0 0 3.85946; 0 0 0 0 0 0 -2
14 0 0 0; 0 0 0 0 0 0 0 0 -(1/0.3) (1/0.3) 0 0; 0
0 0 0 0 -5.208 0 0 -12.5 -12.5 0; 0 0 0 0 0
(fb2)*(ki2) 0 0 0 0 -(ki2); (2*pi*T) 0 0 0 0 -
(2*pi*T) 0 0 0 0 0]
B=[6; 0; 0; 0; 0; 3.85946; 0; 0; 0; 0; 0]
C=[1 0 0 0 0 0 0 0 0 0 0; 0 0 0 0 0 1 0 0 0 0
0]
sys_two_area=ss(A,B,C,0)
Q_req=[0.3 0 0 0 0 0 0 0 0 0 0; 0 19.9 0 0 0 0
0 0 0 0 0; 0 0 1 0 0 0 0 0 0 0 0; 0 0 0 1 0 0 0
0 0 0 0; 0 0 0 0 1 0 0 0 0 0 0; 0 0 0 0 0 0.3 0
0 0 0 0; 0 0 0 0 0 0 15.5 0 0 0 0; 0 0 0 0 0 0
0 5.8 0 0 0; 0 0 0 0 0 0 0 0 5.8 0 0; 0 0 0 0 0
0 0 0 0 5.8 0; 0 0 0 0 0 0 0 0 0 0 5.8]
R_req=[0.001]

[K,P,EV]=lqr(A,B,Q_req,R_req);
Acl_des=(A)-((B)*K);
closed_des=ss(Acl_des,B,C,0);
ClosedLoopEV=eig(Acl_des); %the desired closed
loop
P_input=-0.5
opt_cl=stepDataOptions('InputOffset',0,'StepAmp
litude',P_input);
%opt_cl=stepDataOptions('InputOffset',0,'StepAm
plitude',1);
```

```
[y_cl,t5] = step(closed_des,opt_cl);
controller_response=[y_cl];
figure
plot(t5,controller_response,'LineWidth',1)
hold on
plot(tout,delta_f3)
hold on
plot(tout,delta_f4)
hold on
plot(tout,delta_f,'LineWidth',1)
hold on
plot(tout,delta_f2,'LineWidth',1)
%title('responses of uncontrolled, with PI
only, and with fuzzy logic')
%legend('With integral controller only', 'With
LQR', 'With PI only','With fuzzy and PI')
legend('Area 1 with LQR', 'Area 2 with
LQR','Area 1 with PI', 'Area 2 with PI','Area 1
with fuzzy and PI', 'Area 2 with fuzzy and PI')
legend('Location','southeast')
xlim([0 20])
ylabel('delta f (Hz)')
xlabel('time (s)')
```

FLC initialization for single-area before running Simulink file:

```
close all
clear all
clc
%State space model obtained from MATLAB for PV
system
A=[0,-690857.142857143,0,-136357142857.143,0,-
7.692857142857143e+15,0,0;1,0,0,0,0,0,0,0;0,1,0,
0,0,0,0,0;0,0,1,0,0,0,0,0;0,0,0,1,0,0,0,0;0,0,0
,0,1,0,0,0;0,0,0,0,0,1,0,0;0,0,0,0,0,0,1,0]
B=[1;0;0;0;0;0;0;0]
```

```
C=[0,298775.510203838,0,233775510204.000,0,-
1.09897959183647e+16,0,0]
D=[6001.42857142857]

open_PV_sys=ss(A,B,C,D)
Qc_PV=ctrb(open_PV_sys)
format long
therank_PV=rank(Qc_PV)
Input_current_PV=750;
%Getting the PV output
opt1 =
stepDataOptions('InputOffset',0,'StepAmplitude'
,Input_current_PV);
[y1,t1] = step(open_PV_sys,opt1); %to put the
average power values in a matrix
avg_PV_power=[y1,t1];
figure
plot(avg_PV_power); %with all the samples taken
V =mean(avg_PV_power)
PV_output=V(1)/(10*(10^6)) %to get it in per
unit

%defining P load
P_load=0.5;
%%input as a total effect)
P_input=PV_output-P_load
%The conventional power system in the state
space model
ki=0.6 %gain of the integral controller added,
it should be a small value for the system to be
stable
freq_bias=1 %assuming no frequency bias because
this is single area
%for open loop
A_conv_1=[-1/20 6 0 0 0; 0 -0.1 -1.566 5/3 0; 0
0 -1/0.3 1/0.3 0; -5.21 0 0 -12.5 -12.5;
ki*(freq_bias) 0 0 0 0]
openloopEV= eig(A_conv_1)
```

```
B_conv_1=[6;0;0;0;0] %u input is considered to
be 0
C_conv_1=[1 0 0 0 0] %because the output is the
state variable x1

conventional=ss(A_conv_1,B_conv_1,C_conv_1,0)
%checking the controllability and observability
of the system which are
%important before applying fuzzy logic
Qc_conv=ctrb(conventional)
format long
therank_conv=rank(Qc_conv)

Obs_conv=obsv(conventional)
format long
obsrank_conv=rank(Obs_conv)

%open system response (before controller
opt=stepDataOptions('InputOffset',0,'StepAmplit
ude',P_input);
[y,t4] = step(conventional,opt);
conventional_response=[15];
figure
plot(t4, conventional_response)
title('uncontrolled system response')
ylabel('delta f')
Inform_open=lsiminfo(y,t4)
%fuzzy controller design
trial3_rules4=readfis('trial3_rules4.fis')
trialtrial3=readfis('trialtrial3.fis')

%Inform_closed=lsiminfo(delta_f,tout,0) %this
line is to show the information
%gensurf(trial3_rules4)
```